DSPACE

https://dspace.org/

Effects of alcohol and combined antiretroviral drug interactions on pulmonary histomorphology in diabetic male Sprague Dawley rats

Mahloko, Mmotong Potego

2025
University of the Witwatersrand, Johannesburg
https://hdl.handle.net/10539/49842

Mahloko, Mmotong Potego . (2025). Effects of alcohol and combined antiretroviral drug interactions on pulmonary histomorphology in diabetic male Sprague Dawley rats [Master's dissertation, University of the Witwatersrand, Johannesburg]. WIReDSpace. https://hdl.handle.net/10539/49842

Downloaded from a DSpace repository. https://dspace.org/

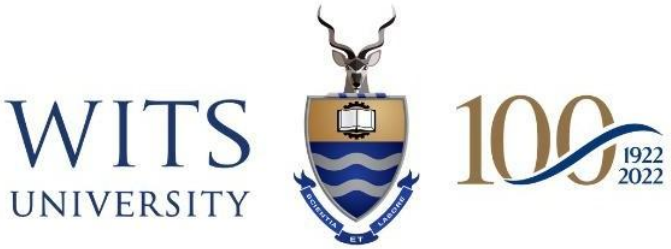

Effects of alcohol and combined antiretroviral drug interactions on pulmonary histomorphology in diabetic male Sprague Dawley rats

Mmotong Potego Mahloko

Student number: 1863024

A dissertation submitted to School of Anatomical Sciences, Faculty of Health Sciences, University of the Witwatersrand, Johannesburg, in fulfilment of the requirement for the degree of Master of Science in Medicine

Supervisors
Prof Ejikeme Mbajiorgu (PhD)
Dr Jaclyn Johnson (PhD)

DECLARATION

I, the undersigned, hereby declare that this dissertation is my own original work and that I have not previously in its entirety or in part submitted it to any university for a degree.

Signature



Full Names: Mmotong Potego Mahloko

Date: 27/10/2025

DEDICATION

To six-year-old me, here we are!!

PRESENTATIONS ARISING FROM THIS RESEARCH PROJECT

1. School of Biomedical Sciences 1st Research Day 2025

Title: Antiretroviral (Atripla) toxicity in combination with alcohol and type 2 diabetes in male Sprague Dawley rats: A pulmonary study.

Authors: Mr Mmotong Mahloko, Dr Jaclyn Johnson, Prof Ejikeme Mbajiorgu

Presentation Type: Poster

Place: Holiday Inn, Sunnyside Park hotel, Parktown, JHB

Date: 17 September 2025

2. Molecular Biosciences Research Thrust (MBRT) Research Symposium 2024

Title: Morphological and biochemical effects of combination antiretroviral (cART) drug on HIV-naïve male diabetic rat lungs.

Authors: Mr Mmotong Mahloko, Dr Jaclyn Johnson & Prof Ejikeme Mbajiorgu

Presentation Type: Oral

Place: Public Health Auditorium, WITS Education Campus, Parktown, JHB

Date: 03 December 2024

3. Johannesburg Health District 2023 Research Conference

Title: Effects of Atripla® on pulmonary histomorphology of HIV-naïve diabetic Sprague Dawley male rats.

Authors: Mr Mmotong Mahloko, Dr Jaclyn Johnson & Prof Ejikeme Mbajiorgu

Presentation Type: Poster

Place: Public Health Auditorium, WITS Education Campus, Parktown, JHB

Date: 23 November 2023

ABSTRACT

Combination antiretroviral therapy (cART) has been utilized for decades as main therapy against Human Immunodeficiency Virus (HIV) progression and transmission and recently for prevention. The research and usage of cART highlighted its effectiveness against HIV, albeit documented unintended effects such as diabetes induction. Further, diabetes affects millions of adults globally and is characterized by high blood glucose levels caused by lifestyle factors such as sedentary behaviour and excessive alcohol intake. Moreover, alcohol consumption is a major contributor of global burden of disease and death. Diabetes, cART, and alcohol are reported to independently impact the respiratory system and its functionality. However, their combined impact is lacking in literature, especially in HIV-negative individuals on preventative cART regime. This study aimed to fill this knowledge gap by investigating the histomorphological and biochemical effects of cART and alcohol treatment in HIV-naïve diabetic rat lungs.

Forty adult Sprague Dawley (SD) male rats were divided into eight groups of five rats each and treated accordingly for 90 days. The groups included untreated negative control (NC), cART-treated (CA), alcohol-treated (AL), cART and alcohol-treated (CAAL), diabetic (DB), diabetic and cART-treated (CADB), diabetic and alcohol-treated (DBAL), and diabetic, cART and alcohol-treated (CAALDB) groups. Blood samples were analyzed for glucose levels and oxidative stress changes using enzyme-linked immunosorbent assay (ELISA) for glutathione peroxidase-1(GPx1) and thiobarbituric acid (TBA) analysis for malondialdehyde (MDA). Lung histomorphological analysis focused on tracheal, bronchiole, vascular, and parenchymal changes using hematoxylin and eosin (H&E), Gordon & Sweet, modified Pentachrome, and Verhoeff van Gieson stains. Additionally, pulmonary inflammation was investigated through C-reactive protein (CRP) expression using immunohistochemistry (IHC).

In this study, cART and alcohol co-administration attenuated oxidative stress, tunica media thickness, reticular fibre hyperplasia in the respiratory bronchiole and parenchyma, and induced minimal CRP inflammation in bronchial vasculature. The cART-diabetes interaction resulted in lung surface area reduction, tracheal and bronchial atrophy, and oxidative stress exacerbation. Further, this morbidity induced parenchymal replacement fibrosis (elevated collagen, reduced elastic and reticular fibres) and CRP inflammation (endothelium, muscularis mucosa, and vascular smooth muscle). Alcohol and diabetes interaction exacerbated weight loss, tracheal and bronchial atrophy, and CRP inflammation (bronchial vein and parenchyma).

In diabetes, alcohol and cART exacerbated oxidative stress (reduced GPx1 and elevated MDA

levels), while CRP inflammation was observed in the bronchial epithelium and smooth muscle, vasculature, alveoli and alveolar macrophages. Histomorphologically, the triple-morbidity induced tracheal, bronchial artery, and vein atrophy. Such combined impact suggests detrimental capacity against the respiratory system and, consequently, may compromise the functionality. As such, this study calls for persistent pulmonary health monitoring in diabetic individuals on cART regime who regularly consume alcohol.

ACKNOWLEDGEMENTS

My gratitude extends to:

- Prof. EF Mbajiorgu and Dr. JA Johnson for your mentorship and leadership throughout.
- Mrs. H Ali for the warmth and guidance you have provided during my lab activities.
- Ms. M Zwane for the artistry you have contributed to our project.
- My family and friends for believing in my aptitude for this work.

TABLE OF CONTENTS

CHAPTER ONE: Introduction....1

1.1. Introduction....1

1.2. Rationale....2

1.3. Aim, Hypothesis and Objectives....3

1.3.1. Aim....3

1.3.2. Hypothesis....3

1.3.3. Objectives....3

CHAPTER TWO: Literature Review....5

2.1. Brief Background on Antiretroviral Therapy as HIV/AIDS regimen....5

2.1.1. Complexity of Lifestyle and HIV/AIDS....6

2.1.2. Combination Antiretroviral Drug....6

2.1.3. Impact and Efficacy of Antiretroviral Therapy in HIV Management....9

2.2. Alcohol Consumption: Prevalence and Health Implications....9

2.3. Alcohol and cART as Risk Factors for Type 2 Diabetes....10

2.4. The Global Diabetes Epidemic: Causes and Consequences....11

2.5. Overview of the Respiratory System Structure and Function….....12

2.5.1. Comparative Gross Anatomy of Human and Rodent Lungs….....13

2.5.2. Microanatomy and Function of the Lung....14

2.6. Independent Respiratory Effects of Diabetes, Alcohol, and cART....15

2.6.1. Oxidative Stress Induced by Diabetes, Alcohol, and cART....15

2.6.2. Mechanisms and Implications of Pulmonary Fibrosis....16

2.6.3. Inflammatory Responses Associated with Diabetes, Alcohol, and cART....17

2.6.4. Thrombosis and Vascular Disruption in Pulmonary Health....19

2.7. Choice Of Experimental Model and Treatment….....21

CHAPTER THREE: Methods and Materials....22

3.1. Ethics....22

3.2. Animal studies....22

3.2.1. Samples & Animal husbandry 22
3.2.2. Diabetes Induction 22
3.2.3. Fasting Blood Glucose 22
3.3. Chemicals and Reagents 23
3.4. Treatments and Termination 23
3.4.1. Groups Treatments 23
3.4.2. Termination and Dissection 24
3.5. Gross Morphological Analysis 24
3.5.1. Body And Lungs Weights 24
3.5.2. Lung Morphology 25
3.6. Serum Biochemical Analysis 25
3.6.1. Bradford Method For Protein Detection 25
3.6.2. Lipid Peroxidation Thiobarbituric Acid (TBA) assay for MDA 26
3.6.3. Glutathione Peroxidase (GPx1) detection (ELISA) 26
3.7. Tissue Processing and Sectioning 26
3.8. Routine Staining 27
3.8.1. Hematoxylin & Eosin Stain 27
3.8.2. Modified Verhoeff's Stain 27
3.8.3. Modified Pentachrome Stain 27
3.8.4. Gordon & Sweets' Stain 28
3.9. Histomorphometry 28
3.9.1. Histological Analysis 28
3.9.1.1. Tracheal Epithelial Height, Cartilage Width and Lacunae Size 28
3.9.1.2. Bronchiole Epithelial Height, Muscularis Mucosa Width and Mucosal Reticular Fibers 29
3.9.1.3. Bronchia Arterial Wall and Tunica Media Heights 30
3.9.1.4. Bronchial Vein Wall, Tunica Media, Tunica Adventitia Heights, Collagen, and Elastic Fibers Percentage Area Fraction 31
3.9.1.5. Parenchymal Collagen, Elastic, and Reticular Fibers Percentage Area Fraction 32

3.10. Immunohistochemical Staining 33

3.10.1. C-Reactive Protein 33

3.11. Statistical Analysis 34

CHAPTER FOUR: Results 35

4.1. ANTIRETROVIRAL TOXICITY 35

4.1.1. Fasting Blood Glucose 35

4.1.2. Gross Morphological Analysis 36

4.1.2.1. Mean Body and Lung Weights and Relative Lung Weight 36

4.1.2.2. Right Lung Surface Area 37

4.1.3. Biochemical Analysis 38

4.1.3.1. Oxidative Stress: Serum MDA and GPx1 Concentrations and MDA: GPx1 Ratio 38

4.1.4. Histological Analysis 40

4.1.4.1. Tracheal Epithelial Height 40

4.1.4.2. Tracheal Cartilage Width 41

4.1.4.3. Tracheal Lacunae Area 42

4.1.4.4. Bronchiole Epithelial Height 44

4.1.4.5. Bronchiole Muscularis Mucosa Width 45

4.1.4.6. Bronchiole Mucosal Reticular Fibres 46

4.1.4.7. Thickness of Bronchial Arterial Wall 47

4.1.4.8. Bronchial Arterial Tunica Media Thickness 48

4.1.4.9. Thickness of The Bronchial Vein Wall 49

4.1.4.10. Bronchial Vein Tunica Media Thickness, Tunica Adventitia Thickness and Collagen Fibres 51

4.1.4.11. Bronchial Vein Elastic Fibres 53

4.1.4.12. Parenchymal Collagen Fibres 54

4.1.4.13. Parenchyma Reticular Fibres 55

4.1.4.14. Parenchymal Elastic Fibres 57

4.1.5. Immunohistochemical Analysis 58

4.1.5.1. C-Reactive Protein IHC Expression....58
4.1.5.2. TGFβ1, MDA and Caspase 3 Trials....61
4.2. DIABETES AND ALCOHOL INTERACTION....61
4.2.1. Fasting Blood Glucose....61
4.2.2. Body and Lung Weights and Right Lung Surface Area....63
4.2.3. Mean Serum MDA and Gpx1 Concentrations and MDA to GPx1 Ratio....64
4.2.4. Tracheal Epithelial Height, Cartilage Width and Lacunae Area....65
4.2.5. Bronchiole Epithelial Height, Muscularis Mucosa Width and Mucosal Reticular Fibre Profile....67
4.2.6. Bronchial Artery and Vein....69
4.2.7. Parenchymal Collagen, Reticular and Elastic Fibre Profile....72
4.2.8. Immunohistochemical Analysis....74
4.2.8.1. C-Reactive Protein IHC Expression....74
4.2.8.2. TGFβ1, MDA and Caspase 3 Trials....77
CHAPTER FIVE: Discussion....78
CHAPTER SIX: Conclusion....83
REFERENCES....84
APPENDICES....104
7.1. Microscope slide-coating....104
7.1.1. Saline....104
7.1.2. Gelatine....104
7.2. Serum biochemical analysis....104
7.2.1. TBA test for MDA....104
7.2.2. ELISA for GPx1....106
7.2.3. Optical density for concentration calculation....106
7.3. Routine stains....107
7.3.1. H&E stain....107
7.3.2. Modified Verhoeff's van Gieson stain....107
7.3.3. Modified pentachrome stain....108
7.3.4. Gordon and sweets stain....108
Ethics Approval....109

LIST OF FIGURES

Figure 2.1: HIV Medication Chart.
Figure 2.2: Different formulations of cART drugs.
Figure 2.3: Overview of the Respiratory System Structure.
Figure 2.4: Comparative Gross Anatomy of Human and Rodent Lungs.
Figure 2.5: Overview of the respiratory tree histology
Figure 2.6: Pulmonary fibrosis-induced organ size increase.
Figure 2.7: A flow diagram illustrating the interactions between alcohol, diabetes and cART and their respective effects.
Figure 3.1: A flow diagram illustrating the treatments and techniques of the study.
Figure 3.2: Illustration of ventral and dorsal surface area of lungs measurements.
Figure 3.3: Illustration of the tracheal epithelial height, cartilage width and lacunae area measurements.
Figure 3.4: Illustration of the measurements of the bronchiole epithelial height, muscularis mucosa width and mucosal reticular fibers.
Figure 3.5: Illustrations of the bronchial arterial wall and tunica media heights measurements.
Figure 3.6: Illustration of the bronchial vein wall height, tunica media and adventitia heights measurements and collagen and elastic fibers quantification.
Figure 3.7: Illustration of parenchymal collagen, reticular and elastic fibers quantification.
Figure 4.1: Mean Biweekly Fasting Blood Glucose Across Groups.
Figure 4.2: Body, Lung And Relative Lung Weights.
Figure 4.3: Mean Right Lung Total Surface Area.
Figure 4.4: Mean Serum MDA and GPx1 Concentrations and MDA To GPx1 Ratio.
Figure 4.5: Tracheal Epithelial Height.
Figure 4.6: Tracheal Cartilage Width.
Figure 4.7: Tracheal Lacunae Area.
Figure 4.8: Bronchiole Epithelial Height.
Figure 4.9: Muscularis Mucosa Width.
Figure 4.10: Bronchiole Mucosal Reticular Fibres.
Figure 4.11: Bronchial Artery Wall Thickness.
Figure 4.12: Bronchial Artery Tunica Media Thickness.
Figure 4.13: Bronchial Vein Wall Thickness.
Figure 4.14: Bronchial Vein Tunica Media and Adventitia Thickness and Collagen Fibres.

Figure 4.15: Bronchial Vein Elastic Fibres.
Figure 4.16: Parenchymal Collagen Fibres.
Figure 4.17: Parenchymal Reticular Fibres.
Figure 4.18: Parenchymal Elastic Fibres.
Figure 4.19: CRP Expression in The Bronchiole epithelium and Alveolar Spaces.
Figure 4.20: CRP Expression in The Bronchial Artery and Vein.
Figure 4.21: Non-expression trials for TGFβ1, MDA and Caspase 3.
Figure 4.22: Mean Right Lung Total Surface Area.
Figure 4.23: Tracheal Epithelial Height, Cartilage Width, and Lacunae Area.
Figure 4.24: Bronchiole Epithelial Height Muscularis Mucosa Width, and Mucosal Reticular Fibre Profile.
Figure 4.25: Bronchial Artery (Tunica Media and Adventitia Thickness) and Vein (Wall, Tunica Media and Adventitia Thickness, and Collagen and Elastic Fibre Profile).
Figure 4.26: Parenchymal Collagen, Reticular and Elastic Fibre Profile.
Figure 4.27: CRP Expression in The Bronchiole and Alveolar Spaces.
Figure 4.28: CRP Expression in The Bronchial Artery and Vein.
Figure 4.29: Non-expression trials for TGFβ1, MDA and Caspase 3.
Figure 7.1: Preparation of the standard working solution.
Figure 7.2: Equation to convert optical density to concentration.

LIST OF TABLES

Table 4.1: Mean Fasting Blood Glucose, Body and Lung Weights, Relative Lung Weight, Right Lung Surface Area, Serum MDA and GPx1 Concentrations and MDA To GPx1 Ratio.

Table 4.2: Bronchiole Epithelial Height, Muscularis Mucosa Width and Mucosal Reticular Fibre Profile.

Table 4.3: Bronchial Artery (Tunica Media and Adventitia Thickness) and Vein (Wall, Tunica Media and Adventitia Thickness, and Collagen and Elastic Fibre Profile).

Table 4.4: Parenchymal Collagen, Reticular and Elastic Fibre Profile.

Table 7.1: The preparation of the TBA assay.

Table 7.2: Preparation of standard curve.

Table 7.3: Optical density for concentration formular values.

LIST OF ABBREVIATIONS

AIDS	Acquired Immune Deficiency Syndrome
AL	Alcohol
ANOVA	Analysis for Variance
AGE	Advanced Glycation End-Products
AZT	Anti-retroviral drug
BSA	Bovine Serum Albumin
cART	Combination Antiretroviral Therapy
CANFAR	The Canadian Foundation for AIDS Research
CRP	C-reactive protein
DB	Diabetes
DF	Disoproxil Fumarate
DTG	Dolutegravir
ECM	Extracellular Matrix
EDTA	Ethylenediaminetetraacetic Acid
ELISA	Enzyme-linked Immunosorbent Assay
EMT	Epithelial to Mesenchymal Transition
eNOS	Endothelial Nitric oxide synthase
FBG	Fasting Blood Glucose
FDA	Food and Drug Administration
FEV1	Forced Expiratory Volume
FVC	Forced Vital Capacity
GM-CSF	Granulocyte-Macrophage Colony Stimulating Factor
GPx1	Glutathione Peroxidase 1
GRID	Gay-Related Immune Deficiency
GSH	Glutathione
GSSG	Glutathione Disulfide
HIV	Human immunodeficiency virus
IDF	International Diabetes Federation

IHC	Immunohistochemistry
IRIS	Immune Reconstruction Inflammatory Syndrome
MDA	Malondialdehyde
NC	Negative Control
NNRTI	Non-Nucleoside Reverse Transcriptase Inhibitor
NO	Nitric Oxide
NRTI	Nucleoside Reverse Transcriptase Inhibitors
OD	Optical Density
OGTT	Oral Glucose Tolerance Tests
PBS	Phosphate Buffered Saline
PIs	Protease Inhibitors
RNFBG	Random Non-Fasting Blood Glucose
SD	Sprague Dawley
SEM	Standard Error of The Mean
SOD	Superoxide Dismutase
SPSS	Statistical Package for Social Science
T1DM	Type 1 Diabetes Mellitus
T2DM	Type 2 Diabetes Mellitus
TBA	Thiobarbituric Acid
TGF	Transforming Growth Factor
WHO	World Health Organization

CHAPTER ONE: Introduction

1.1. Introduction

The use of various combinations of antiretroviral therapies (cART) to manage Human immunodeficiency virus (HIV) has significantly reduced the transmission and progression rate of the virus while improving life quality and expectancy of infected individuals (Otieno *et al*., 2019). Recently, the World Health Organization (WHO) estimated more than 39.9 million HIV-infected individuals globally, of which roughly 80% are on cART (WHO, 2024: HIV). In addition to managing HIV transmission and progression, cART is also used as both pre- and post-exposure preventative measure for individuals with high probability of HIV exposure and infection (Baeten *et al*., 2012).

While cART unburdens some of the HIV-related complications in infected individuals (Vaillant and Naik 2023), pulmonary complications, including inflammatory and fibrotic illnesses, persist (Fitzpatrick *et al*., 2018). In HIV patients, cART is associated with recurring respiratory health complications in conjunction with elevated baseline CRP (Sereti *et al*., 2017). Other studies also showed cART's capacity to induce oxidative stress through downregulation of superoxide dismutase (SOD) and GPx1 (Sharma, 2014). Pulmonary effects of cART include alveolar tears, which impair gaseous exchange and incidences of emphysema in HIV patients (Twigg III and Knox, 2013). Moreover, cART use has been associated with metabolic dysfunction and, consequently, diabetes induction in HIV-positive individuals (Gebrie *et al*., 2020). However, combined pulmonary effects of cART and diabetes are lacking, especially in HIV-negative individuals who may receive routine cART treatment as both pre- and post-exposure preventative prophylaxis.

Similarly, diabetes affects more than 800 million adults worldwide, with the majority originating from developing countries and comprised of Type 1 diabetes mellitus (T1DM) induced by faulty insulin secretion and Type 2 diabetes mellitus (T2DM) due to insulin resistance (Zheng *et al*., 2018). Further, T2DM is diagnosed in 9 out of 10 diabetes cases, perpetuated by factors such as sedentary habits, poor diet, chronic alcohol abuse, and cART treatment (Lazic *et al*., 2025; Bailin *et al*., 2020; Sapra and Bhandari, 2023). Moreover, diabetes has been associated with lung complications such as microvascular damage, vascular inflammation, and pulmonary fibrosis through hyperglycaemic influence and pro-inflammatory pathways (Khateeb *et al*., 2019). Chronic inflammation is reported as one of the main causes of T2DM pathogenesis, as evidenced

by systemic CRP overexpression (Stanimirovic *et al*., 2022). Other studies have shown T2DM capacity to induce pulmonary oxidative stress through lipid peroxidation and lung parenchymal SOD downregulation (Forgiarini *et al*., 2009; Hamden *et al*., 2009). Further, diabetes-induced redox imbalance is suggested to induce pulmonary fibrosis (Talakatta *et al*., 2018).

On the other hand, the prevalence of alcohol consumption globally is at its highest in history, especially in South African rural regions, where more than half of HIV patients are reported to consume alcohol (Mpinganjira *et al*., 2023). Further, alcohol use is estimated to contribute to 10% of the yearly death rate in South Africa, with 60% of the mortality emerging from underprivileged households (Probst *et al*., 2018). Pulmonary alcohol toxicity includes oxidative stress leading to MDA upregulation and subsequent bronchial pro-inflammatory response, potentially harmful to the respiratory epithelium (Wyatt *et al*., 2012; Kaphalia and Calhoun, 2013). Moreover, alcohol-induced pulmonary redox imbalance is reported to downregulate alveolar macrophages, possibly impairing immune response and surveillance (Joshi *et al*., 2005). Additionally, moderate alcohol consumption is linked with lower CRP baseline in the adult population, highlighting alcohol's potential deleterious effect on the immune response (Stewart *et al*., 2002). Present studies report that cART, diabetes, and alcohol independently affect pulmonary histomorphology and function through oxidative stress, fibrosis, and inflammatory perturbations (Knoop *et al*., 2018; Kaphalia *et al*., 2024). As such, it was hypothesized that combining cART, diabetes, and alcohol would collectively induce an adverse effect on lung histomorphology in an HIV-naive context.

To investigate, we examined oxidative stress through GPx1 and MDA using ELISA and TBA analysis, respectively. Further, H&E stain was used to assess tracheal, bronchiole, and bronchial vasculature layers and histomorphology, whereas Modified Pentachrome, Gordon & Sweet and Verhoeff van Gieson stains were used to assess pulmonary collagen, reticular and elastic fibre configuration, respectively. Pulmonary inflammation was examined through CRP expression in the bronchiole, and pulmonary vasculature, and parenchyma using immunohistochemistry technique (IHC). Thus, this study will provide histopathological insight on the pulmonary condition in diabetic individuals on cART who frequently consume alcohol and will enable careful management of underlying conditions that may arise when prescribing cART drugs.

1.2. Rationale.

Diabetes, alcohol use, and cART regimen (as HIV treatment and prevention) are extremely prevalent in society, especially in low socioeconomic settings with all three factors occurring in one individual. However, the present literature only reports independent effects of diabetes, cART, and alcoholism on the respiratory system. Therefore, a comparative histopathological study of the combinatorial effects of this multiple morbidity is invaluable in bridging the gap in literature and consequently in the management of respiratory health of diabetic individuals on cART who drink alcohol regularly.

1.3. Aim, Hypothesis and Objectives.

1.3.1. Aim.

To investigate the adverse effects of combined alcohol and cART on lung histopathology and relative functionality in adult male diabetic Sprague Dawley rats.

1.3.2. Hypothesis.

H_0: Alcohol and cART (Atripla®) will have no significant effects on lung histopathology in a HIV-naive diabetic condition.

H_1: It is hypothesized that alcohol and cART (Atripla®) will exert detrimental effects on the lung histopathology in a HIV-naive diabetic condition.

1.3.3. Objectives.

To determine the effects of alcohol and cART therapy, diabetes, and their combinations on male Sprague Dawley (SD) rats by evaluating:

1. The surface area analysis of the right lung (superior, middle, accessory, and inferior lobes) using stereoscopic imaging and ImageJ software.

2. Oxidative stress analysis of serum MDA and GPx using TBA analysis and ELISA to profile lipid peroxidation and antioxidant activity, respectively.

3. Histomorphological analysis of the following using H&E, modified Pentachrome, Verhoeff's Van Gieson and Gordon & Sweet stains, and ImageJ software.

    a) Epithelial height, cartilage width and lacunae area of the trachea.

b) Epithelial height, muscularis mucosa width and mucosal reticular fibres of the bronchiole.

c) Bronchial vein wall, tunica media and adventitia width, collagen, and elastic fibres profiles of the bronchial vein.

d) Bronchial artery wall and tunica media thickness of the bronchial artery.

4. Pulmonary fibrosis analysis by quantifying collagen, elastic, and reticular fibers in the lung parenchyma using modified Pentachrome, Verhoeff's Van Gieson and Gordon & Sweet stains, and ImageJ software.

5. Assessing pulmonary inflammatory state using IHC to profile CRP expression in pulmonary venules, bronchial epithelium, and type II pneumocytes, respectively.

CHAPTER TWO: Literature Review.

2.1. Brief Background on Antiretroviral Therapy as HIV/AIDS regimen.

The Human Acquired Immune Deficiency Syndrome (AIDS), caused by HIV types 1 and 2 lentiviruses, was identified and documented as a deadly new infectious disease in 1981 (Caterino-de-Araujo *et al*., 2022). After numerous deaths of same-sex (homosexual) men caused by uncommon malignant conditions and opportunistic infections, AIDS was coined Gay-Related Immune Deficiency (GRID) believed to affect only gay men (Greene, 2007). Further, the disease is believed to originate in monkeys and apes from Central and West Africa regions, in 1982, and it was then renamed AIDS (Melhuish & Lewthwaite, 2022; Canadian Foundation for AIDS Research, 2017: History of HIV/AIDS | CANFAR; Be in the KNOW, 2023: Origin of HIV and AIDS).

Right from the inception of the pandemic, AIDS has been a subject of extreme research relative to its unexpected development, spread and rare pathogenicity. Today, HIV/AIDS is reported as a sexually transmitted disease which also spreads by percutaneous and perinatal routes (Bogers *et al*., 2021). In 1987, the Anti-retroviral drug (AZT) discovery and approval for use by the US Food and Drug Administration led to a significant decrease in the fatality associated with the HIV/AIDS pandemic. Later followed the development of a combination drug therapy (3TC) in 1996, which led to a drastic reduction of about 60 to 80% in AIDS-related deaths and hospitalization, however, the drug was unaffordable to the majority of infected individuals (Canadian Foundation for AIDS Research, 2017: History of HIV/AIDS | CANFAR; Melhuish & Lewthwaite, 2022)

The WHO experts (WHO, 2024) showed that HIV infection is still a major global public health issue, causing more than 41 million deaths to date, with spread persisting, especially in developing countries. By the end of 2023, about 40 million people were living with HIV while 65% was accounted for by the WHO African Region residents. During that year (2023), estimated new HIV infections was approximated 1.3 million and HIV-related death toll stood at about 630 000 lives. Additionally, HIV/AIDS has no cure, but improved risk reduction with therapy. Detection and therapy allow for a sustainable chronic illness, providing infected individuals with better quality of life. Further, HIV/AIDS has huge national and global disease burden, therefore, the target 3.3 strategy of the Sustainable Development Goals (SDGs) by WHO, UNAIDS and Global Fund was established to end the AIDS epidemic by 2030. As such, the success of national and international HIV/AIDS treatment programs enabled 86% of infected individuals to know

their status in 2023, with 77% receiving antiretroviral therapy and 72% achieving viral suppression.

2.1.1. Complexity of Lifestyle and HIV/AIDS.

Lifestyle factors like alcohol abuse, poor diet, lack of exercise, drug use, and stress are believed to significantly worsen HIV/AIDS progression and complications (Baum *et al*., 2022). Alcohol abuse and cART may independently contribute to diabetes and obesity in HIV patients (Bailin *et al*., 2020). Alcohol abuse among HIV-positive individuals with diabetes heightens the risk of health complications due to potential toxicity from alcohol-cART interactions (Kumar *et al*., 2012). This study investigates this complex scenario of alcohol abuse in conjunction with cART in diabetes, focusing on their combined effects on respiratory histomorphology, morphometry, biochemical and histochemical outcomes.

2.1.2. Combination Antiretroviral Drugs.

Combination antiretroviral therapy (cART) is an antiretroviral drug typically involving three drug variants and delivered as a once-daily pill. This combination includes efavirenz, a non-nucleoside reverse transcriptase inhibitor (NNRTI), and tenofovir disoproxil fumarate (DF) and emtricitabine, both nucleoside reverse transcriptase inhibitors (NRTI) (Deeks and Perry, 2010; Horberg and Klein, 2010). South Africa is reckoned to have effective, prominent antiretroviral treatment programs due to the extreme commonness of HIV/AIDS in the Southern Africa region (Juta *et al*., 2024). Worldwide, cART is reported as highly proficient in restraining HIV virulence in the peripheral (bodily fluids) and central environments (major organs) of HIV patients (Kanters *et al*., 2020). Moreover, the regimen is affordable and accessible, and therefore, employed to contain the spread and transmission of the virus (Meintjes *et al*., 2017). The FDA-approved different antiretroviral formulations charts displaying discontinued and currently in use treatments are presented below (Fig. 2.1 and 2.2).

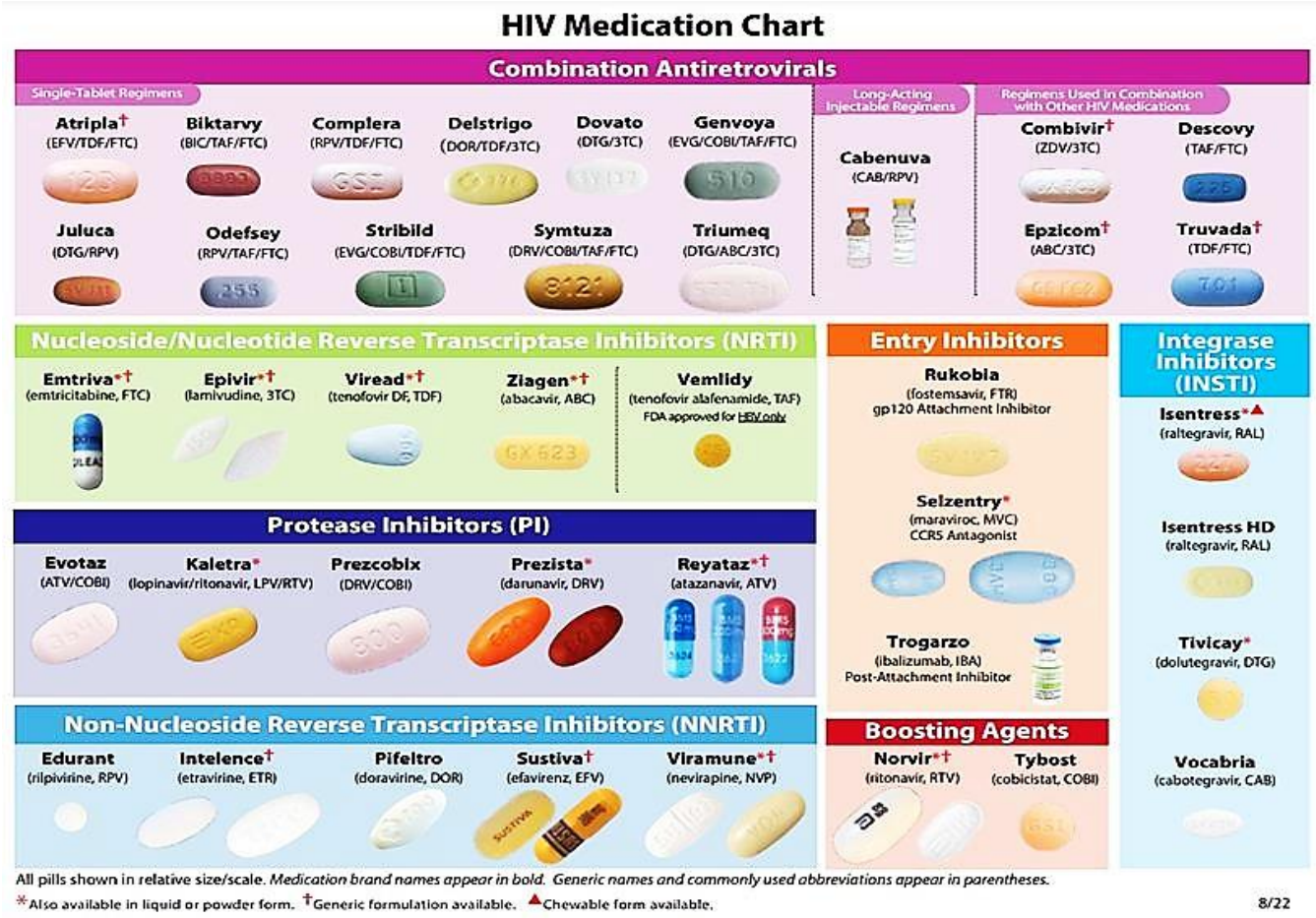

Figure 2.1: HIV Medication Chart.

A HIV medication chart illustrating different combination antiretroviral therapy drugs. (The Mountain West AIDS Education and Training Center (MWAETC) HIV Medication Chart)

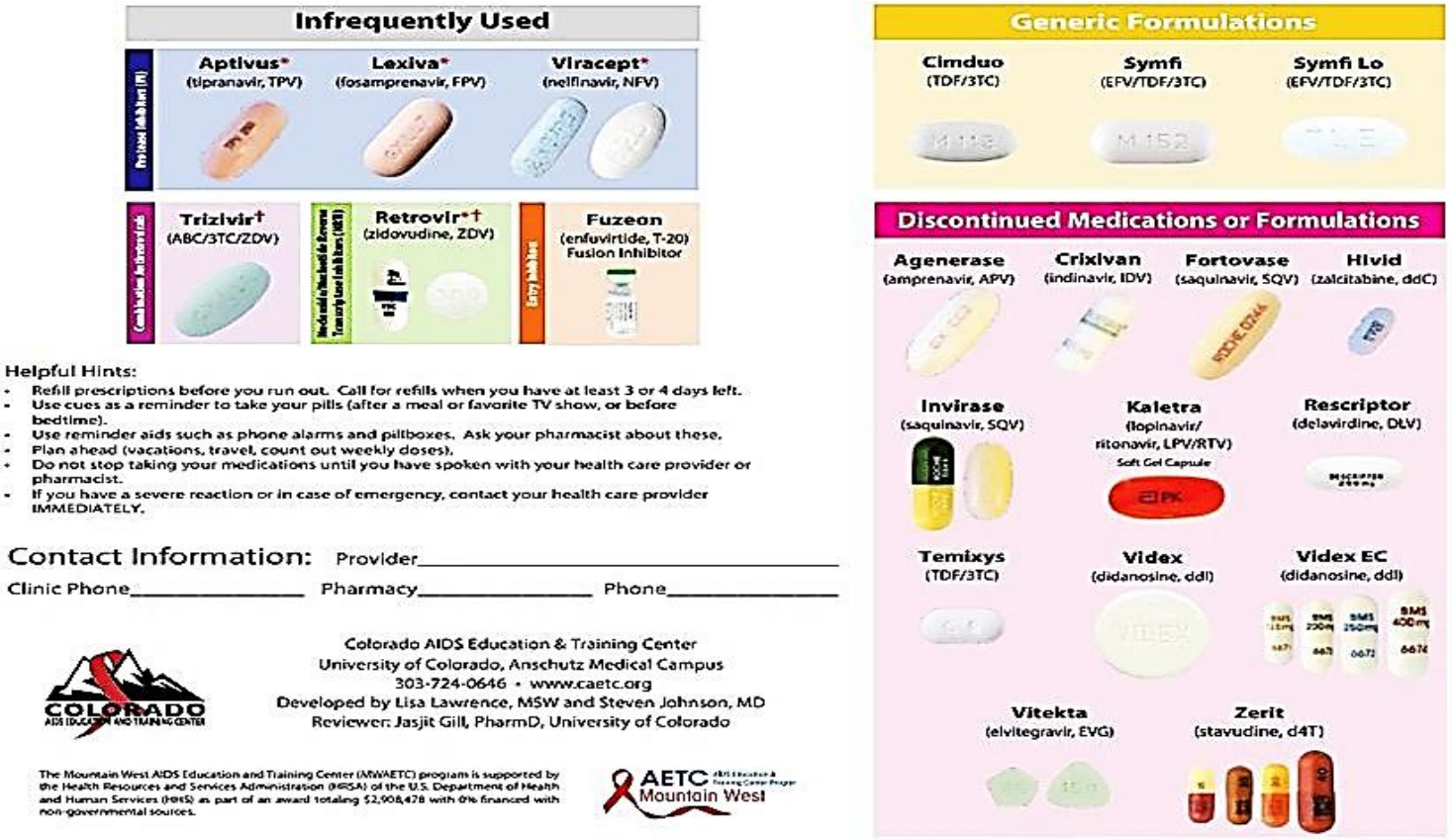

Figure 2.2: Different formulations of cART drugs.

Combination antiretroviral therapy drugs usage and formulations chart. (The Mountain West AIDS Education and Training Center (MWAETC): Different formulations of cART drugs)

2.1.3. Impact and Efficacy of Antiretroviral Therapy in HIV Management.

The World Health Organization (WHO) approximated 1.5 million new HIV infections worldwide in 2021 (UNAIDS, 2024). The scourge of HIV infections affects and claims a substantial number of lives yearly (UNAIDS, 2024). However, the introduction of combination antiretroviral therapy (cART) treatment lessened the HIV infection rates and deaths compared to previous years (Lau & Wong, 2013; Otieno *et al*., 2019). Antiretroviral therapy is the first treatment implemented immediately following a HIV-positive diagnosis, and it is aimed at evading viral resistance and increasing cluster of differentiation 4 count (CD4) (Clumeck *et al*., 2008). Nevertheless, the treatment may be associated with underlying co-morbidities, such as the development of metabolic syndrome conditions like T2DM (Gebrie *et al*., 2020). Furthermore, antiretroviral therapy is reported as an effective preventative prophylaxis for HIV infection and is often employed as a pre- and post-exposure prophylaxis for high HIV risk occupations (Baeten *et al*., 2012). Individuals in these occupations, such as healthcare professionals who are continuously exposed to HIV/AIDS patients, infected human remains, or fluid specimens, and as well sex workers, and individuals with multiple sex partners, amongst others.

Antiretroviral therapy is associated with significant improvements in opportunistic infections within the lungs of HIV patients (Vaillant and Naik 2023). Inversely, post-mortem studies report that cART regimen in HIV-positive individuals causes damage to alveolar epithelium and consequently the collapse and rupture of the alveoli (Twigg III & Knox, 2013). The alveoli rupture is associated with larger air sacs and shortness of breath or otherwise emphysema compared to healthy controls (Hale *et al*., 2018). Considering the high population of HIV-infected patients and HIV-naïve individuals who are regularly exposed to prophylaxis of cART regimen, it is therefore important to investigate the sub-chronic chemo-toxic effect of cART in the respiratory system involving alcohol abuse as a lifestyle factor (McCance-Katz *et al*., 2012).

2.2. Alcohol Consumption: Prevalence and Health Implications.

Among other pressing medical factors, alcohol consumption is a major etiologic factor of preventable death and a significant contributor of global burden of disease and death (Taylor *et al*., 2010; Witkiewitz *et al*., 2019). Reports by the WHO demonstrate that alcohol use is implicated in 10% of overall annual mortality in South Africa, and 5.3% of daily mortality worldwide (Schneider *et al*., 2007; Probst *et al*., 2018). In 2015, reports indicated that alcohol abuse claimed about 62 300 adult lives in South Africa, 60% of which are from lower

socioeconomic status households (Probst *et al*., 2018). This highlights the severity and prevalence of alcoholism, especially on individuals from middle to low-socioeconomic status countries.

Additionally, alcohol-induced dysregulation of antioxidant and oxidant systems (Liang *et al*., 2012) in the lungs is associated with downregulation of granulocyte-macrophage colony stimulating factor (GM-CSF) receptors in dust cells and consequently implicated in impaired alveoli inflammatory response (Joshi *et al*., 2005). Moreover, a study on United States adult population associated moderate alcohol consumption with decreased likelihood of C-reactive protein (CRP) elevation (Stewart *et al*., 2002). Additionally, an in vivo study by the American Association of Immunologists highlighted CRP as an inflammatory promoter through activation of phagocytic cells such as human macrophages (Newling *et al*., 2019). Further, CRP has been shown to promote lung metastases in mice through inhibition of pulmonary macrophage and, consequently impairing immune surveillance (Feng *et al*., 2024), highlighting the significant role played by CRP in lung macrophage functioning. However, alcohol combinatorial impact with other factors such as cART and diabetes on the respiratory immune response of HIV naïve individuals or models has not been fully elucidated.

2.3. Alcohol and cART as Risk Factors for Type 2 Diabetes.

Alcohol is associated with diabetes induction through its metabolism by reducing insulin effectiveness, as such, pancreatic beta cells respond to this malfunction by increasing insulin secretion (Kim and Kim, 2012). However, high blood insulin concentrations with continued heavy alcohol intake results in decreased insulin efficacy, leading to induction of insulin resistance and prediabetic state (Steiner *et al*., 2015). Prediabetes. also termed glucose intolerance, manifests through low insulin-dependent glucose cell intake within the hepatic, adipose, and muscle tissues (Rahman *et al*., 2021). Therefore, alcohol use is one of the major contributors to compromised glucose tolerance and consequently T2DM induction (Lam *et al*., 2021).

Studies have shown that alcohol use exacerbates glucose metabolism in diabetic rats compared to non-diabetic rats, further underlining the harmful effects of alcohol abuse in diabetics (Jung *et al*., 2011; Kim and Kim, 2012). Moreover, alcohol consumption is reported to induce a five-fold increase in transforming growth factor (TGFβ1) synthesis in alveolar epithelium associated with alveolar epithelial damage during inflammatory response (Guidot and Hart, 2005). However, the respiratory effect of alcohol in a diabetic state is lacking in literature. Similarly,

the popularized use of cART has gained attention concerning the association between antiretroviral drugs and diabetes induction. A retrospective analysis of chronic cART treatment on plasma glucose concentrations in HIV patients associated Tenofovir with hyperglycemia and pancreatitis (García-Benayas *et al*., 2006) and consequently increased chances of T2DM occurrence. Additionally, other cART components, such as protease inhibitors (PIs), are implicated in direct induction of insulin resistance and interference with glucose transporter (Arafath *et al*., 2018), which may eventually cause prediabetes. Furthermore, glucose dysregulation, oxidative DNA damage and insulin resistance are reported to be more prevalent in individuals on cART regimen compared to cART-naïve patients (Jantarapakde *et al*., 2014; Tangvarasittichai, 2015; Honnapurmath and Patil, 2017).

In addition to contributing to T2DM induction, cART treatment is reported to downregulate systemic GPx in HIV-infected individuals (Sharma, 2014), an antioxidant agent involved in respiratory epithelial protection against oxidative stress-induced damage through glutathione (GSH) activation (Schamberger *et al*., 2016). Therefore, the development of T2DM diabetes may stem from lifestyle factors such as alcohol abuse and cART therapy amongst others. Considering this scenario, the use of these drugs in a diabetic condition demands evaluation and documentation of possible adverse effects relative to the respiratory system.

2.4. The Global Diabetes Epidemic: Causes and Consequences.

Diabetes is characterized by elevated blood glucose levels resulting from malfunctioning of insulin action, or insulin secretion, or both (American Diabetes Association, 2010). The battle against diabetes mellitus is one of the longest battles that humanity has fought and is still fighting. Alcoholism, metabolic syndrome, sedentary lifestyle, genetics, and chronic drug therapies such as antiretroviral drugs are few of the factors fueling diabetes induction and progression (Malecki, 2005; Wu *et al*., 2014). In the year 2000, the International Diabetes Federation (IDF) and WHO estimated the number of diabetic individuals globally between 151 and 171 million (Zimmet, 2017). In 2024, about 830 million individuals were considered diabetic, with attendant effects on the quality of life, especially in developing countries (WHO, 2024; Diabetes). The impact of diabetes on cognitive, cardiovascular, and endocrine health has received attention, which has also gained momentum on respiratory health following the COVID-19 global pandemic. In post-mortem studies, thickening of the pulmonary capillary and epithelial basal laminas was reported in T2DM compared to unaffected controls of similar age (Pitocco *et al*., 2012). Further, the thickened pulmonary basal laminas are associated with

increased collagen fibres within the lung parenchyma, which may reduce lung elastic recoil in diabetic patients (Zhang *et al.*, 2024b). As such, the collative effects of diabetes on respiratory health require attention relative to other chemotherapeutic factors such as alcohol and cART use. The outcomes of this study will therefore be invaluable for documentation of adverse effects of this complex combination of diabetes, cART, and alcohol, especially in the respiratory-pulmonary system (Respiro-pulmonary system).

2.5. Overview of the Respiratory System Structure and Function.

The respiratory system is a complex arrangement of organs and tissues that transport exogenous air from the nasal and oral cavities to the alveoli for gaseous exchange (Wagner, 2015). Fractionated into two components: Upper respiratory tract, which ranges from nasal cavity to terminal bronchioles, and lower respiratory tract, which ranges from respiratory bronchioles to alveoli (Fig. 2.3) (Wagner, 2015).

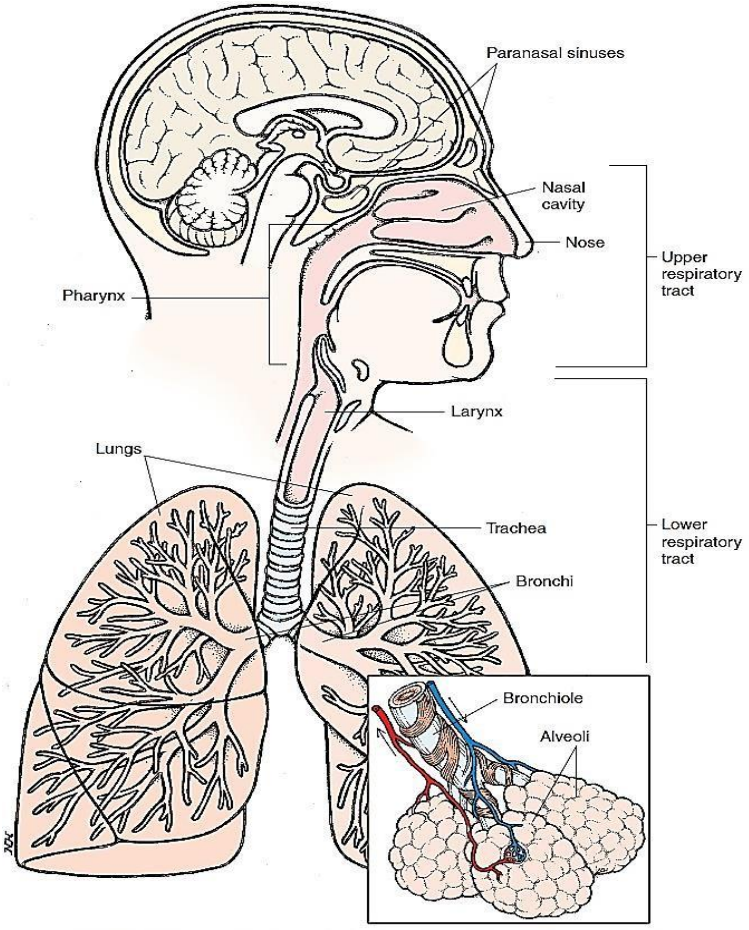

Figure 2.3: Overview of the Respiratory System Structure.
Overview of the upper and lower respiratory tract. (Overview of the Respiratory System Structure)

2.5.1. Comparative Gross Anatomy of Human and Rodent Lungs.

In contrast to the human lung, which is composed of three right lobes (Upper, middle, and lower lobes) and two left upper and lower lobes (Patwa and Shah, 2015). The rodent lung is composed of a solitary left lobe and four lobes in the right lung, upper, middle, caudate, and lower lobes (cranial to caudal) as illustrated in Figure 2.4 (Sato *et al*., 2015; Zhang *et al*., 2024a). However, both mammals maintain similar respiratory systems, a trachea that bifurcates into the respiratory tree, on the medial side of the lung is a hilum which accommodates the entry of pulmonary vasculature and lymphatics, main bronchi, bronchial vessels, and phrenic nerve (Chaudhry *et al*., 2024).

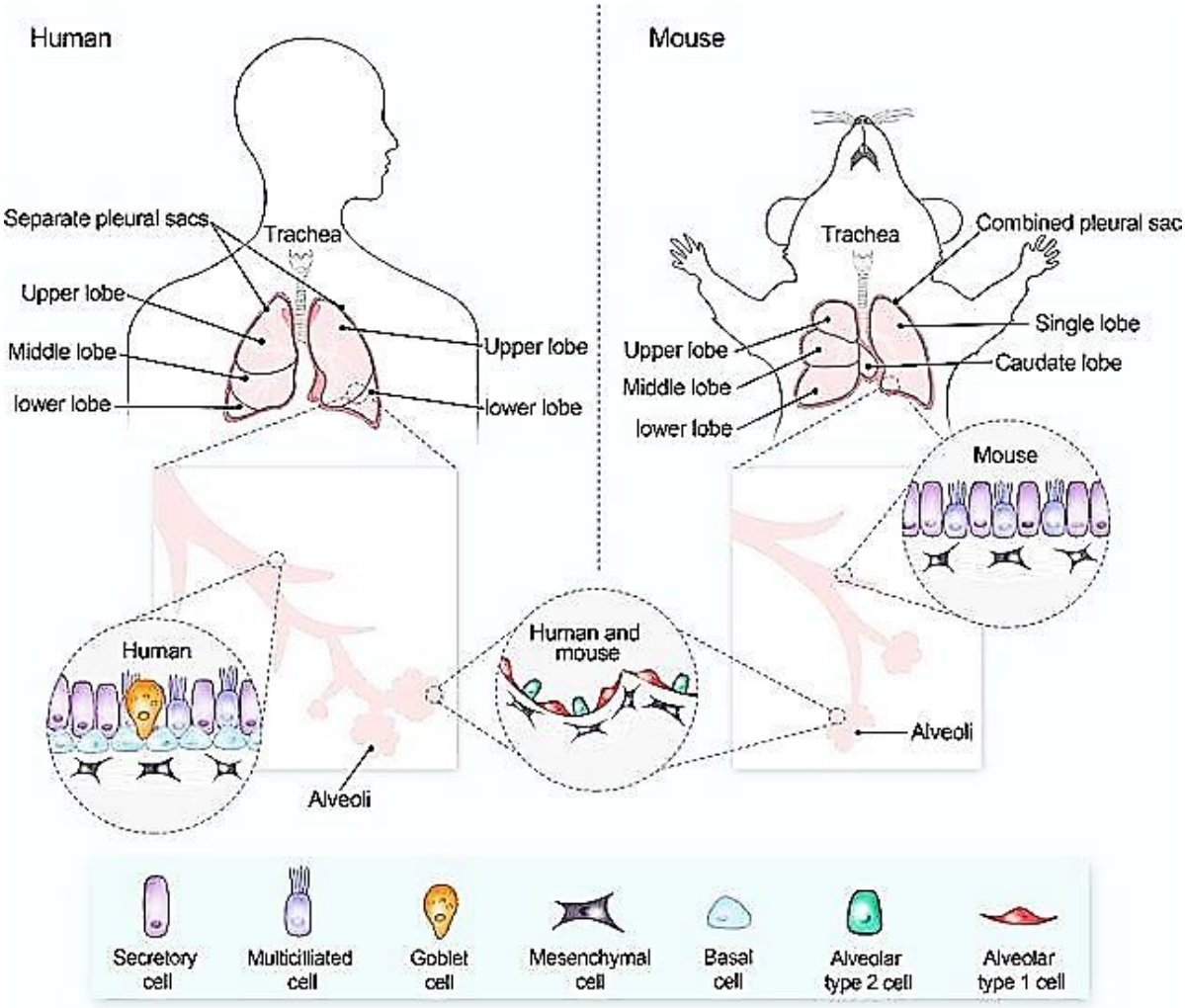

Figure 2.4: Comparative Gross Anatomy of Human and Rodent Lungs.
Similarities and differences in human and rodent lungs (Zhang *et al*., 2024a)

2.5.2. Microanatomy and Function of the Lung.

The epithelial lining of the respiratory tree ranges from ciliated pseudostratified columnar epithelium with the goblet, serous and mucous cells (trachea and bronchi), ciliated simple low cuboidal epithelium (bronchioles and respiratory bronchioles) to simple squamous epithelium (alveolar ducts and alveoli) (Fig. 2.5) (Zhang *et al*., 2024a) with the primary role of protection against inhaled xenobiotic materials. The bronchioles consist of a muscularis mucosa, which separates the mucosa and submucosa and consists of a smooth muscle layer that aids in contraction and relaxation of the lumen. Additionally, clusters of collagen and elastic fibres and smooth muscle cells surround alveolar ducts and sacs and facilitate the elasticity demand during breathing. While reticular fibres in the alveolar septa provide support for the septa and regulation of capillary distention at the blood-air barrier (Suki and Bates, 2008; Bara *et al*., 2010).

The blood-air barrier, comprised of type I pneumocytes, which allow for gaseous exchange, and type II pneumocytes, which are classified as simple cuboidal epithelium and synthesize pulmonary surfactants to ease the surface tension of the lumen (Cerrada *et al*., 2015). The surfactants contribute to the breakdown of xenobiotic material trapped by the epithelial fluid of the respiratory lining (Harkema *et al*., 2013). Alcohol, cART, and diabetes independently affect these basic pulmonary structures and associated functions (Lieber, 2004; Wang *et al*., 2009). Therefore, it is essential to gain histopathological insight regarding the combinatorial impact of these factors on the lungs.

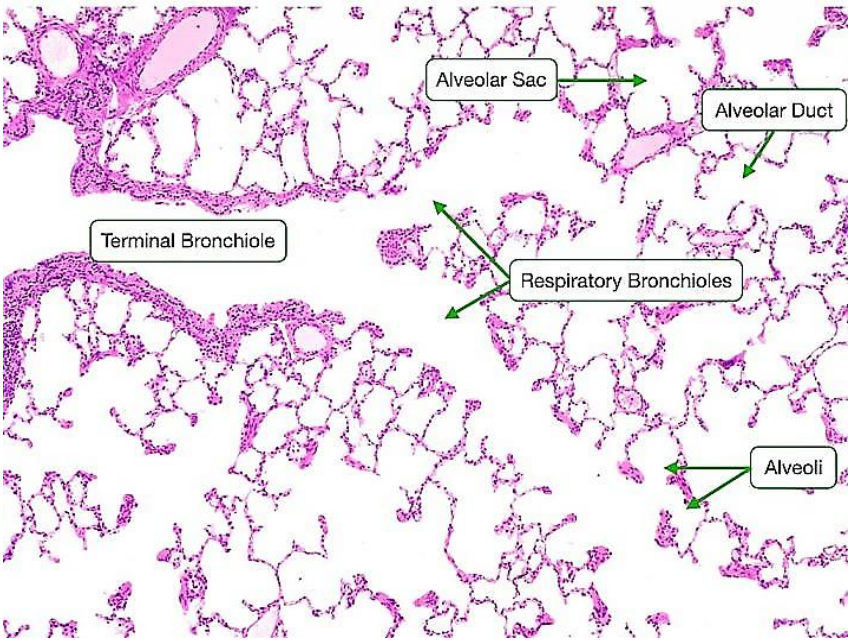

Figure 2.5: Overview of the respiratory tree histology.

Histological overview of the terminal and respiratory bronchioles and alveoli. (Overview of the respiratory tree histology)

2.6. Independent Respiratory Effects of Diabetes, Alcohol, and cART.

Alcohol, cART, and diabetes are independently associated with chronic health issues such as hypertension, hyperglycemia and liver toxicity with associated complications that may be overlooked by the public and clinicians (Simet and Sisson, 2015). These factors are independently associated with oxidative stress, fibrotic processes, inflammatory response, thrombotic and vasculature perturbations (Talakatta *et al*., 2018; Thapa and Shrestha, 2022), which may lead to respiratory system compromise.

2.6.1. Oxidative Stress Induced by Diabetes, Alcohol, and cART.

Studies have demonstrated that in addition to the liver as a major site for alcohol metabolism, the lungs also metabolize alcohol dependent on the amount ingested (Qin and Meng, 2006). During long-term alcohol abuse, alcohol metabolism is undertaken particularly by antioxidant enzymes which are implicated in redox imbalance within the lungs (Lieber, 2004). These antioxidant enzymes are expressed ambiguously within the lungs by Clara cells, alveolar macrophages, bronchial and bronchiolar epithelium and pneumocytes II (Hukkanen *et al*., 2002). Alcohol oxidation in the lungs has been shown to generate oxidative radicals that can cause lipid peroxidation and produce malondialdehyde (MDA) (Kaphalia and Calhoun, 2013) and induce pro-inflammatory response in bronchial epithelium (Wyatt *et al*., 2012; Kaphalia and Calhoun, 2013). Alcohol-induced redox imbalance is also reported to increase serum glutathione disulfide (GSSG) and depletion of GSH in type II pneumocytes and alveolar macrophages of alcohol abusers and alcohol-fed mice respectively (Liang *et al*., 2012).

Additionally, cART is independently associated with elevated oxidative stress through inhibition of antioxidant agents including GPx1 and superoxide dismutase (SOD) in HIV patients in contrast to healthy controls (Hurwitz *et al*., 2004; Sharma, 2014). Also, another study reported increased serum oxidative stress markers (elevated MDA and decreased GSH) in cART-treated HIV-positive individuals compared to pre-cART and healthy uninfected controls (Ivanov *et al*., 2016). However, reports on cART effects on oxidative stress specific to the respiratory system are lacking in literature, necessitating this study especially in HIV-naïve diabetic incidences.

Furthermore, high glucose levels in T2DM have been shown to induce redox imbalance through

lipid peroxidation which is associated with aggressive macrophage infiltration and consequently chronic inflammation, creating a positive feedback loop between chronic inflammation and redox imbalance (Oguntibeju, 2019). Other reports demonstrate increased pulmonary lipid peroxidation detected by MDA levels through thiobarbituric acid reactive substance (TBARS) and diminished SOD activity in erythrocytes and lung parenchyma of diabetic rats (Forgiarini *et al*., 2009; Hamden *et al*., 2009). Moreover, the oxidative stress induced by diabetic-hyperglycemia, alcohol metabolism, and cART consequently upregulates myofibroblast-induced collagen synthesis, which may elicit fibrosis (Lieber, 2004). However, there is dearth of information on the impact of diabetic-cART-alcohol interaction on these parameters on pulmonary system in HIV-naïve rats.

2.6.2. Mechanisms and Implications of Pulmonary Fibrosis.

Hyperglycemia in diabetes and alcohol-induced oxidative stress have been shown to induce pulmonary fibrosis through TGF-β1-induced epithelial to mesenchymal transition (EMT) (Pohlers *et al*., 2009; Sueblinvong *et al*., 2014). Particularly, EMT gives rise to highly proliferative fibroblast-like mesenchymal cells which deposit excess extracellular matrix (ECM) structures, resulting in high cell and collagen density as well as reduced alveoli density (Pohlers *et al*., 2009). Also, diabetes is reported to induce pulmonary fibrosis through redox imbalance (Talakatta *et al*., 2018). Both hyperinsulmenia and hyperglycemia are reported to downregulate antioxidant molecules in the lungs, which may allow for aggressive inflammatory processes which can cause vascular injury (Jagadapillai *et al*., 2016). As a response to vascular injury and inflammation, a redox imbalance-inflammation positive feedback loop is initiated and activates unregulated wound healing processes resulting in pulmonary fibrosis (Savin *et al*., 2022).

Additionally, studies have reported collagen fibre deposition within the lungs during pulmonary fibrosis to be associated with perturbation in gross morphology such as increased lung size in length and width (Fig. 2.6) (Birbrair *et al*., 2014). Another study associated lung fibrosis with bosselated or cobblestone appearance on the pleural surface and enlarged airspaces with fibrotic retraction of mid-lobe on a cut section (Wolters *et al*., 2014). Therefore, gross morphology measurements and examination of the lung could provide supporting structural evidence for fibrosis as previously reported (Birbrair *et al*., 2014). Since both alcohol and diabetes are implicated in lung fibrosis, and attendant reduced access of deoxygenated blood to ventilated alveoli (Wheatley *et al*., 2011; Pitocco *et al*., 2012), it is vital to document their combinatorial effects.

On the other hand, despite reduced mortality and improved lifespan in HIV-positive individuals on cART, pulmonary complications are still largely high including lung fibrosis (Fitzpatrick *et al*., 2018). Some studies suggest that cART exerts an insignificant influence against chronic HIV- related lung illnesses, implicating HIV residual replication, proximity to airborne toxicants and poor penetration of cART in lung deep tissues and persistent inflammation (Martinez-Picado and Deeks, 2016; Marsh Sung and Margolis *et al*., 2018; Alexandrova *et al*., 2022). Furthermore, other factors such as aggressive inflammation have been shown to lead to highly progressive fibrosis in mice lungs (Wynn and Ramalingam, 2012).

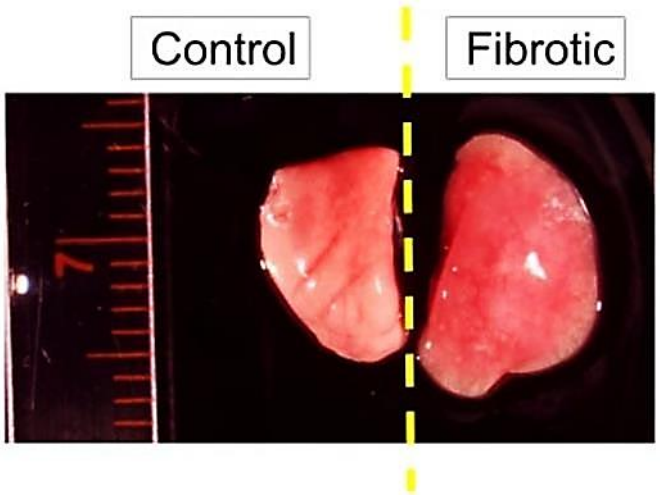

Figure 2.6: Pulmonary fibrosis-induced organ size increase.

Mice fibrotic lung tissue (right) exhibits an increase in size (surface area) (Birbrair *et al*., 2014).

2.6.3. Inflammatory Responses Associated with Diabetes, Alcohol, and cART.

Subclinical chronic inflammation has been reported as a foundation for T2DM pathology, and its mechanism of induction is associated with excess body weight through adipose-induced CRP upregulation (Kanmani *et al*., 2019; Stanimirovic *et al*., 2022). Further, other factors associated with T2DM development such as high blood glucose levels, insulin resistance and obesity are linked with increased CRP levels (Festa *et al*., 2002; Obradovic *et al*., 2015). The liver is known as the primary site for CRP gene activity (Boras *et al*., 2014). However, CRP expression is reported in extrahepatic sites such as lung epithelium and parenchyma as well as alveolar macrophages (López-Campos *et al*., 2013; Feng *et al*; 2024). While effects of diabetes on lung CRP expression are lacking in literature, diabetes is linked with elevated levels of CRP in other tissues (Khateeb *et al*., 2019; Dungu *et al*., 2023).

Moreover, elevated CRP levels are associated with impaired lung health as demonstrated by low forced expiratory volume (FEV_1) and forced vital capacity (FVC) (Zhang *et al*., 2020). Reduced FEV_1 and FVC are also reported in T2DM, which indicates a restrictive pattern of lung dysfunction associated with reduced elastic capacity and lung volume (Agarwal *et al*., 2021). Diabetes is also associated with elevated levels of GM-CSF, a pro-inflammatory agent known for its activation of phagocytic capacity in alveolar macrophages (Slovinsky *et al*., 2019; McCormick *et al*., 2022). Further, elevated serum GM-CSF levels are reported in T2DM patients and adult rodent studies, indicating hypersensitive pathogen detection and phagocytosis (Foster *et al*., 2010); Surendar *et al*., 2011; Knoop *et al*., 2018). Such diabetes-induced aggressive immune response is associated with damaged alveolar epithelium (Forgiarini *et al*., 2009).

On the other hand, alcohol use is known to suppress inflammatory processes and response (Bektas *et al*., 2016). Moreover, oxidative stress in chronic alcohol use is reported to downregulate pulmonary pro-inflammatory proteins (Brown *et al*., 2004; Joshi and Guidot, 2007). The alcohol disruption of inflammatory response extends to reduction in phagocytic capacity of alveolar macrophages and consequently deposit of debris in the alveolar spaces which may impede gaseous exchange processes (Alvarado and Arce, 2016 Kaphalia *et al*., 2019; Slovinsky *et al*., 2019). Further, moderate alcohol use is associated with low likelihood of CRP overexpression in drinking adult population (Stewart *et al*., 2002). Also, lowest baseline CRP concentration has been linked to both moderate and heavy drinking compared to non-drinkers (Albert *et al*., 2003; Sexton, 2003).

Furthermore, cART is implicated with a significant decrease of alveolar macrophage activation and downregulated expression of pro-inflammatory factors in alveolar epithelial milieu of HIV patients (Twigg and Knox, 2013). In HIV positive individuals, cART is reported to ease systemic inflammation, however, inflammatory markers such as CRP remain high compared to healthy individuals (Sereti *et al*., 2017). This elevation of CRP is associated with persistent inflammation that may increase the chances of other respiratory health complications occurring (Sereti *et al*., 2017). Contrary to alcohol effects, cART is shown to induce elevated baseline levels of CRP in cART-treated individuals with HIV, and this has been linked with high bacterial pneumonia occurrence (Bjerk *et al*., 2013). Studies show that in response to cART regime, HIV leans towards the lung mucosa as a reservoir which sets up HIV-infected individuals on cART for a lifelong inflammatory pathology of the respiratory system (Triplette *et al*., 2018; Alexandrova *et al*., 2022). As such, the documentation of alcohol and cART effects

on respiratory CRP expression and lung histomorphology in a diabetic condition will be clinically important.

2.6.4. Thrombosis and Vascular Disruption in Pulmonary Health.

Diabetes is reported as a key contributor for thrombosis-induced cardiovascular pathology, constituting over half of diabetes mortality (Pignone *et al*., 2010; Ferreiro & Angiolillo, 2011; Xiang *et al*., 2015). Research shows that diabetes downregulates pulmonary endothelial nitric oxide synthase (eNOS) which results in endothelial dysfunction (Mzimela *et al*, 2024). This dysfunction further exacerbates the prothrombotic environment through upregulated thrombogenic factors and downregulation of anti-thrombotic factors such as NO (Mzimela *et al*, 2024). Both diabetes-induced oxidative stress and systemic inflammation are reported to induce vascular injury and pulmonary fibrosis through platelet-endothelial interaction and low NO levels (Jagadapillai *et al*., 2016). Further, diabetes-induced redox imbalance is suggested to disrupt endothelium-mediated vasodilation in pulmonary arteries of STZ-induced diabetic male SD rats (Lopez-Lopez *et al*., 2008), which may contribute to narrowing of the arteries and consequently increased inflammatory responses.

Parallel to diabetes, alcohol is shown to induce hypercoagulability through endothelial dysfunction, associated with thrombosis (Shen *et al*., 2017). Also, high alcohol intake is reported to downregulate NO production and induce endothelial apoptosis, arresting pulmonary vascular cell proliferation through persisting apoptosis pattern (Liu *et al*., 2002; Kuhlmann *et al*., 2004; Silva *et al*., 2021). Another study showed that chronic alcohol use affects blood-air barrier qualities including permeability implicated in disturbances of gaseous exchange and consequently respiratory failure (Burnham *et al*., 2009).

Just as diabetes and alcohol are associated with endothelial dysfunction through oxidative stress, cART is similarly reported to induce oxidative stress in both human and porcine pulmonary artery endothelial cells which may be associated with high occurrence of pulmonary arterial hypertension (Wang *et al*., 2009). As reported in HIV patients, cART use is implicated in pulmonary immune reconstruction inflammatory syndrome (IRIS)-associated narrowing of bronchial and alveolar blood vessels in contrast to healthy controls (Shelburne *et al*., 2002). On the other hand, alcohol abuse is associated with the induction of pronounced stromal proliferation of bronchial and alveolar vasculature in male mice that later developed emphysema and alveolar hyperplasia (Balansky *et al*., 2016). Similarly, diabetes is associated with vascular perturbations such as narrowing of pulmonary vessels (Takahashi *et al*., 2018)

and alveolar capillaries (Pechlivani and Ajjan, 2018).

However, it is not known how cART will influence pulmonary vasculature in HIV-naïve individuals especially in the light of alcohol use and in diabetes. Though these independent effects of diabetes, alcohol and cART perturbations exist in the lungs (Fig. 2.7), this study proposes to investigate their combined effects relative to pulmonary fibrosis, thrombosis, oxidative stress, inflammation and histomorphology of the respiratory tract and vasculature.

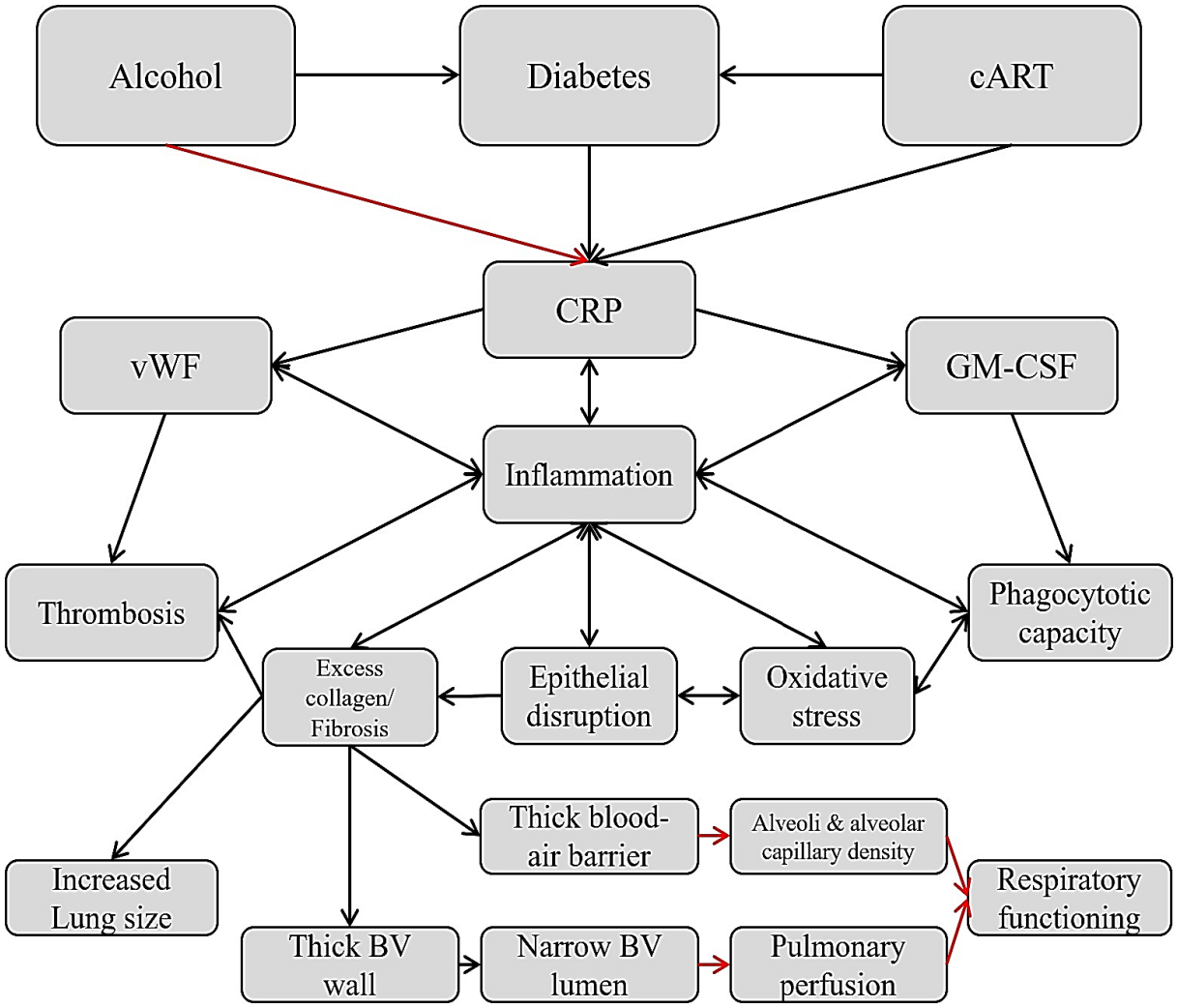

Figure 2.7: A flow diagram illustrating the interactions between alcohol, diabetes and cART and their respective effects.

Single arrow: Induction, double arrow: Positive feedback loop and red arrow: Inhibition. cART: Combination antiretroviral therapy, GM-CSF: Granulocyte-macrophage colony- stimulating factor, vWF: Von Willebrand factor, and BV: Blood vessel.

2.7. Choice Of Experimental Model and Treatment.

This study is designed to evaluate the in vivo combinatorial impact of diabetes, alcohol, and cART on the lungs, as such, an animal model is required. The SD rat is an ideal animal model for imitation of a human sub-chronic study (Bryda, 2013). Because of possible influence of female endocrine hormones and cycle on our diabetic model (Gambineri and Pelusi, 2019), a male SD rat with approximate body weight of 270- 320 grams was selected as an animal model for this study.

Atripla® and Dolutegravir (DTG)-based antiretroviral therapy drugs are the commonly used HIV treatments and preventative prophylaxes approved by the Food and Drug Administration (FDA) in 2006 and 2013 respectively (Stewart, 2021). However, DTG was discontinued due to high rate of adverse effects, especially neuropsychiatric adverse effects in patients with psychiatric disorders (Fernandez-Bargiela *et al*., 2022). Therefore, Atripla® was chosen as the treatment model for this study and administered at the direct extrapolated equivalent to human daily dose of 23.22 mg/Kg body weight.

CHAPTER THREE: Methods and Materials

3.1. Ethics.

This study is an extension of a larger study, ethical clearance for the original study and a subsequent modification and extension approval of the project were obtained from the Wits Research Animal Facility (WRAF) at the University of Witwatersrand, under the same ethics number: 2018/011/58/C.

3.2. Animal studies.

Adult male Sprague Dawley rats obtained from WRAF, aged approximately 10 weeks, were used in the original study. In the present study, preserved tissue samples from the original study were used.

3.2.1. Samples & Animal husbandry.

Tissue samples for this study were obtained from an already conducted larger study tissue bank to reduce both animal suffering and operational costs. The animals were bred and housed at the WRAF, University of Witwatersrand, within the temperature range of 21 ˚C and 23 ˚C with a light-dark cycle of 12 hours in a sterilized environment. Each animal was allowed free movement and kept in individual cages of dimensions 200 millimetres (mm) in height, 430 mm in length, and 220mm in width. Standard rodent diet and water were available *ad libitum* for the rats for the duration of the 90 days treatment.

3.2.2. Diabetes Induction.

To induce diabetes, the animals in the diabetic groups received a 20% fructose diet composed of mixed fructose (Nature's Choice) (Dischem pharmacies, Durban, South Africa) for 14 days. Further, the animals were given a once-off intraperitoneal administration of 40mg/kg body weight of Streptozotocin (STZ) in newly made 0.05 M of citrate buffer (pH 4.5) (Sigma, St. Louis, MO, United States of America) according to Asouzu-Johnson *et al*., (2023). At week 3 following the initiation of high-fructose feed, glucose levels of 250 mmol/L or more were considered diabetic following a random non-fasting blood glucose (RNFBG).

3.2.3. Fasting Blood Glucose.

Following diabetic state confirmation, routine biweekly fasting blood glucose (FBG) evaluations were done through tail vein prick following 12h fasting (8pm to 8 am or 20:00 to

08:00) using Accu-Chek meter and glucose strips. Additionally, biweekly RNFBG levels were evaluated during the evening hours using glucose strips through tail prick and the Accu-Chek meter, to ensure that diabetic condition was maintained in the animals over the span of the study. Furthermore, monthly oral glucose tolerance tests (OGTT) were additionally performed to monitor the diabetic condition (Furman, 2021). The animals were subjected to 12 hours of overnight fasting before a 2 g/kg body weight glucose solution oral administration and tail prick glucose measuring using glucose strips at 0 minutes, quarter-hour, half-hour and hourly interludes after glucose loading. (Abu-Abeeleh *et al*., 2010).

3.3. Chemicals and Reagents.

Malondialdehyde (MDA) Colorimetric Assay Kit (TBA Method) (E-BC-K025-M), Rat GPX1 (Glutathione Peroxidase 1) ELISA Kit (E-EL-R2491), Goat anti-rabbit 1Gg (H+L) Biotinylated (BA-1000), Vectastatin Elite ABC kit Peroxidase (Standard)(PK-6100), Sigma Bradford Reagent (Catalogue No. B6916), Hematoxylin & eosin stain, Gordon & Sweets' stain (Sodium nitrate, Potassium permanganate, Oxalic acid, Iron alum, Sodium thiosulfate), Modified pentachrome stain (Nitric acid, Toluidine blue, Picrosirius), Modified Verhoeff's stain (Ferric chloride, Iodine iodide, alcoholic hematoxylin), Periodic Acid Schiff's stain (Schiff's reagent), rabbit polyclonal anti-CRP antibody (AB227507).

3.4. Treatments and Termination.

3.4.1. Groups Treatments.

Forty animals were divided into two major groups: non-diabetic and diabetic. The non-diabetic animals were divided into four sub-groups. Group 1 (Negative Control: NC) which comprised of non-diabetic and untreated rats; group 2 (Alcohol: AL) treated with 10% (v/v) ethanol in drinking water as a recommended concentration for representation of lifestyle alcohol use in rodent models (Green & Grahame, 2008). Group 3 (cART: CA), received cART (Bristol-Myers Squibb & Gilead Sciences LLC, United States of America) administered at an extrapolated daily adult dose (23.22 mg /Kg body weight) and group 4 (cART and Alcohol: CAAL), treated with cART plus 10% ethanol in drinking water *ad libitum*.

The diabetic animals also included four sub-groups. Group 5 (Diabetes: DB) consisting of untreated diabetic animals and group 6 (cART and Diabetes: CADB); which are diabetic animals treated with cART. Group 7 (Diabetes and Alcohol: DBAL); which included diabetic animals treated with (v/v) 10% ethanol in drinking water and group 8, (cART, Alcohol and

Diabetes: CAALDB); diabetic animals treated with cART, and 10% (v/v) ethanol in drinking water.

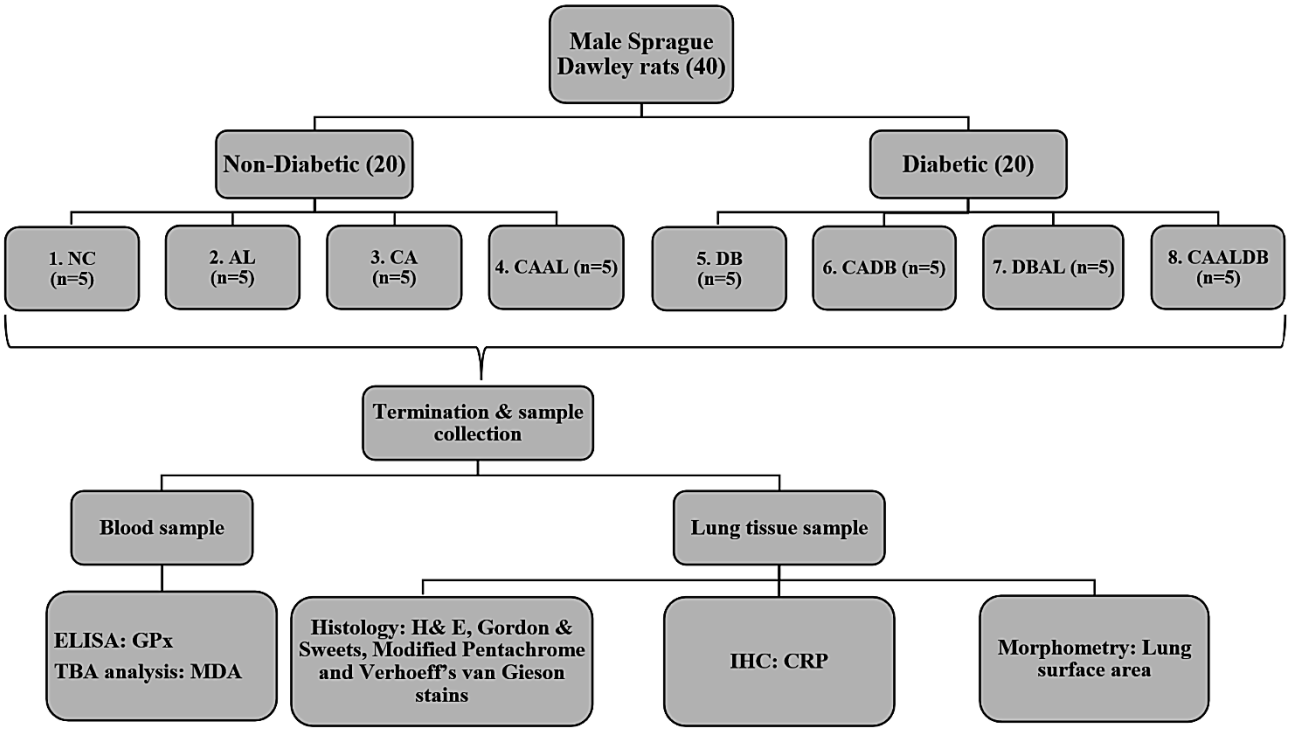

Figure 3.1: A flow diagram illustrating the treatments and techniques of the study.

Group acronyms: **1:** NC= Negative Control, **2:** AL= Alcohol, **3:** CA= cART, **4:** CAAL= cART and Alcohol, **5:** DB= Diabetes, **6:** CADB= cART and Diabetes, **7:** DBAL= Diabetes and Alcohol, **8:** CAALDB= cART, Alcohol and Diabetes.

3.4.2. Termination and Dissection.

At the end of the study (90 days), the animals were anesthetized with 9.1 mg/mL of Sodium pentobarbitone and terminated. Blood samples were collected using a 5 mL syringe and instantly transferred to 4 mL vials containing 7.2 mg ethylenediaminetetraacetic acid (EDTA) for serum preparation. Then the animals were perfused with 0.9% saline, and the lungs were fixed in 10% buffered formalin. The blood and tissue samples were stored for further analysis at -80 ℃ and room temperature, respectively.

3.5. Gross Morphological Analysis.

3.5.1. Body And Lungs Weights.

Prior to termination, the animals were weighed and recorded, and immediately after termination

the lungs were dissected out and weighed. A body-to-lung weight ratio was calculated to evaluate lung efficiency per body size.

3.5.2. Lung Morphology.

The surface area measurements of the right lung were performed using ImageJ software (free-hand tool) on both the ventral and dorsal surface areas as illustrated in Figure 3.2A-B. The morphological analysis of ventral and dorsal surfaces of the lungs was performed through the Nikon-Model C-DSS230 stereomicroscope with an Olympus EP50 camera and measurements were performed through the ImageJ using hand tool functionality. The right lobes were arranged in the anatomical position ventrally, with the top part of the inferior lobe resting on the bottom part of the middle lobe and the top part of the middle lobe resting on the bottom part of the superior lobe.

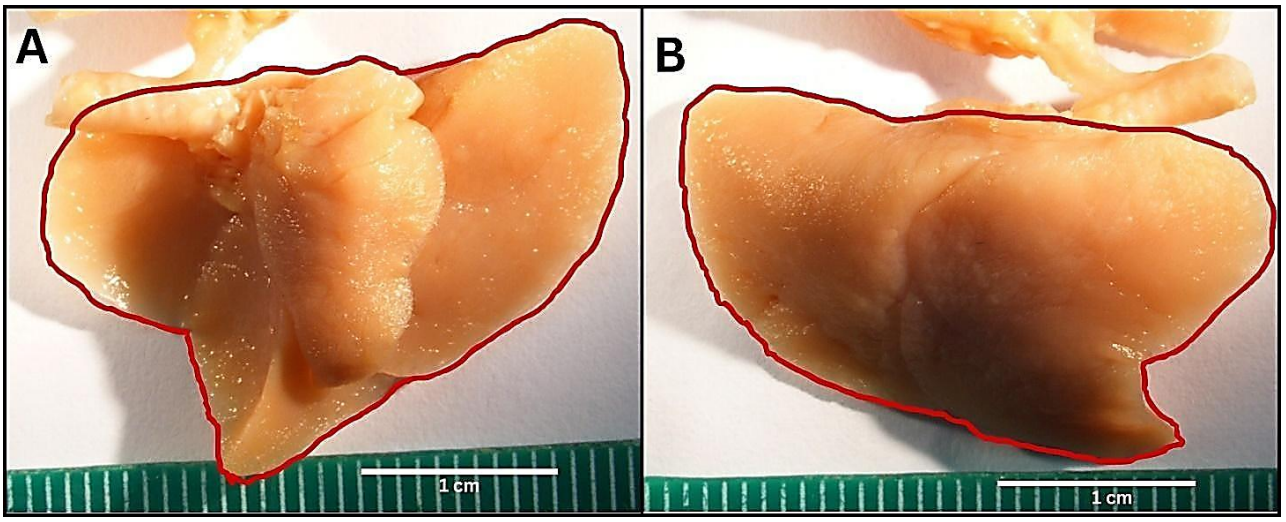

Figure 3.2: Illustration of ventral and dorsal surface area of lungs measurements.

Ventral (A) and dorsal (B) surface area measurements of the right lung (superior, middle, and inferior lobes). Red borderline: Indicate the area selected and measured on ImageJ software (free-hand tool).

3.6. Serum Biochemical Analysis.

3.6.1. Bradford Method For Protein Detection.

Collected blood samples were transferred to 4 mL vials containing 7.2 mg EDTA for serum preparation. For protein detection, serum samples were diluted with distilled water at 1:20 (sample: distilled water) and 5 µL of the diluted samples and standard solutions made up of

bovine serum albumin (BSA) were added to appropriate wells of 96 sterile well plates. Each well was filled with Bradford reagent (250 µL), followed by 30 seconds on a shaker then 10 minutes incubation at room temperature. The optical density (OD) was read at 595 within 30 minutes using Anthos 2010, Austria plate reader coupled to Anthos ADAP software revision 1.2 of the experiment. The total protein concentration calculated from the standard curve was expressed as µg/ml (Appx. 7.2.3).

3.6.2. Lipid Peroxidation Thiobarbituric Acid (TBA) assay (colorimetric) for Malondialdehyde (MDA).

Samples were diluted and mixed with stipulated amounts of reagents into Eppendorf tubes and incubated at 100 ℃ for 40 minutes according to the manufacturer's protocol (Appendix 7.2.1). Afterward, the tubes were cooled to room temperature and centrifuged for 10 minutes at 10,000 g. Then 0.25 mL of the supernatant was micro-pipetted from each tube into the control and sample microplates in duplicates respectively (Appx. 7.2.1). The OD was measured at 532 nm with a microplate reader. According to the manufacturer's recommendation, the OD values of the control and sample tubes in combination with the total protein concentration were used to calculate the concentration of MDA in each sample expressed in µmol/g protein as stipulated in Appendix. 7.2.3.

3.6.3. Glutathione Peroxidase (GPx1) detection (ELISA).

Each serum sample and standard were diluted in the provided sample and standard diluent, respectively and pipetted into respective wells in duplicates. The samples were then incubated at 37 ℃ for 90 minutes. Subsequently, Biotinylated Detection Ab working solution was added to each well and incubated at 37 ℃ for an hour. Followed by a triple wash in the provided buffer, soaking then aspiration. Provided HRP conjugated working solution was added to each well, sealed, and then incubated at 37 ℃ for 30 minutes followed by five times wash in the provided buffer, soaking then aspiration. Finally, the provided substrate reagent was added to each well, sealed, and incubated at 37 ℃ for 15 minutes under protection from light (Appx 7.2.2). Followed by a stop solution and optical density was determined at 450 nm. The concentration of GPx in each sample was expressed as µmol/ml as stipulated in Appendix. 7.2.3.

3.7. Tissue Processing and Sectioning.

The inferior lobe of the right lung tissue was placed in histology tissue caskets and routinely

processed with an automated tissue processor (Citadel 2000, Thermo Scientific) for 18 hours and embedded in paraffin wax. The tissues were sectioned with a rotatory microtome (Leica RM2125 RTS) in the transverse plane at 5 μm for IHC staining and 7 μm for routine staining. For routine staining, one of the four series of sections was made for H& E, Verhoeff's Van Gieson, modified Pentachrome, and Gordon & Sweets stains respectively, and mounted on 1% Gelatine-coated microscope slides.

3.8. Routine Staining.

3.8.1. Hematoxylin & Eosin Stain.

The first series of sections were dewaxed and hydrated, then stained for 10 minutes in Hematoxylin solution, washed with tap water, followed by rinsing in acid alcohol and treated in Scott's tap water for 5 minutes then washed with tap water. The sections were then stained with Eosin stain for 2 minutes and rinsed in tap water, dehydrated, and mounted. Solutions protocols are as stipulated in Appendix 7.3.1. This stain was used to conduct histomorphology analysis on tracheal and bronchiole epithelial heights, lacunae area, cartilage width, bronchial vein, and arterial wall heights measurements.

3.8.2. Modified Verhoeff's Stain.

After dewaxing and hydrating, the second series of sections were stained for 7 minutes in Verhoeff's solution at room temperature and rinsed in tap water. Followed by differentiation in 0.4% Ferric chloride and washed in tap water then hydrated and mounted. In these sections, elastic fibers and nuclei stain black to blue-black. Solutions protocols are as stipulated in Appendix 7.3.2. This stain was used to conduct histomorphology analysis on bronchial vein and parenchymal elastic fibers quantifications.

3.8.3. Modified Pentachrome Stain.

Following the dewaxing and hydrating, the third series of sections were pre-treated with 6% Nitric acid for 5 minutes. The sections were then stained in 0.5% Toludine blue solution for 5 minutes and washed in distilled water, followed with staining in Picrosirius solution for 5 minutes then washed in distilled water. Followed by alcohol series, then mounted. In these sections cytoplasm stains yellow, smooth muscle fibers stain yellow-orange, collagen fibers stain red, and sulphated polysaccharide concentration in tracheal cartilage stains violet. The preparation of the solutions is stipulated in Appendix 7.3.3. In this, histomorphology analysis

on muscularis mucosa width, bronchial vein and artery tunica media heights, bronchial vein tunica adventitia height measurements and bronchial vein and parenchymal collagen fibers quantifications were carried out and recorded.

3.8.4. Gordon & Sweets' Stain.

Following dewaxing and hydrating, the fourth series of sections were treated with 1% potassium permanganate solution for 5 minutes and rinsed in tap water then bleached in 1% oxalic acid solution. The sections were then treated with 2.5% iron alum solution for 18 minutes and washed in several changes of distilled water. Afterward, the sections were stained with silver solution for 2 minutes and washed in several changes of distilled water, then reduced in 10% aqueous formalin solution for 2 mins and rinsed in tap water. The sections were then treated with 5% sodium thiosulfate and rinsed in tap water, then dehydrated and mounted. The preparation of the solutions is illustrated in Appendix 7.3.4. The Gordon & Sweets stain sections were used to conduct histomorphology analysis on bronchiole mucosal and parenchymal reticular fibers quantifications.

3.9. Histomorphometry.

The Leica DM750 microscope coupled to a Leica ICC50w camera was used to capture images of routine-stained slides using the LAS EZ software at the magnification of 40x, further, measurements were performed through Image J software.

3.9.1. Histological Analysis.

3.9.1.1. Tracheal Epithelial Height, Cartilage Width, and Lacunae Size.

Measurements of the tracheal epithelial height, cartilage width, and lacunae area were made in each H&E-stained field of view as illustrated in Figure 3.3. A total of 360 measurements for the epithelial height were performed from 120 fields of view (photomicrograph). For each field of view, three measurements of epithelial height were taken at three different regions of the epithelium, and a mean was calculated. The epithelial height was measured from the basement membrane to the apical end below the cilia (double-ended arrow, Fig. 3.3). For cartilage width, a total of 200 measurements were performed from 40 fields of view, five measurements were taken at 5 regions of the cartilage, and a mean was calculated. The cartilage width was measured from both ends of the perichondrium (double-ended broken arrow, Fig. 3.3). A total of 200 lacunae area measurements were performed from 40 fields of view, 5 lacunae were measured

by tracing the edge of the capsular matrix, and a mean was taken (circle, Fig. 3.3). The ImageJ line tool was used to measure both epithelial height and cartilage width and ImageJ freehand tool was used to measure lacunae area.

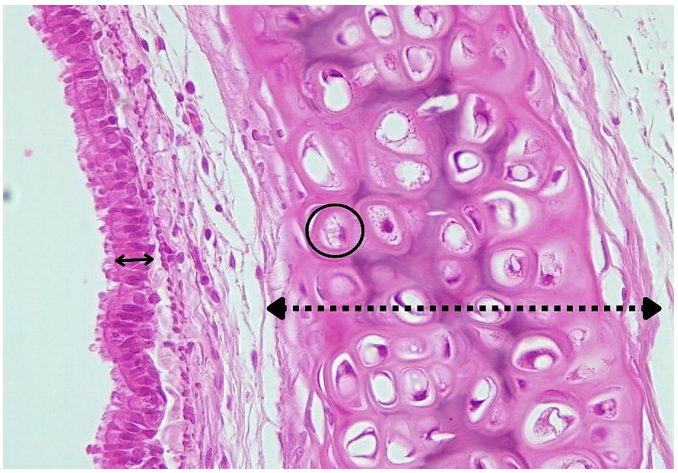

Figure 3.3: Illustration of the tracheal epithelial height, cartilage width, and lacunae area measurements. Epithelial height is illustrated by a double arrow, Cartilage width is illustrated by a dashed double arrow, and Lacunae area is illustrated by a circle stained with H&E.

3.9.1.2. Bronchiole Epithelial Height, Muscularis Mucosa Width and Mucosal Reticular Fibers.

Measurements of the bronchiole epithelial height, muscularis mucosa width and mucosal reticular fibers in H&E, modified Pentachrome and Gordon & Sweet stains respectively are illustrated in Figure 3.4A-C. A total of 360 measurements were performed from 120 fields of views for the epithelial height and muscularis mucosa width respectively (Fig. 3.4A-B). For both epithelial height and muscularis mucosa width, 3 measurements were taken at 3 different regions per field of view using the ImageJ line tool and a mean was taken. The epithelial height was measured from the basement membrane to the apical end below the cilia and the muscularis mucosa width was measured from end to end. For the mucosal reticular fibers, a total of 160 measurements were performed from a total of 20 fields of view per group. The ImageJ grid method was used to quantify the reticular fibers profile (arrows, Fig 3.4C) in the mucosa (double arrow, Fig 3.4) of the bronchiole.

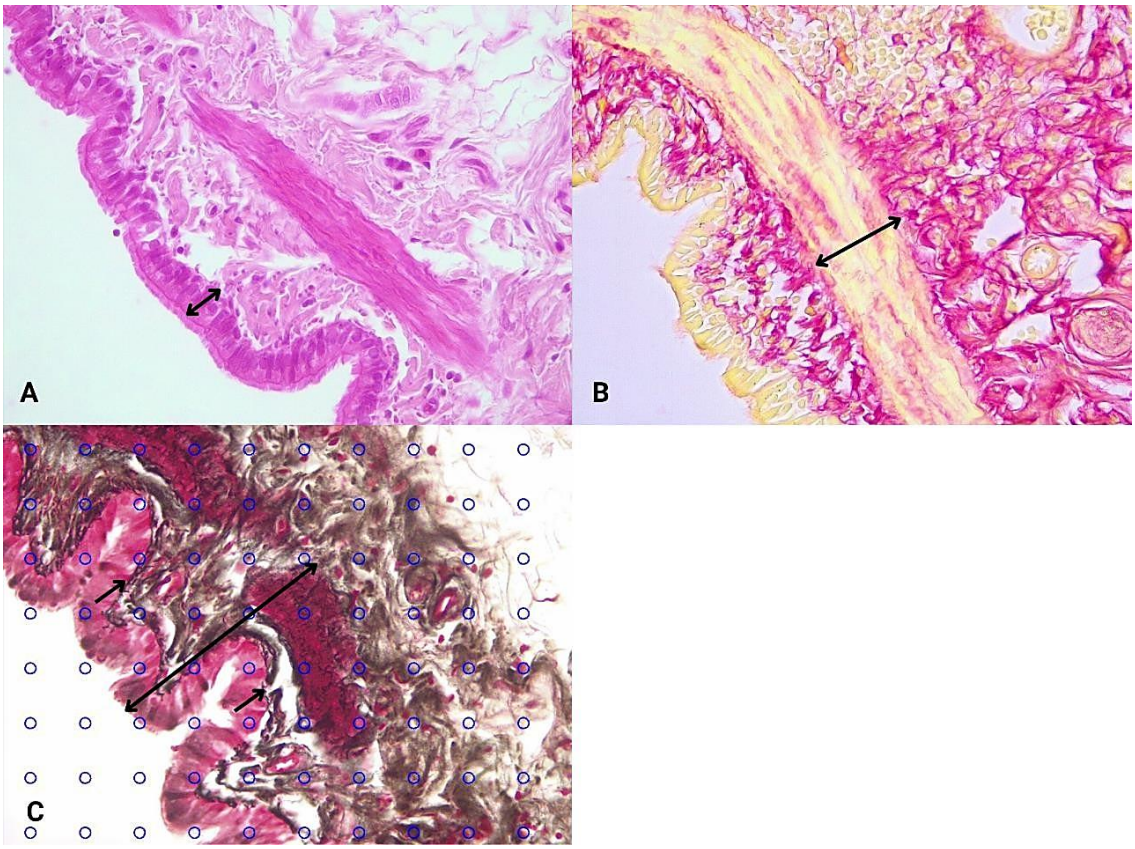

Figure 3.4: Illustration of the measurements of the bronchiole epithelial height, muscularis mucosa width and mucosal reticular fibers.

A: Epithelial height stained with H&E illustrated by double arrow. **B:** Muscularis mucosa width stained yellow with modified Pentachrome illustrated by double arrow. **C:** Reticular fibers stained black with Gordon & Sweet stain illustrated by single arrow.

3.9.1.3. Bronchial Arterial Wall and Tunica Media Heights.

Measurements of the bronchial artery wall and tunica media heights are presented in H &E and modified Pentachrome stains are as illustrated in Figure 3.4 A and B, respectively. A total of 360 measurements were performed from 120 fields of views for the bronchial artery wall and tunica media heights respectively using ImageJ line tool. The wall height was measured from the base of the tunica adventitia to the edge of the tunica intima(double arrow: 1-wall thickness, 2-tunica intima, 3-tunica media and 4-tunica adventitia, Fig. 3.4A), and tunica media was measured from the internal elastic lamina (single arrow, Fig 3.4B) to the junction with the tunica adventitia.

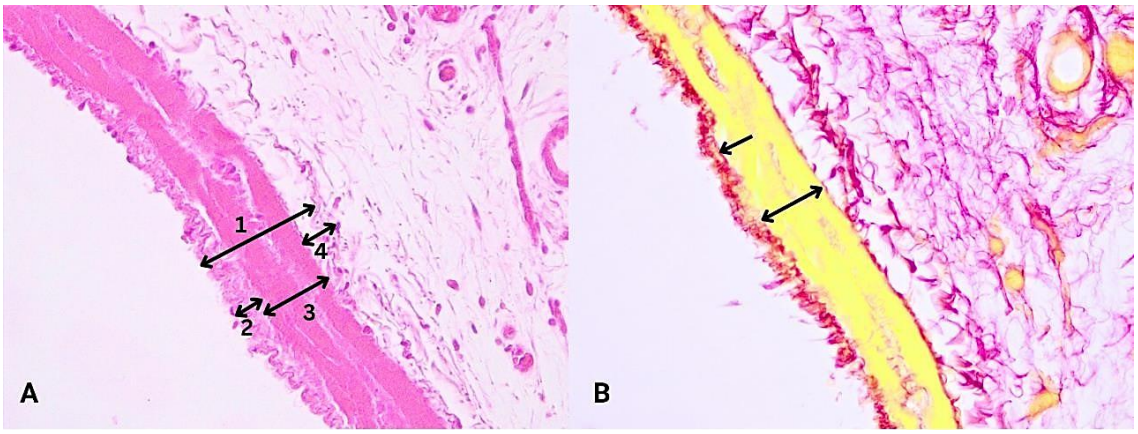

Figure 3.5: Illustrations of the bronchial arterial wall and tunica media heights measurements.

A: Bronchial arterial wall height stained with H&E illustrated by double arrow (1- total arterial wall thickness, 2- tunica intima thickness, 3- tunica media thickness, 4- tunica adventitia thickness). **B:** Bronchial artery tunica media height stained yellow with modified Pentachrome, illustrated by a double arrow.

3.9.1.4. Bronchial Vein Wall, Tunica Media, Tunica Adventitia Heights, Collagen, and Elastic Fibers Percentage Area Fraction.

Measurements of the venal wall, tunica media, and adventitia heights and the quantification of the collagen and elastic fibers are presented in Figure 3.6. A total of 360 measurements were performed from 120 fields of view for the bronchial vein wall, tunica media, and adventitia heights, respectively, using ImageJ line tool (Fig. 3.6A-B). To measure the venal wall, tunica media, and adventitia heights, 3 measurements were performed on different sites, and a mean was taken per field of view. The venal wall height was measured from the base of the tunica adventitia to the edge of the tunica intima. Tunica media was measured from the internal elastic lamina (single arrow) to the junction with the tunica adventitia and tunica adventitia was measured from the junction with tunica media and the junction with parenchyma.

A total of 160 quantifications were performed from 160 fields of view for the collagen and elastic fibers, respectively, and the ImageJ grid method was used to quantify the fibers respectively (Fig. 3.6C-D). To measure the percentage area occupied by collagen and elastic fibers, respectively, the number of circles intersecting with each type of fibre within the bronchial vein wall (double arrow) was counted and the percentage was calculated per field of view, respectively.

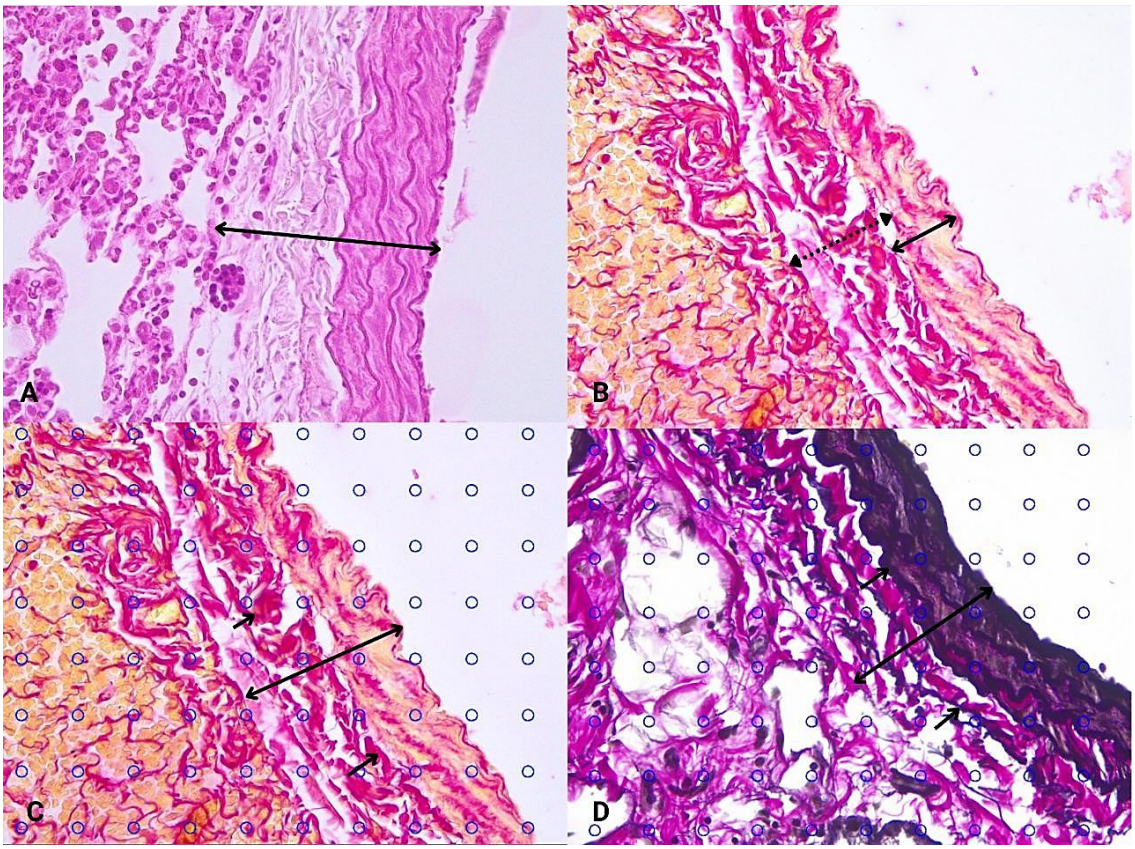

Figure 3.6: Illustration of the bronchial vein wall height, tunica media and adventitia heights measurements and collagen and elastic fibers quantification.

A: Venal wall height stained with H&E illustrated by double arrow. **B:** Tunica media (yellow) illustrated by double arrow and tunica adventitia illustrated by dashed double arrow stained with modified Pentachrome. **C:** Collagen fibers (red) stained with modified Pentachrome. **D:** Elastic fibers stained black with Verhoeff van Gieson stain.

3.9.1.5. Parenchymal Collagen, Elastic, and Reticular Fibers Percentage Area Fraction.

Quantifications for collagen, reticular, and elastic fibers were obtained from sections stained with Modified Pentachrome stain, Gordon and Sweets stain and Modified Verhoeff's van Gieson stains respectively are presented in Figure 3.7. For each type of fibers, collagen, elastic and reticular fibers, a total of 160 quantifications were performed from 160 fields of views. The ImageJ grid method tool was used to count the number of intersections/ small circles to calculate the percentage area fraction occupied the respective fibers.

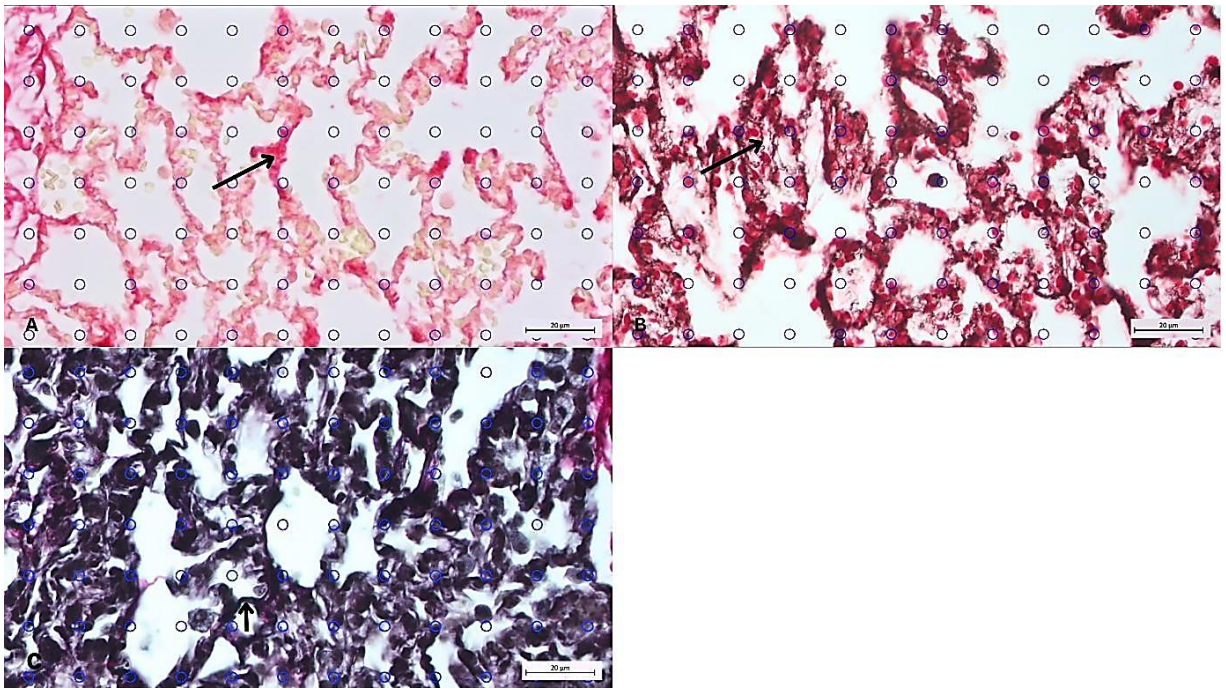

Figure 3.7: Illustration of parenchymal collagen, reticular and elastic fibers quantification.

Quantification of **A:** Collagen (stained red) with modified Pentachrome annotated with single arrow. **B:** Reticular (stained black) with Gordon & Sweets annotated with a single arrow. **C:** Elastic fibers stained black with Verhoeff's van Gieson annotated with single arrow.

3.10. Immunohistochemical (IHC) Staining.

For IHC analysis, 3 series of sections were made for C- reactive protein (CRP) then mounted on 3% Saline-coated microscope slides. Tissue sections were deparaffinized then incubated in citrate buffer (pH= 6) overnight at 60 ℃ water bath for antigen retrieval. The sections were then rinsed in PBS for 5 minutes, blocked in 3% hydrogen peroxidase and washed in PBS for x5 minutes. Then the sections were incubated in 5% normal goat serum for an hour at room temperature, the serum was tapped off the sections then incubated in appropriate primary antibodies overnight at 1: 250 in goat serum ratio for and CRP (AB227507) as shown in Table 3.1. The sections were washed in PBS and incubated with the secondary antibody (1:1000 in PBS) for 30 minutes, washed and incubated with ABC, washed, and incubated with DAB working solution then washed in running tap water. Subsequently, the sections were dehydrated in a series of alcohol (100%, 95% and 75%) and cleared in xylene then mounted.

3.10.1. C-Reactive Protein.

A total of 10 Fields of view per animal were captured for the respiratory (tracheal, bronchial,

and alveolar epithelium) from which areas immunolocalized CRP were analysed using the imageJ grey scale threshold tool. In total, 50 fields of view were analysed for CRP localization per group. The quantification of CRP was used as a marker of inflammation within the lung tissue (Gould and Weiser, 2001; Agassandian *et al*., 2014).

3.11. Statistical Analysis.

The statistical analysis was performed using Statistical Package for Social Science (SPSS) version 27.0 as follows; Normality test was performed with Shapiro-Wilk test where $p>0.05$ signified parametric data. Hypothesis testing for parametric data was performed with Independent-Samples T Test. For non-parametric data, hypothesis testing was performed with Independent Samples Kruskal-Wallis test with Bonferroni-correction. The significant level for both data types was considered at $p<0.05$ and a confidence level of 95%.

CHAPTER FOUR: Results

For better understanding of the effects induced by the treatments and their combinations, the results section has been divided into two themes,

- Theme 1: Describes antiretroviral and alcohol toxicity with/ without the diabetic condition.
- Theme 2: Describes diabetic condition and alcohol interaction.

4.1. ANTIRETROVIRAL TOXICITY.

The effect of antiretroviral therapy and alcohol with or without diabetic condition is analyzed for differential interactive toxicities induced by the therapy.

4.1.1. Fasting Blood Glucose.

The mean biweekly fasting blood glucose levels (FBG) are presented in Figure 4.1. At the end of week 2, the non-diabetic groups: NC, CA, and CAAL presented insignificant differences in average FBG of 4.83, 5.38, and 4.72 mmol/L, respectively (Fig. 4.1). Diabetic groups: CADB and CAALDB presented average FBG of 8.52 and 10.98 mmol/L, respectively at the 2nd and maintained this increase in the 12th week (Fig. 4.1). Group CADB showed a significant increase in FBG compared to NC, CA and CAAL in weeks 4 to 12 ($p < 0.05$ respectively). Group CAALDB showed a significant increase compared to NC and CA in weeks 2, 6, 8, and 10, whereas a significant decrease against CAAL was observed in weeks 6 to 12 ($p<0.05$, respectively) (Fig. 4.1).

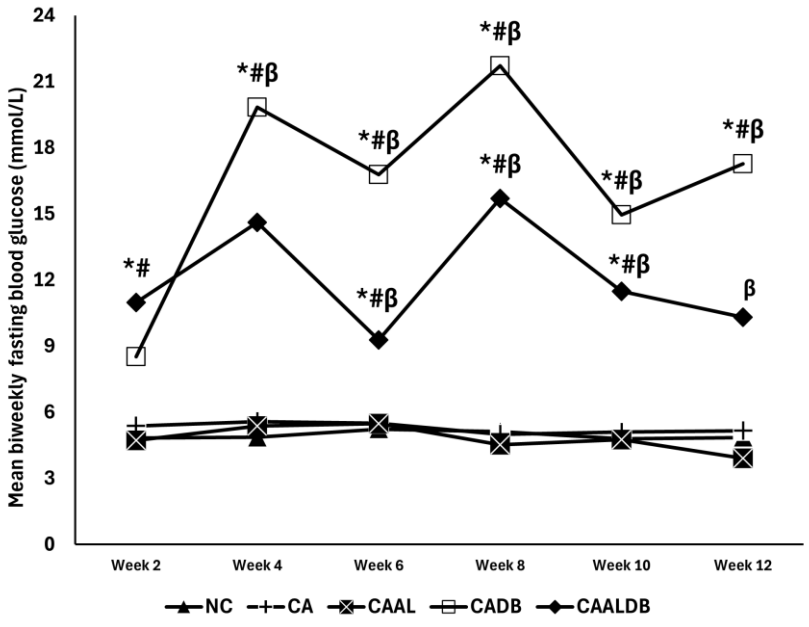

Figure 4.1: Mean Biweekly Fasting Blood Glucose Across Groups.

FBG; End of week 2: CAALDB showed significant increase compared to NC and CA (Independent-Samples T Test, p= 0.036 and 0.015, respectively). **End of week 4:** CADB was significantly increased against NC and CA (Independent-Samples T Test, p= 0.009 and 0.002, respectively). **End of week 6:** CADB showed significant increase compared to NC, CA, and CAAL (Independent-Samples T Test, p= 0.049, 0.018, and 0.018, respectively), and CAALDB showed significant increase compared to NC, CA, and CAAL (Independent-Samples T Test, p= 0.017, 0.005, and 0.005, respectively). **End of week 8:** CADB showed a significant increase against NC, CA, and CAAL (Independent-Samples T Test, p< 0.001 respectively), whereas CAALDB showed significant increase compared to NC, CA and CAAL (Independent-Samples T Test, p= 0.033, 0.032, and 0.027 respectively). **End of week 10:** CADB was significantly increased against NC, CA, and CAAL (Independent-Samples T Test, p= 0.033, 0.037, and 0.033, respectively) and CAALDB showed a significant increase against NC, CA and CAAL (Independent-Samples T Test, p= 0.002, respectively). **End of week 12:** CADB showed significant increase compared to NC, CA and CAAL (Independent-Samples T Test, p= 0.003, 0.003 and 0.002 respectively). CAALDB showed a significant decrease against CAAL (Independent-Samples T Test, p= 0.045). **'*'** indicates significant difference compared to NC, **'#'** against CA and 'β'against CAAL.

Key: NC= negative control; CA= cART; CAAL= cART and alcohol; CADB= cART and diabetes; CAALDB= cART, alcohol and diabetes.

4.1.2. Gross Morphological Analysis.

4.1.2.1. Mean Body, Lung and Relative Lung Weights.

The mean body and lung weights are illustrated as in Figure 4.2. The CA group showed a significant increase in body weight compared to the NC (Fig. 4.2A, p< 0.05), whereas groups CAAL, CADB, and CAALDB showed a significantly reduced body weight against NC and CA (Fig. 4.2A, p< 0.05, respectively). Moreover, CADB and CAALDB exhibited significantly reduced body weight against CAAL (Fig. 4.2A, p< 0.05, respectively). The lung weight was significantly reduced in groups CAAL, CADB, and CAALDB compared to NC and CA (Fig. 4.2B, p< 0.05, respectively).

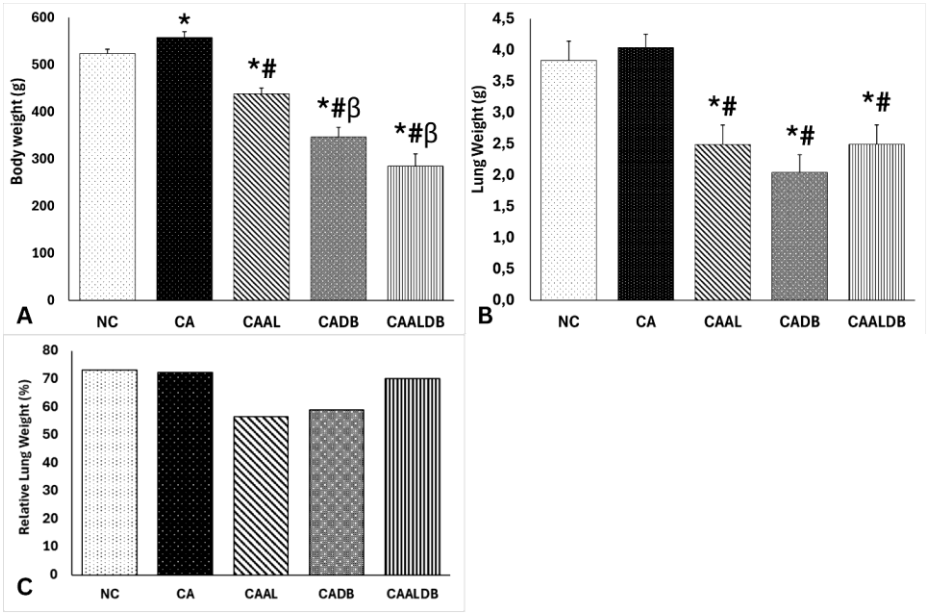

Figure 4.2: Body, Lung and Relative Lung Weights.

A: Body weight; Significant difference was observed (One-way ANOVA, $p< 0.001$). CA showed a significant increase compared to NC (Independent-Samples T Test, $p= 0.030$; 0.060), while CAAL, CADB, and CAALDB showed a significant decrease against NC and CA (Independent-Samples T Test, $p<0.001$, respectively). CADB and CAALDB were significantly reduced compared to CAAL (Independent-Samples T Test, $p= 0.003$ and <0.001, respectively). **B:** Lung weight; Significant difference across groups (One-way ANOVA, $p< 0.001$). CAAL, CADB, and CAALDB showed a significant decrease against NC (Independent-Samples T Test, $p= 0.008$, 0.001 and 0.014, respectively) and CA (Independent-Samples T Test, $p= 0.002$, <0.001, and 0.004, respectively). **C:** Relative Lung Weight; No significant difference recorded. **'*'** indicates significant difference compared to NC, **'#'** against CA and 'β'against CAAL.

Key: NC= negative control; CA= cART; CAAL= cART and alcohol; CADB= cART and diabetes; CAALDB= cART, alcohol, and diabetes.

4.1.2.2. Right Lung Surface Area.

The representative photomicrographs and estimated total right lung surface area (combination of right superior, middle, and inferior lobes) are illustrated in Figure 4.3. The different lobes are annotated with respective shapes. Significant reduction in total right lung surface area was observed in group CADB compared to NC and CA (Fig. 4.3, $p< 0.05$ respectively), whereas groups CAAL and CAALDB showed significant reduction only against CA (Fig. 4.3, $p< 0.05$).

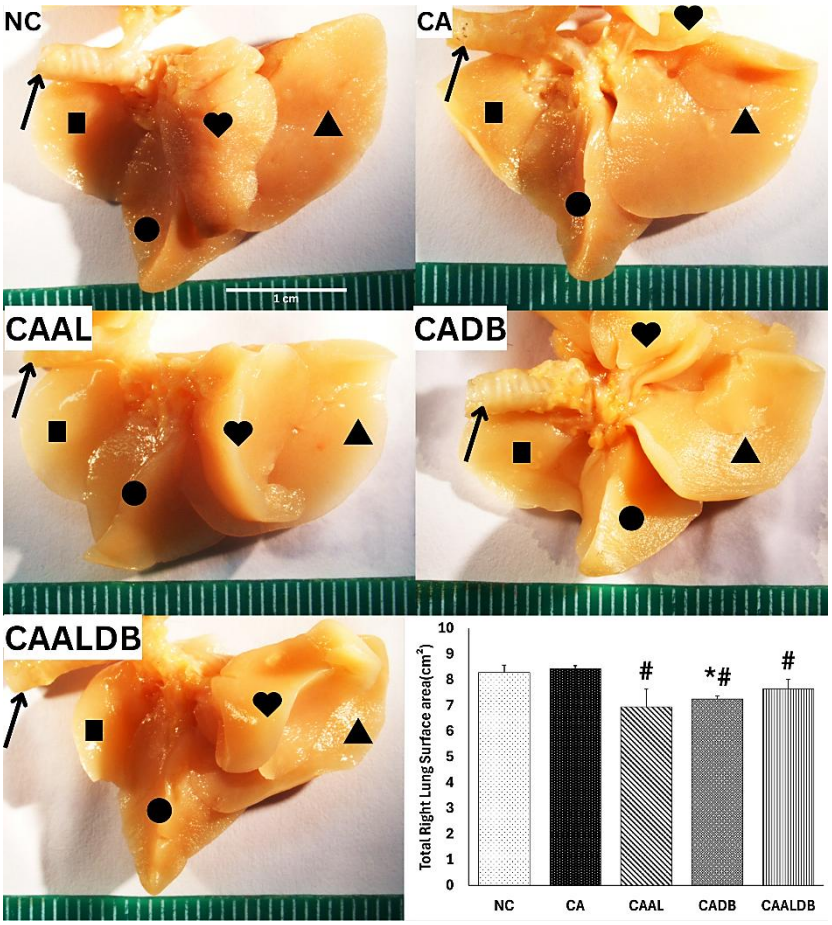

Figure 4.3: Mean Right Lung Total Surface Area.

Right lung surface area: Comparison across groups (One-way ANOVA, p= 0.053). CADB showed a significant decrease against NC and CA (Independent-Samples T Test, p= 0.005 and <0.001 respectively). CAAL and CAALDB showed significant decrease against CA (Independent-Samples T Test, p= 0.034 and 0.040, respectively). Single arrow: Trachea, ■: Right superior lobe, ▲: Right inferior lobe, ●: Right middle lobe and ♥: Post caval lobe. **'*'** indicates significant difference compared to NC and **'#'** against CA.

Key: NC= negative control; CA= cART; CAAL= cART and alcohol; CADB= cART and diabetes; CAALDB= cART, alcohol, and diabetes.

4.1.3. Biochemical Analysis.

4.1.3.1. Oxidative Stress: Serum MDA and GPx1 Concentrations and MDA: GPx1 Ratio.

Following the analysis of serum oxidative stress, the concentrations of serum MDA and GPx1 and the ratio of MDA to GPx1 are displayed in Figure 4.4A-C. Groups CADB and CAALDB showed a significant increase in serum MDA concentration compared to NC and CA (Fig. 4.4A, p< 0.05 respectively). Moreover, a significantly increased MDA was observed in CADB against CAAL whereas a significantly decreased MDA was noted in CAALDB against CADB

(Fig. 4.4A, p< 0.05, respectively). Further, groups CADB and CAALDB showed a significant decrease in GPx1 concentration compared to NC, CA, and CAAL (Fig. 4.4B, p< 0.05), whereas CA showed a significant GPx1 compared to NC (Fig. 4.4B, p< 0.05). Both groups CADB and CAALDB showed a significant increase in MDA to GPx1 ratio against NC, CA, and CAAL Additionally, the oxidative ratio was significantly decreased in CAALDB against CADB (Fig. 4.4C, p< 0.05 respectively).

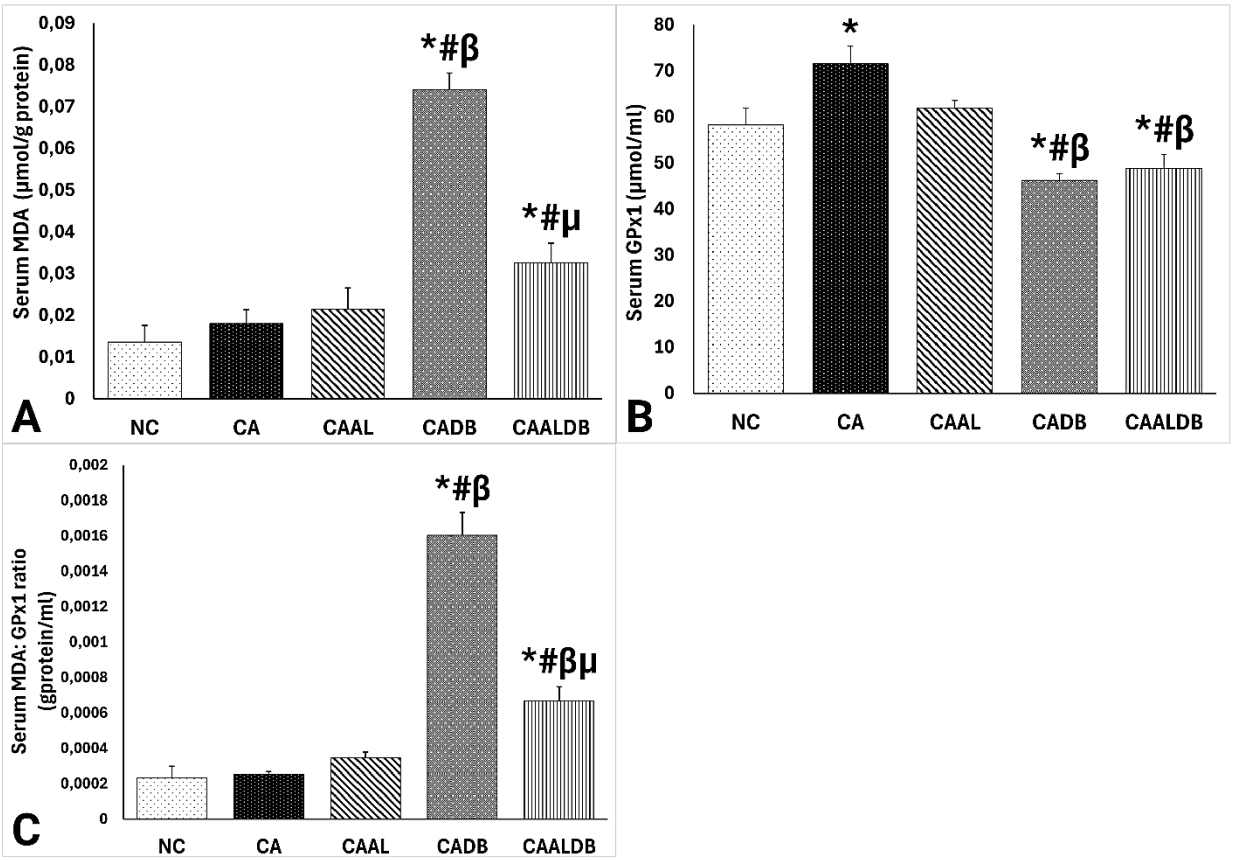

Figure 4.4: Mean Serum MDA and GPx1 Concentrations and MDA To GPx1 Ratio.

A: Serum MDA concentration. Significant difference across groups (One-way ANOVA, p< 0.001). CADB and CAALDB showed significant increase in MDA compared to NC (Independent-Samples T Test, p= 0.002 and 0.010, respectively) and CA (Independent-Samples T Test, p= 0.028 and 0.005, respectively). CADB showed significant increase in MDA against CAAL (Independent-Samples T Test, p= 0.009) and CAALDB a significant decrease against CADB (Independent-Samples T Test, p= 0.005). **B:** Significant difference in serum GPx1 concentration across groups (One-way ANOVA, p< 0.001). CA showed a significant increase in GPx compared to NC (Independent-Samples T Test, p= 0.018), whereas CADB and CAALDB showed a significant decrease against NC (Independent-Samples T Test, p= 0.008 and 0.044, respectively), CA (Independent-Samples T Test, p< 0.00, respectively), and CAAL (Independent-Samples T Test, p< 0.001 and 0.011, respectively). **C:** Significant difference in serum MDA to GPx1 ratio across groups (One-way ANOVA, p< 0.001). Significant ratio increase in CADB and CAALDB against NC (Independent-Samples T Test, p< 0.001 and

0.013, respectively), CA (Independent-Samples T Test, p= 0.002 and 0.002, respectively), and CAAL (Independent-Samples T Test, p< 0.001 and 0.009, respectively), moreover, CAALDB showed a significant decrease against CADB (Independent-Samples T Test, p< 0.001). **'*'** indicates significant difference compared to NC, **'#'** against CA, 'β' against CAAL, and 'μ' against CADB.

Key: NC= negative control; CA= cART; CAAL= cART and alcohol; CADB= cART and diabetes; CAALDB= cART, alcohol, and diabetes.

4.1.4. Histological Analysis.

4.1.4.1. Tracheal Epithelial Height.

The mean epithelial height of the trachea is presented in Figure 4.5 (epithelial height; double arrow and cilia; single arrow). Groups CAAL and CADB showed significantly decreased tracheal epithelial heights against NC and CA (Fig. 4.5, p< 0.05 respectively), but CAALDB showed a significantly decreased epithelial height compared to NC and a significant increase against CADB (Fig. 4.5, p< 0.05, respectively).

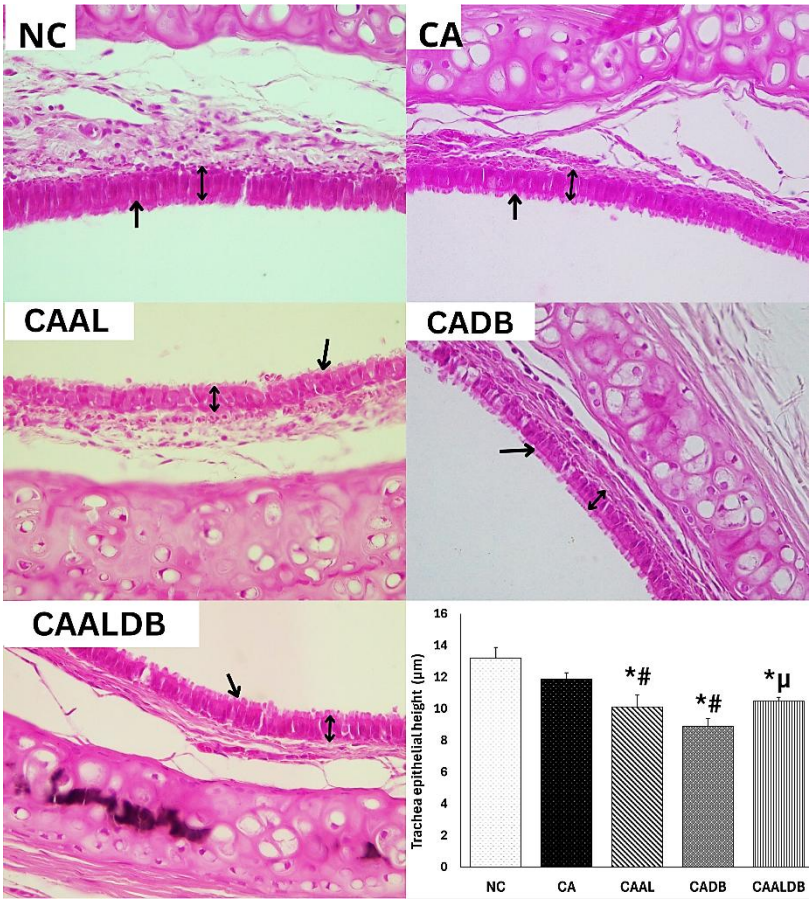

Figure 4.5: Tracheal Epithelial Height.

Epithelial height: Significant difference across groups (One-way ANOVA, $p< 0.001$). CAAL and CADB showed a significant decrease against NC (Independent-Samples T Test, $p= 0.008$ and < 0.001, respectively) and CA (Independent-Samples T Test, $p= 0.036$ and < 0.001, respectively), whereas CAALDB showed a decrease against NC (Independent-Samples T Test, $p= 0.002$) and a significant increase against CADB (Independent-Samples T Test, $p= 0.009$). Single arrow: Cilia and Double arrow: Epithelial height. **'*'** indicates a significant difference compared to NC, **'#'** against CA and 'µ' against CADB.

Key: NC= negative control; CA= cART; CAAL= cART and alcohol; CADB= cART and diabetes; CAALDB= cART, alcohol and diabetes.

4.1.4.2. Tracheal Cartilage Width.

The morphological changes in the tracheal cartilage were determined by analyzing the trachea width as presented in Figure 4.6 (double arrow; trachea width and double broken arrow; perichondrium width). Groups CA, CAAL and CADB showed significantly decreased cartilage width compared to NC (Fig. 4.5, $p< 0.05$, respectively). Moreover, CAAL and CADB showed a significantly reduced cartilage width against CA, whereas CADB showed a significant decrease against CAAL and CAALDB a significant increase against CADB (Fig. 4.5, $p< 0.05$, respectively).

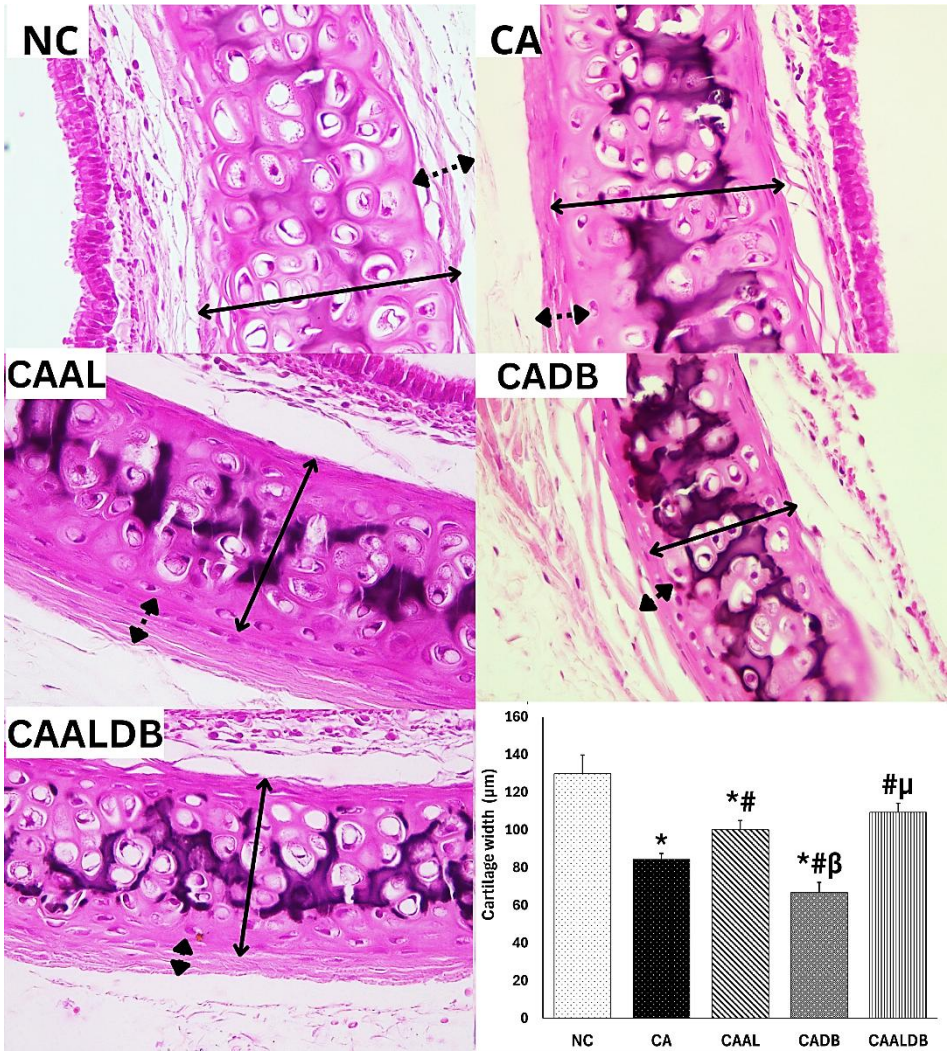

Figure 4.6: Tracheal Cartilage Width.

Cartilage width: Significant difference across groups (One-way ANOVA, p< 0.001). CA, CAAL, and CADB showed a significant decrease against NC (Independent-Samples T Test, p= 0.001, 0.014 and <0.001, respectively). CAAL and CAALDB showed a significant increase against CA (Independent-Samples T Test, p= 0.014 and 0.001, respectively) and CAALDB showed a significant increase against CA (p= 0.001), whereas CADB showed a significant decrease against CA (Independent-Samples T Test, p= 0.012). Moreover, CADB showed a significant decrease against CAAL (Independent-Samples T Test, p= 0.001), and CAALDB showed a significant increase against CADB (Independent-Samples T Test, p< 0.001). Double arrow: Cartilage width and Double broken arrow: Perichondrium width. **'*'** indicates a significant difference compared to NC, **'#'** against CA, 'β' against CAAL and 'µ' against CADB.

Key: NC= negative control; CA= cART; CAAL= cART and alcohol; CADB= cART and diabetes; CAALDB= cART, alcohol and diabetes.

4.1.4.3. Tracheal Lacunae Area.

The mean lacunae area (circled, Fig 4.7) within the tracheal cartilage are presented in Figure

4.7. All the treated groups showed a significantly decreased lacunae area compared to NC (Fig. 4.7, $p < 0.05$, respectively). But CAAL and CAALDB groups showed significant increases against CA (Fig. 4.7, $p < 0.05$, respectively). Moreover, CADB and CAALDB showed a significantly lower lacunae area compared to CAAL (Fig. 4.7, $p < 0.05$, respectively).

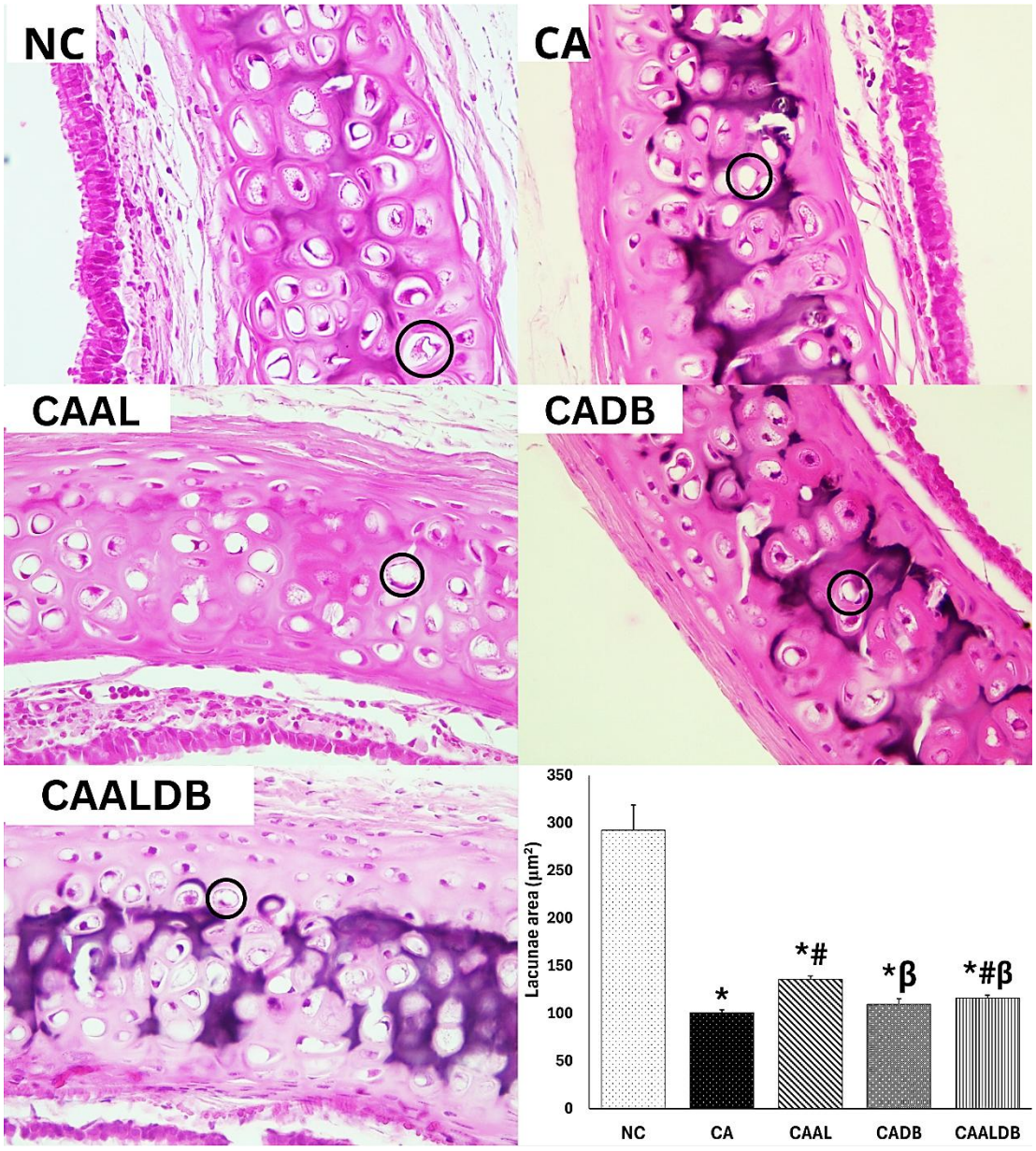

Figure 4.7: Tracheal Lacunae Area.

Lacunae area: Significant difference across groups (One-way ANOVA, $p < 0.001$). CA, CAAL, CADB and CAALDB showed a significant decrease against NC (Independent-Samples T Test, $p < 0.001$ respectively). CAAL and CAALDB showed a significant increase against CA (Independent-Samples T Test, $p < 0.001$ and 0.003 respectively). CADB and CAALDB showed a significant decrease against CAAL (Independent-Samples T Test, $p < 0.003$ and 0.002 respectively). Circle: Lacunae. '*' indicates a significant difference compared to NC, '#' against CA and 'β' against CAAL.

Key: NC= negative control; CA= cART; CAAL= cART and alcohol; CADB= cART and diabetes; CAALDB= cART, alcohol and diabetes.

4.1.4.4. Bronchiole Epithelial Height.

The mean bronchiole epithelial height is presented in Figure 4.8 (epithelial height; double arrow, cilia; single arrow and muscularis mucosa: double broken arrow). All the treated groups showed a significantly decreased bronchiole epithelial height compared to NC (Fig. 4.8, $p< 0.05$ respectively). Moreover, CADB showed a significant increase in bronchiole epithelial height compared to CA and CAAL whereas CAALDB showed a significant decrease against CA, CAAL and CADB (Fig. 4.8, $p< 0.05$, respectively).

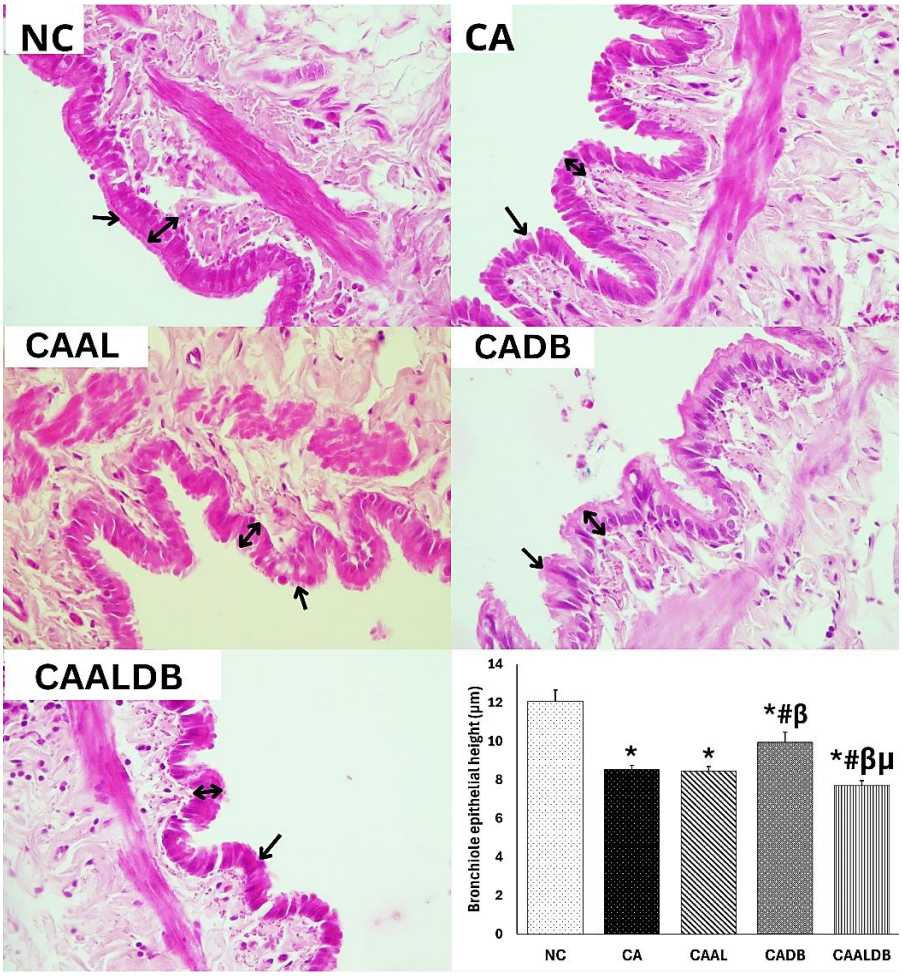

Figure 4.8: Bronchiole Epithelial Height.

Epithelial height: Significant difference across groups (One-way ANOVA, $p< 0.001$). CA, CAAL, CADB and CAALDB showed a significant decrease against NC (Independent-Samples T Test, $p< 0.001$ respectively). CADB showed a significant increase against CA and CAAL (Independent-Samples T Test, $p =0.019$ and 0.016 respectively) and CAALDB showed a significant decrease against CA, CAAL and CADB (Independent-Samples T Test, $p= 0.016$,

0.033 and 0.002 respectively). Single arrow: Cilia and Double arrow: Epithelial height. '*' indicates significant difference compared to NC, '#' against CA, 'β' against CAAL and 'μ' against CADB.

Key: NC= negative control; CA= cART; CAAL= cART and alcohol; CADB= cART and diabetes; CAALDB= cART, alcohol and diabetes.

4.1.4.5. Bronchiole Muscularis Mucosa Width.

The mean width of the bronchial muscularis mucosa is presented in Figure 4.9 (double arrow; muscularis mucosa). Only CAAL showed a significant decrease in bronchial muscularis mucosa width compared to NC and CA whereas CADB and CAALDB showed a significant increase against CAAL (Fig. 4.9, $p < 0.05$ respectively).

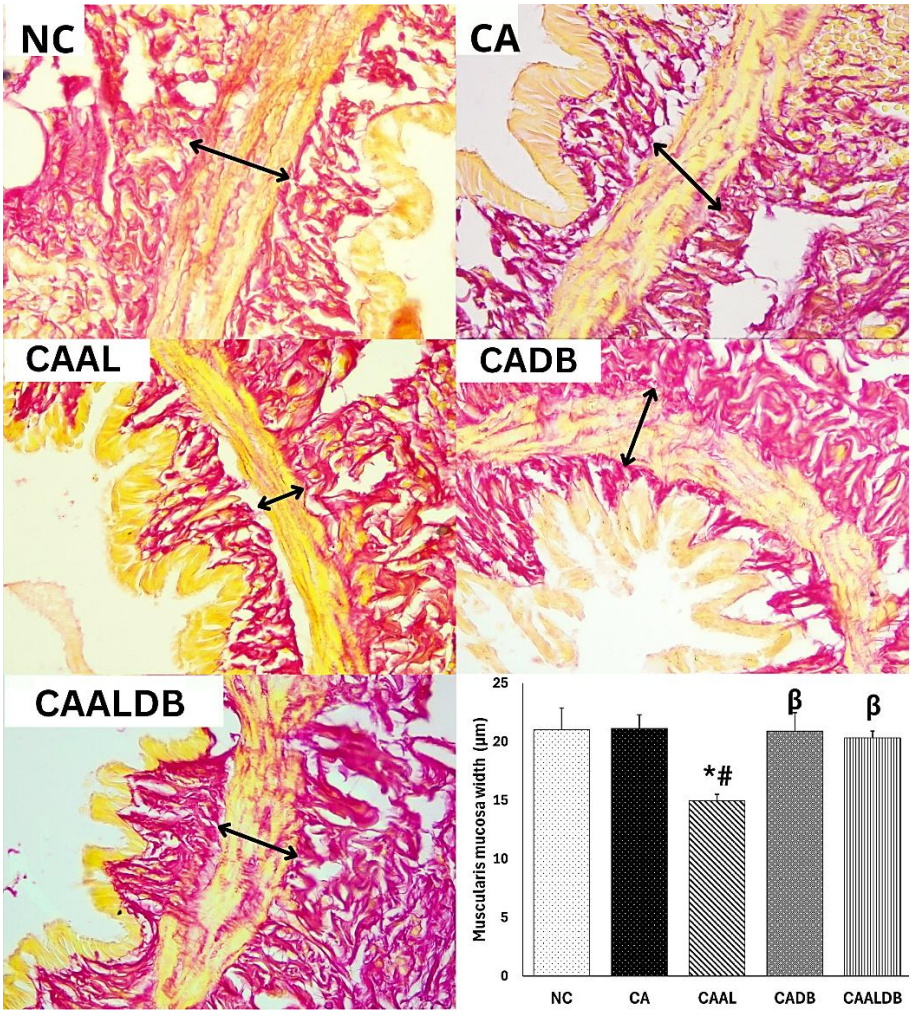

Figure 4.9: Bronchiole Muscularis Mucosa Width

Muscularis mucosa width: Significant difference across groups (One-way ANOVA, p= 0.008). CAAL showed a significant decrease compared to NC and CA (Independent-Samples T Test, p= 0.007 and < 0.001 respectively). CADB and CAALDB showed a significant increase against CAAL

(Independent-Samples T Test, p= 0.003 and <0.001 respectively). Double arrow: Muscularis mucosa width. **'*'** indicates a significant difference compared to NC, **'#'** against CA and 'β' against CAAL.

Key: NC= negative control; CA= cART; CAAL= cART and alcohol; CADB= cART and diabetes; CAALDB= cART, alcohol and diabetes.

4.1.4.6. Bronchiole Mucosal Reticular Fibres.

The mean presence of reticular fibres in the bronchiole mucosa is presented in Figure 4.10 (mucosa; double arrow and reticular fibres/stained black; single arrow). The CA treated showed a significant increase in bronchiole mucosal reticular fibre amount compared to NC (Fig. 10, p< 0.05) and CAAL showed a significant decrease in bronchiole mucosal reticular fibre amount against NC and CA (Fig. 4.10, p< 0.05 respectively). The CADB and CAALDB groups showed a significant decrease in bronchiole mucosal reticular fibre profile compared to CA and a significant increase against CAAL (Fig. 4.10, p< 0.05 respectively).

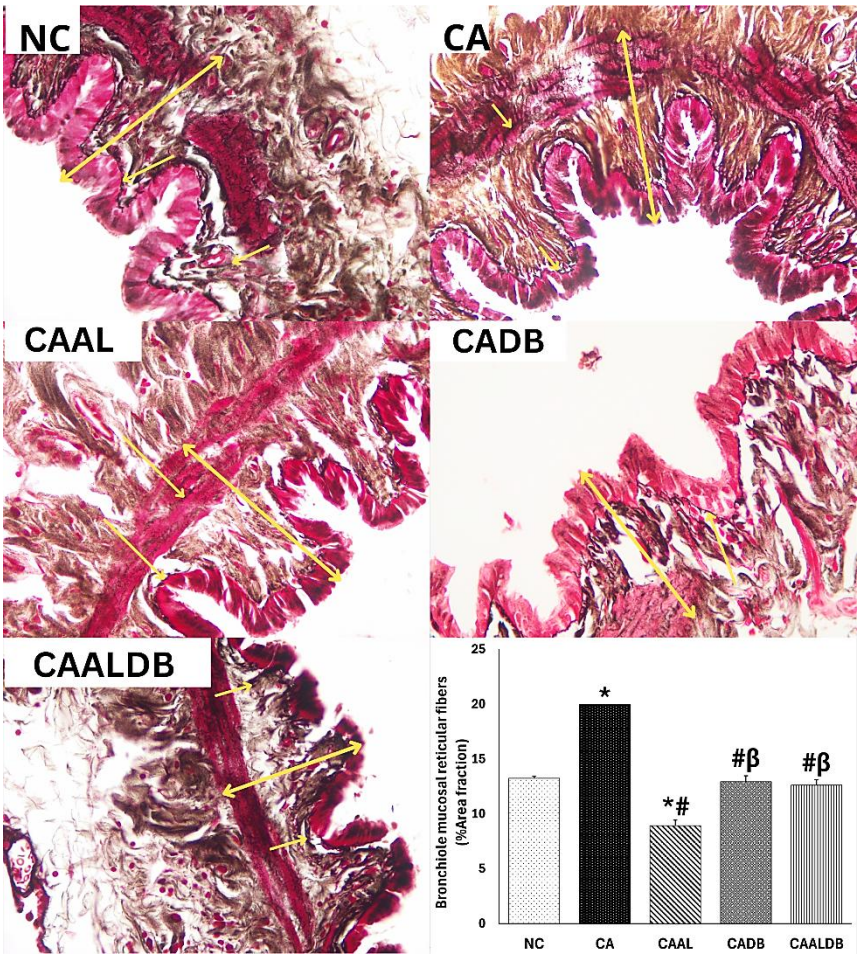

Figure 4.10: Bronchiole Mucosal Reticular Fibres.
Bronchiole mucosal reticular fibres: Significant difference across groups (One-way ANOVA, p< 0.001). CA showed significant increase compared to NC (Independent-Samples

T Test, p< 0.001); CAAL showed significant decrease against NC and CA (Independent-Samples T Test, p< 0.001 respectively). CADB and CAALDB showed a significant decrease against CA (Independent-Samples T Test, p= 0.003 and 0.002, respectively.) and a significant increase against CAAL (Independent-Samples T Test, p< 0.001 respectively). Double arrow: Mucosa and single arrow: Reticular fibres. **'*'** indicates a significant difference compared to NC, **'#'** against CA and 'β' against CAAL.

Key: NC= negative control; CA= cART; CAAL= cART and alcohol; CADB= cART and diabetes; CAALDB= cART, alcohol and diabetes.

4.1.4.7. Thickness of Bronchial Arterial Wall.

The mean bronchial arterial wall thickness (combination of tunica intima, media, and adventitia) is presented in Figure 4.11 (artery wall thickness; double arrow). Group CAALDB showed a significant decrease in bronchial arterial wall thickness compared to NC, CAAL and CADB (Fig. 4.11, p< 0.05 respectively).

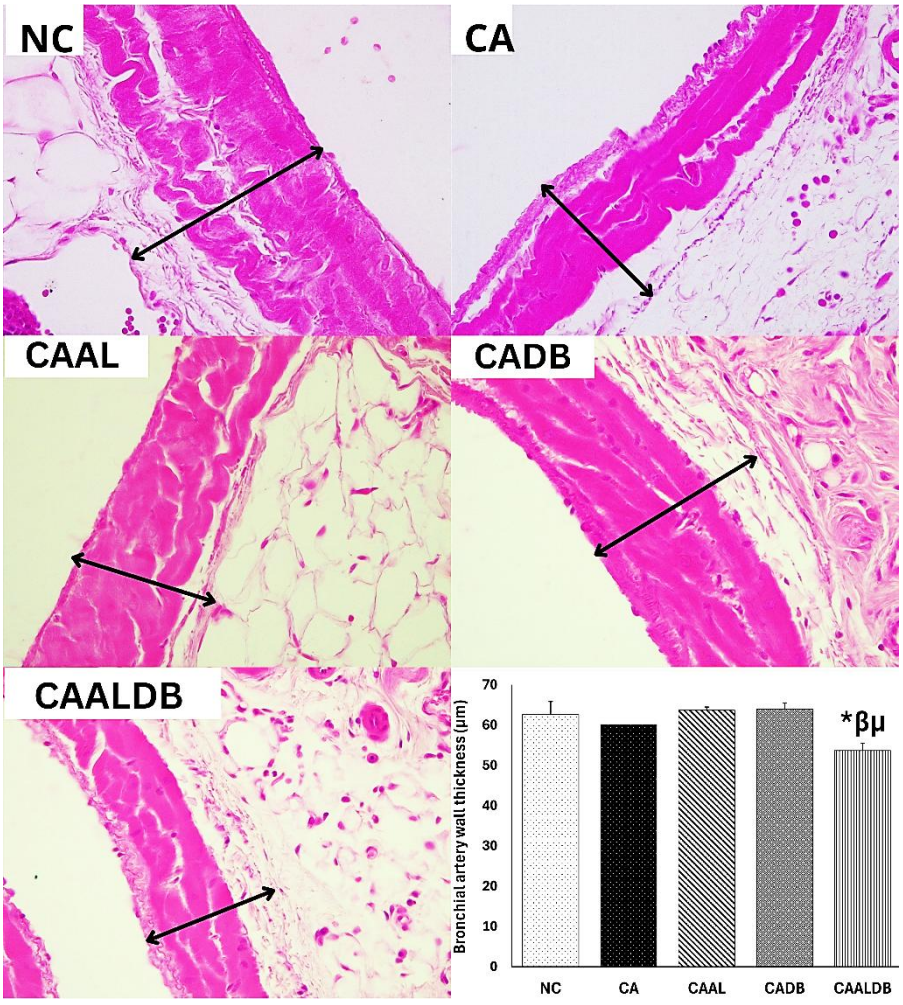

Figure 4.11: Bronchial Artery Wall Thickness.

Wall thickness: Comparison between groups (One-way ANOVA, p= 0.063). CAALDB showed a significant decrease compared to NC, CAAL and CADB (Independent-Samples T Test, p= 0.025, 0.011 and 0.005 respectively). Double arrow: Wall thickness. **'*'** indicates significant difference compared to NC, 'β' against CAAL and 'μ' against CADB

Key: NC= negative control; CA= cART; CAAL= cART and alcohol; CADB= cART and diabetes; CAALDB= cART, alcohol and diabetes.

4.1.4.8. Bronchial Arterial Tunica Media Thickness.

The mean thickness of tunica media in the bronchial artery is as presented in Figure 4.12 (tunica media thickness; double arrow). The CADB group showed a significantly decreased tunica media thickness of the bronchial artery compared to CAAL, moreover, CAALDB showed significant decrease against NC, CAAL and CADB (Fig. 4.12, p< 0.05 respectively).

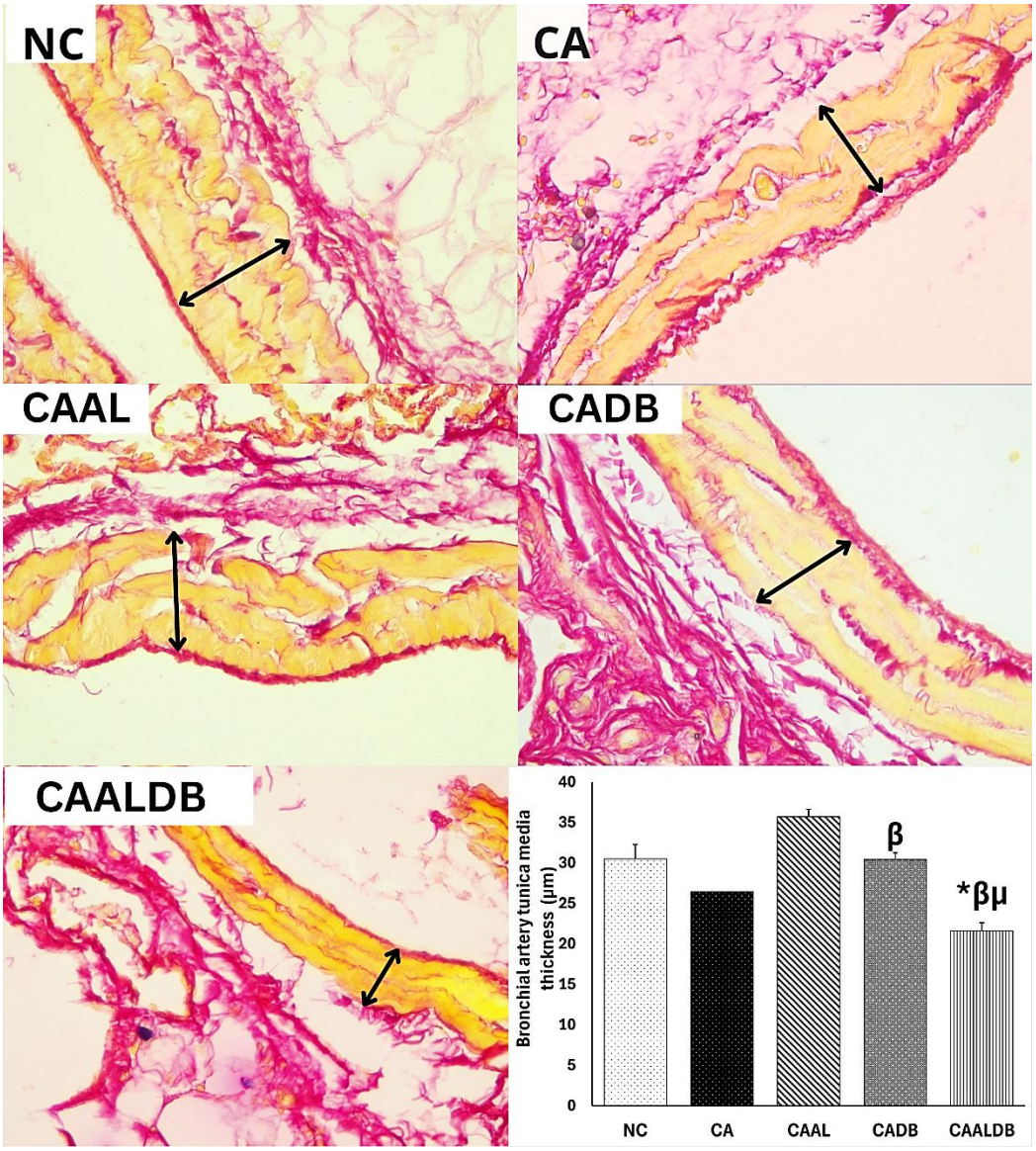

Figure 4.12: Bronchial Artery Tunica Media Thickness.

Tunica media thickness: Significant difference across groups (One-way ANOVA, p= 0.001). CADB showed a significant decrease compared to CAAL (Independent-Samples T Test, p= 0.013). CAALDB showed a significant decrease against NC, CAAL and CADB (Independent-Samples T Test, p= 0.002, <0.001 and 0.001). Double arrow: Tunica media thickness. **'*'** indicates significant difference compared to NC, 'β' against CAAL and 'μ' against CADB.

Key: NC= negative control; CA= cART; CAAL= cART and alcohol; CADB= cART and diabetes; CAALDB= cART, alcohol and diabetes.

4.1.4.9. Thickness of The Bronchial Vein Wall.

The mean bronchial vein wall thickness is presented in Figure 4.13 (wall thickness; double arrow). Groups CAAL, CADB and CAALDB showed a significantly reduced bronchial vein wall height against both NC, Additionally, CAAL showed a significant decrease against CA (Fig. 4.13, p< 0.05 respectively). Moreover, CADB showed a significantly increased bronchial vein wall thickness compared to CAAL whereas CAALDB showed a significant decrease against CA and CADB (Fig. 4.13, p< 0.05).

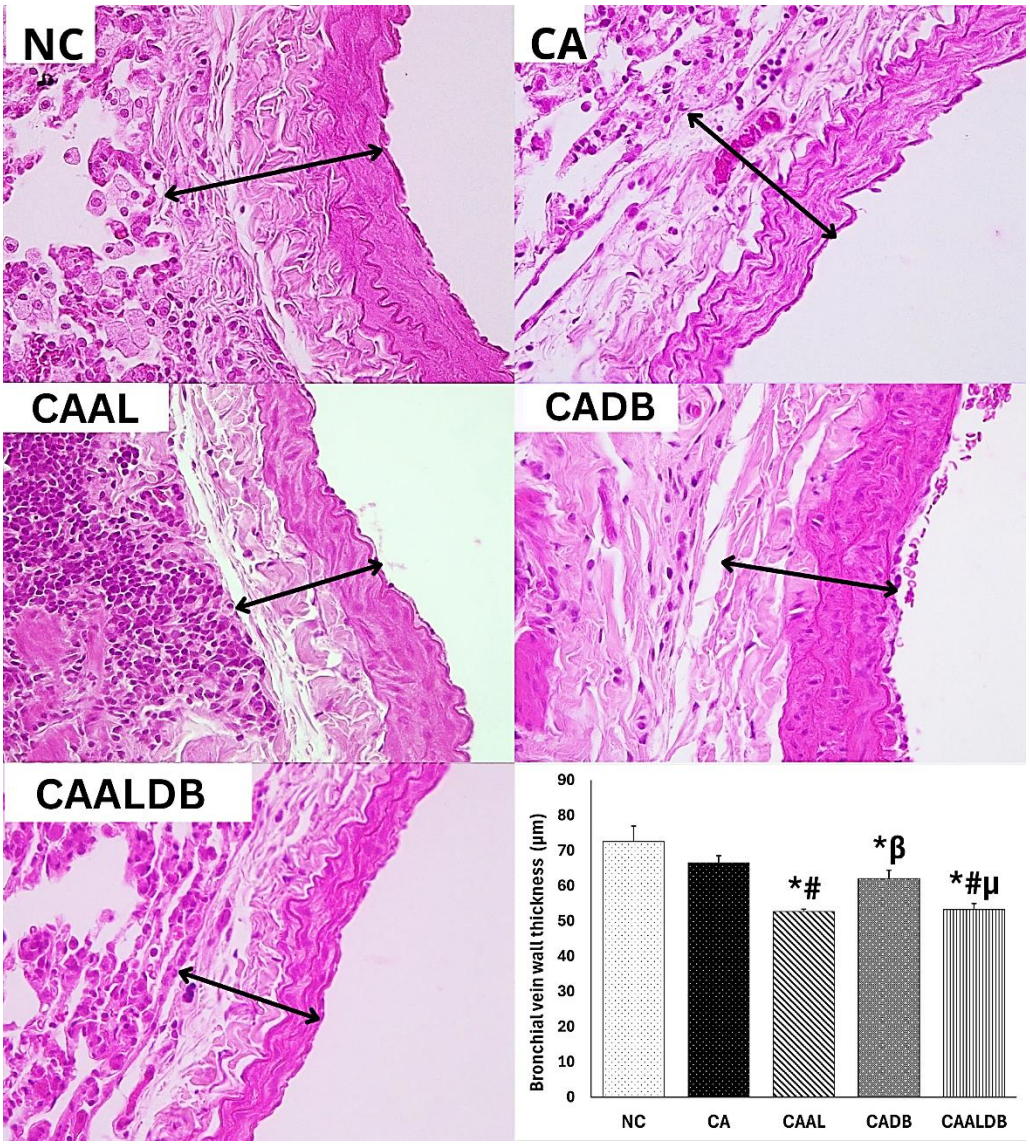

Figure 4.13: Bronchial Vein Wall Thickness.

Wall thickness: CAAL, CADB and CAALDB showed a significantly reduced bronchial vein wall height against both NC (Independent-Samples T Test, p< 0.001, 0.032 and 0.002 respectively). CAAL showed a significant decrease against CA (Independent-Samples T Test, p< 0.001). CADB showed a significantly increased bronchial vein wall thickness compared to CAAL (Independent-Samples T Test, p= 0.003). CAALDB showed a significant decrease against CA and CADB (Independent-Samples T Test, p< 0.001 and 0.008). Double arrow: Wall thickness. '*' indicates significant difference compared to NC, '#' against CA, β' against CAAL and 'µ' against CADB.

Key: NC= negative control; CA= cART; CAAL= cART and alcohol; CADB= cART and diabetes; CAALDB= cART, alcohol and diabetes.

4.1.4.10. Bronchial Vein Tunica Media Thickness, Tunica Adventitia Thickness and Collagen Fibres.

The mean bronchial vein tunica media and adventitia thickness and collagen fibre profile are presented in Figure 4.14A-C respectively (tunica media; double arrow, tunica adventitia; double broken arrow and collagen fibres; single arrow). The CA, CADB, and CAALDB treated groups showed a significantly reduced bronchial vein tunica media thickness against NC (Fig. 4.14A, $p< 0.05$ respectively), whereas CAAL showed a significant decrease against CA (Fig. 4.14A, $p< 0.05$ respectively). Moreover, CADB, and CAALDB showed a significant decrease in bronchial vein tunica media thickness compared to CAAL (Fig. 4.14A, $p< 0.05$ respectively). For bronchial vein tunica adventitia thickness, all the treated groups showed a significant decrease in thickness compared to NC, and CADB showed a significant decrease against CAAL (Fig. 4.14B, $p< 0.05$ respectively). Moreover, a significant reduction of tunica adventitia thickness was observed in CAALDB compared to CA, CAAL and CADB (Fig. 4.14B, $p< 0.05$ respectively). The collagen fibre content was significantly reduced in CADB and CAALDB against NC, CA and CAAL, additionally, the collagen fibres content was also significantly reduced in CAALDB compared to CADB (Fig. 4.14C, $p< 0.05$ respectively).

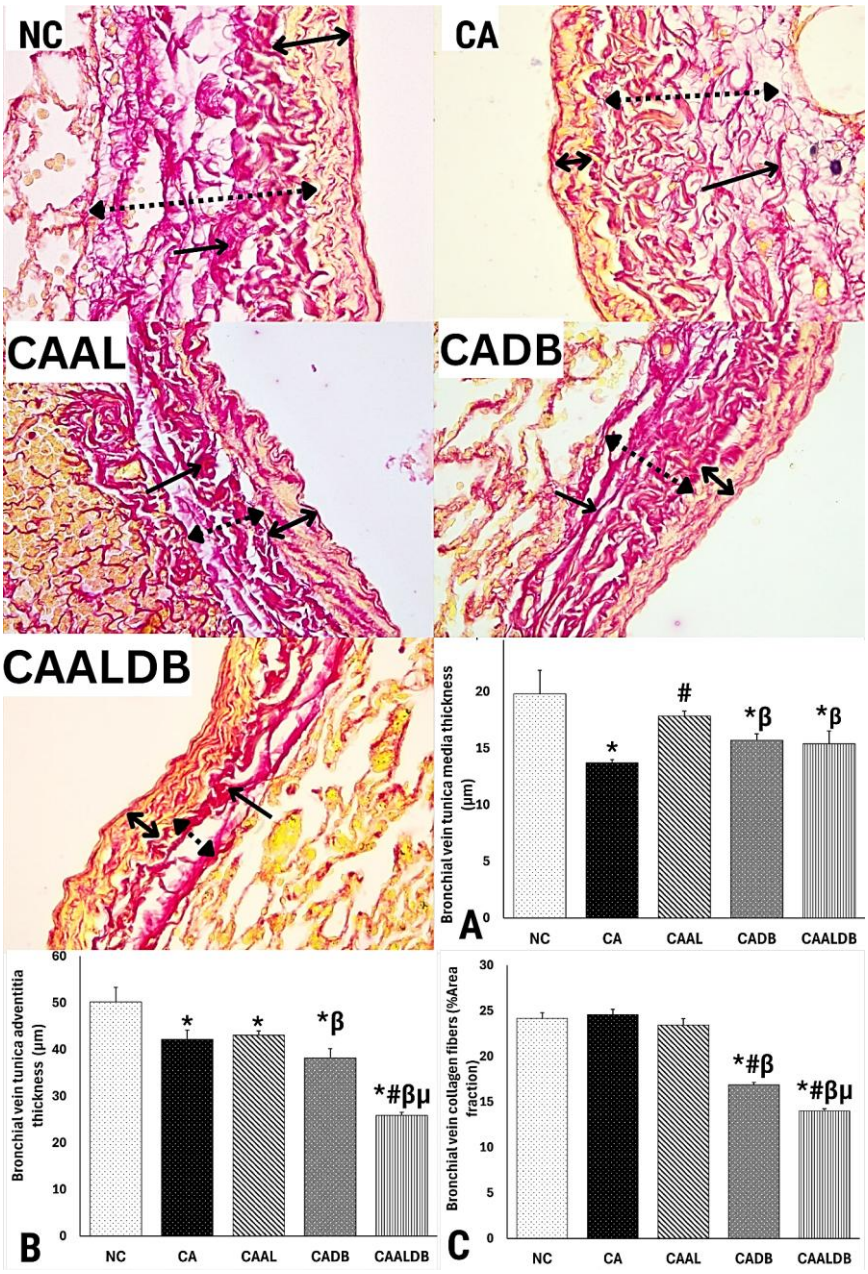

Figure 4.14: Bronchial Vein Tunica Media and Adventitia Thickness and Collagen Fibres.

A: Significant difference across groups in bronchial vein tunica media thickness (One-way ANOVA, p= 0.009). CA, CADB and CAALDB showed a significant decrease compared to NC (Independent-Samples T Test, p= 0.01, 0.046 and 0.049 respectively), whereas CAAL showed a significant increase against CA (Independent-Samples T Test, p< 0.001). CADB and CAALDB showed significant decrease against CAAL (Independent-Samples T Test, p= 0.008 and 0.039 respectively). **B:** Significant difference across groups tunica adventitia thickness (One-way ANOVA, p< 0.001). CA, CAAL, CADB and CAALDB showed a significant decrease against NC (Independent-Samples T Test, p= 0.03, 0.028, 0.006 and <0.001 respectively), CADB showed a significant decrease against CAAL (Independent-Samples T Test, p= 0.029) whereas CAALDB groups showed a significant decrease compared to CA,

CAAL and CADB (Independent-Samples T Test, p< 0.001 respectively). **C:** Significant difference across groups in bronchial vein collagen fibre profile (One-way ANOVA, p< 0.001). CADB and CAALDB showed a significant decrease against NC, CA and CAAL (Independent-Samples T Test, p< 0.001 respectively) and CAALDB a significant decrease against CADB (Independent-Samples T Test, p< 0.001). Double arrow: Tunica media thickness, Double broken arrow: Tunica adventitia and Single arrow: Collagen fibre profile. **'*'** indicates significant difference compared to NC and **'#'** against CA, 'β' against CAAL and 'μ' against CADB.

Key: NC= negative control; CA= cART; CAAL= cART and alcohol; CADB= cART and diabetes; CAALDB= cART, alcohol and diabetes.

4.1.4.11. Bronchial Vein Elastic Fibres.

The mean elastic fibre profile in the bronchial vein is presented in Figure 4.15 (elastic fibres; single arrows/stained in black and the wall of the bronchial vein; double arrow). The elastic fibre content was significantly decreased in CAAL against both NC and CA (Fig. 4.15, p< 0.05 respectively). Moreover, CADB and CAALDB showed a significantly increased bronchial vein elastic fibre content compared to CAAL (Fig. 4.15, p< 0.05 respectively).

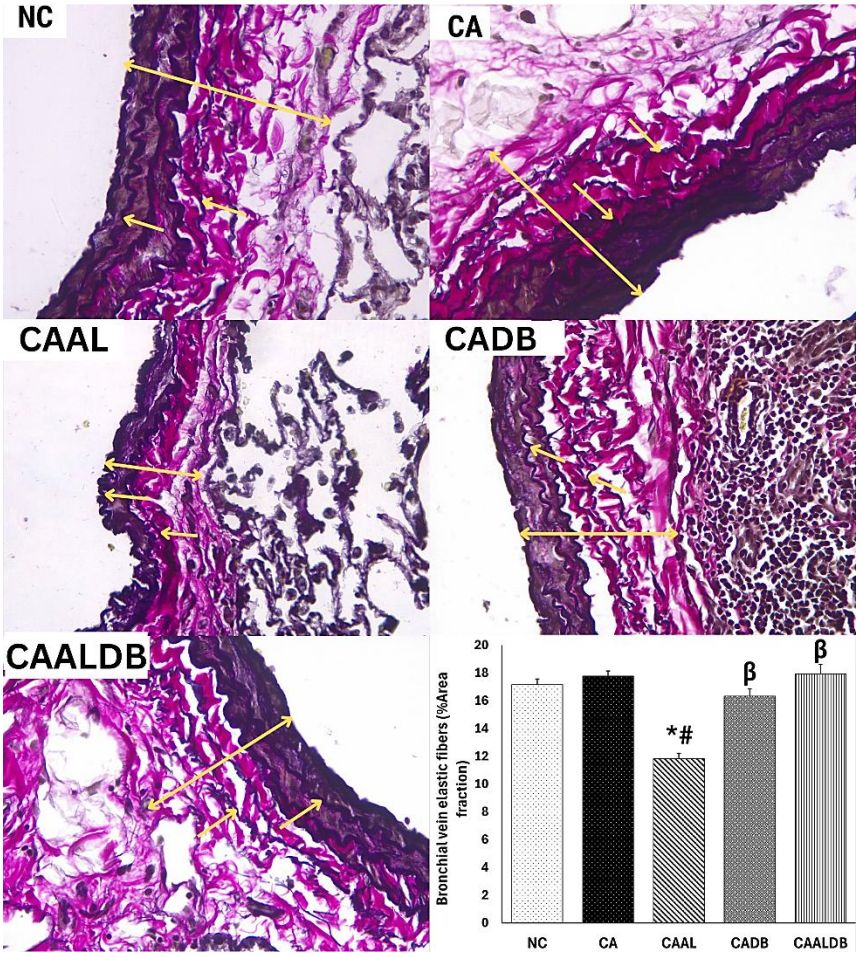

Figure 4.15: Bronchial Vein Elastic Fibres.

Elastic fibres: Significant difference across groups (One-way ANOVA, $p< 0.001$). CAAL showed a significant decrease compared to NC and CA (Independent-Samples T Test, $p< 0.001$ respectively). CADB and CAALDB showed a significant increase compared to CAAL (Independent-Samples T Test, $p< 0.001$ respectively). Double arrow: Bronchiole vein wall and single arrow: Elastic fibres. **'*'** indicates significant difference compared to NC and **'#'** against CA and 'β' against CAAL.

Key: NC= negative control; CA= cART; CAAL= cART and alcohol; CADB= cART and diabetes; CAALDB= cART, alcohol and diabetes.

4.1.4.12. Parenchymal Collagen Fibres.

The mean collagen profile within the lung parenchyma is presented in Figure 4.16 (collagen fibres; stained red /single arrows). Groups CA, CAAL, and CADB showed a significant increase in the amount of parenchymal collagen fibre compared to NC (Fig. 4.16, $p< 0.05$ respectively). Additionally, CADB showed a significant increase in collagen fibre content against CA and CAAL whereas CAALDB showed a significant decrease to CA, CAAL and CADB (Fig. 4.16, $p< 0.05$ respectively).

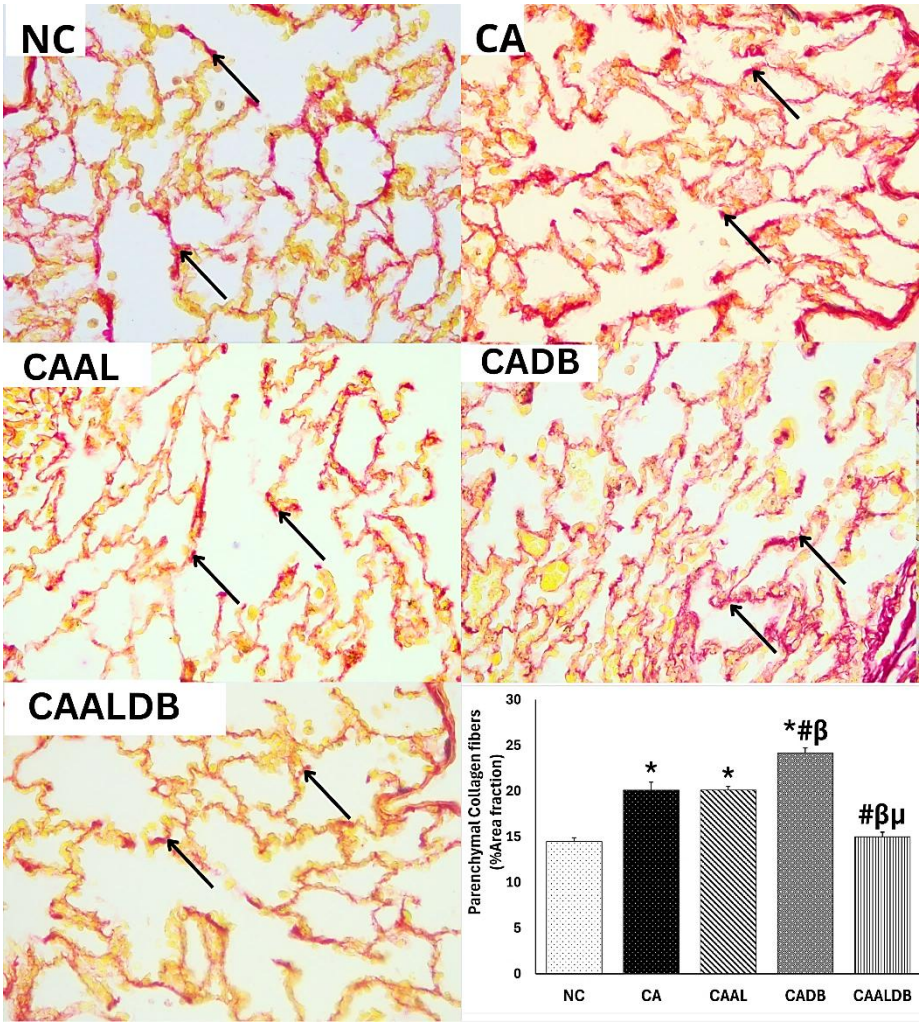

Figure 4.16: Parenchymal Collagen Fibres.

Collagen fibres: Significant difference across groups (One-way ANOVA, p< 0.001). CA and CAAL showed a significant increase compared to NC (Independent-Samples T Test, p< 0.001 respectively) CADB showed a significant increase to NC, CA and CAAL (Independent-Samples T Test, p< 0.001, 0.002 and <0.001 respectively). CAALDB showed a significant decrease against CA, CAAL and CADB (Independent-Samples T Test, p< 0.001, respectively). Single arrow: Collagen fibres. **'*'** indicates significant difference compared to NC, **'#'** against CA, 'β' against CAAL and 'μ' against CADB.

Key: NC= negative control; CA= cART; CAAL= cART and alcohol; CADB= cART and diabetes; CAALDB= cART, alcohol and diabetes.

4.1.4.13. Parenchyma Reticular Fibres.

The mean reticular fibre profile in the lung parenchyma is presented in Figure 4.17 (reticular fibres; stained black/ single arrows). Groups CA and CAALDB showed a significant increase in the parenchymal reticular fibre profile compared to NC (Fig. 4.17, p< 0.05 respectively),

moreover, CAALDB also showed a significantly increased reticular fibre content against CAAL and CADB (Fig. 4.17, $p < 0.05$ respectively). Whereas CAAL and CADB showed a significant decrease in parenchymal reticular fibre profile compared to NC and CA (Fig. $p < 0.05$), additionally, CADB also showed a significant increase against CAAL (Fig. 4.17, $p < 0.05$ respectively).

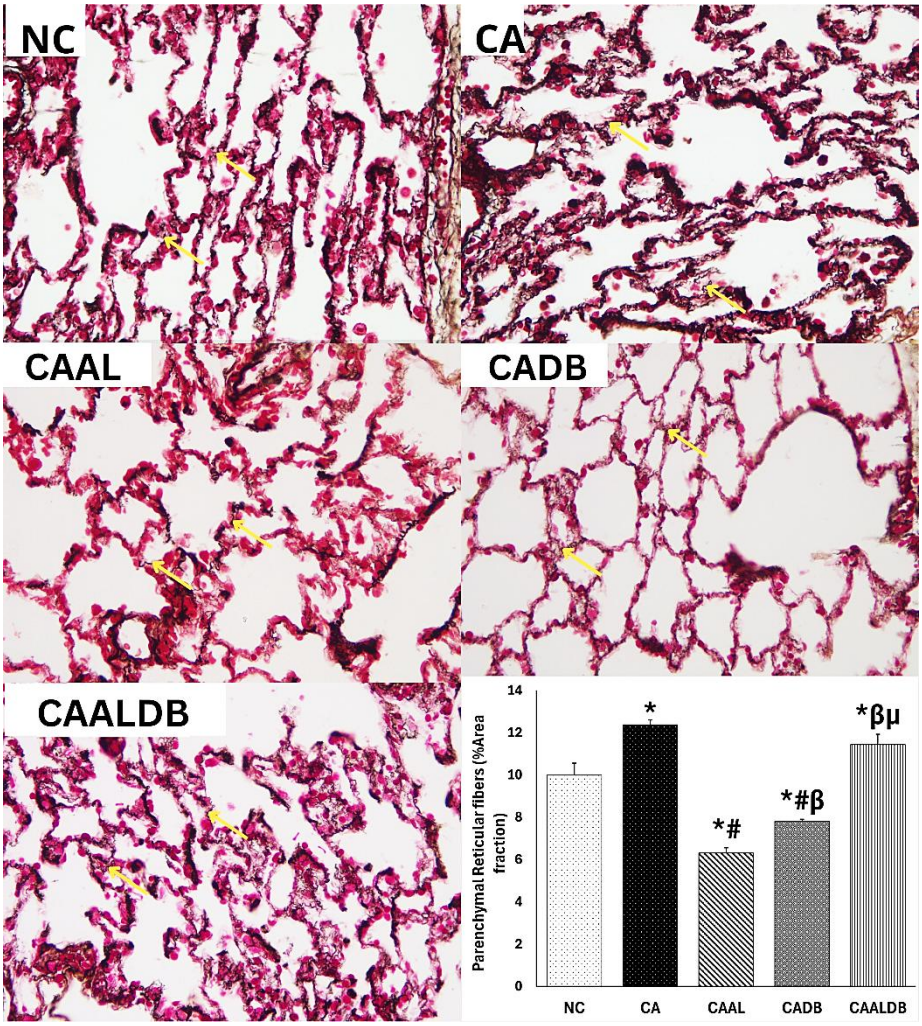

Figure: 4.17: Parenchymal Reticular Fibres.

Reticular fibres: Significant difference across groups (One-way ANOVA, $p < 0.001$). CA and CAALDB showed significant increase against NC (Independent-Samples T Test, $p = 0.002$ and 0.043 respectively). CAAL and CADB showed a significant decrease against NC (Independent-Samples T Test, $p < 0.001$ and 0.002 respectively) and CA (Independent- Samples T Test, $p < 0.001$ respectively). CADB showed a significant increase against CAAL (Independent-Samples T Test, $p < 0.001$) while CAALDB showed a significant increase against CAAL and CADB (Independent-Samples T Test, $p < 0.001$ respectively). Single arrow: Collagen fibres. **'*'** indicates significant difference compared to NC, **'#'** against CA, 'β' against CAAL and 'μ' against CADB.

Key: NC= negative control; CA= cART; CAAL= cART and alcohol; CADB= cART and diabetes; CAALDB= cART, alcohol and diabetes.

4.1.4.14. Parenchymal Elastic Fibres.

The mean parenchymal elastic fibre profile (Stained black) is presented in Figure 4.18, with the elastic fibres annotated with single arrows. Groups CAAL, CADB and CAALDB showed a significant decrease in the amount of parenchymal elastic fibres compared to NC and CA (Fig. 4.18, $p < 0.05$ respectively). Moreover, significantly increased parenchymal elastic content was observed in CADB compared to CAAL whereas CAALDB showed a significant increase against CAAL and a significant decrease compared to CADB (Fig. 4.18, $p < 0.05$ respectively).

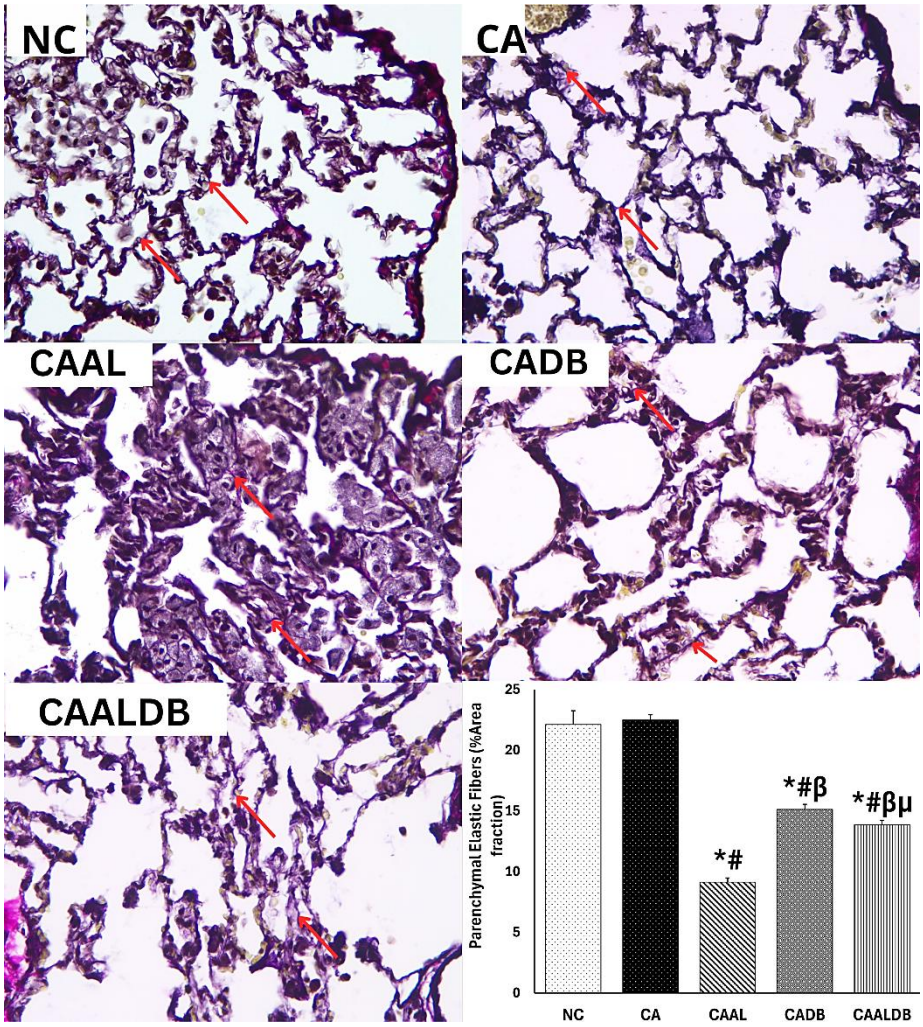

Figure 4.18: Parenchymal Elastic Fibres.

Elastic fibres: Significant difference across groups (One-way ANOVA, $p < 0.001$). CAAL, CADB and CAALDB showed a significant decrease compared to NC and CA (Independent-Samples T Test, $p < 0.001$ respectively). CADB showed a significant increase against CAAL

(Independent-Samples T Test, p< 0.00l) while CAALDB showed a significant increase against CAAL (Independent-Samples T Test, p< 0.001) and a significant decrease against CADB (Independent-Samples T Test, p= 0.025). Singe arrow: Elastic fibres. **'*'** indicates significant difference compared to NC, **'#'** against CA, 'β' against CAAL and 'μ' against CADB.

Key: NC= negative control; CA= cART; CAAL= cART and alcohol; CADB= cART and diabetes; CAALDB= cART, alcohol and diabetes.

4.1.5. Immunohistochemical Analysis.

4.1.5.1. C-Reactive Protein IHC Expression.

The immunohistochemical expression of CRP in the bronchiole lining and alveoli is illustrated in Figure 4.19 and in the bronchial artery and vein presented in Figure 4.20. The bronchiole (Fig. 4.19A-E) demonstrated minimal expression in the epithelium and luminal macrophage nuclei in the NC group and upregulated in CA, CAAL and CADB groups with highest expression observed in CAALDB. Further, CRP expression was observed in the muscularis mucosa of CAAL, CADB and CAALDB (Fig. 4.19C-E). Across all treated groups, clusters of type 2 pneumocytes and alveolar macrophage nuclei showed CRP expression in the alveoli (Fig. 4.19F-J), whereas in NC the expression was minimally observed only in alveolar macrophage nuclei. The CRP expression was also observed in the smooth muscle nuclei of the bronchial artery (Fig. 4.20A-E) and vein (Fig. 4.20F-J) of all treated groups (CA, CAAL, CADB and CAALDB) and the endothelium of both vasculatures in CADB. Only CADB showed CRP expression in endothelial nuclei of both bronchial artery and vein (Fig. 4.20D and I respectively).

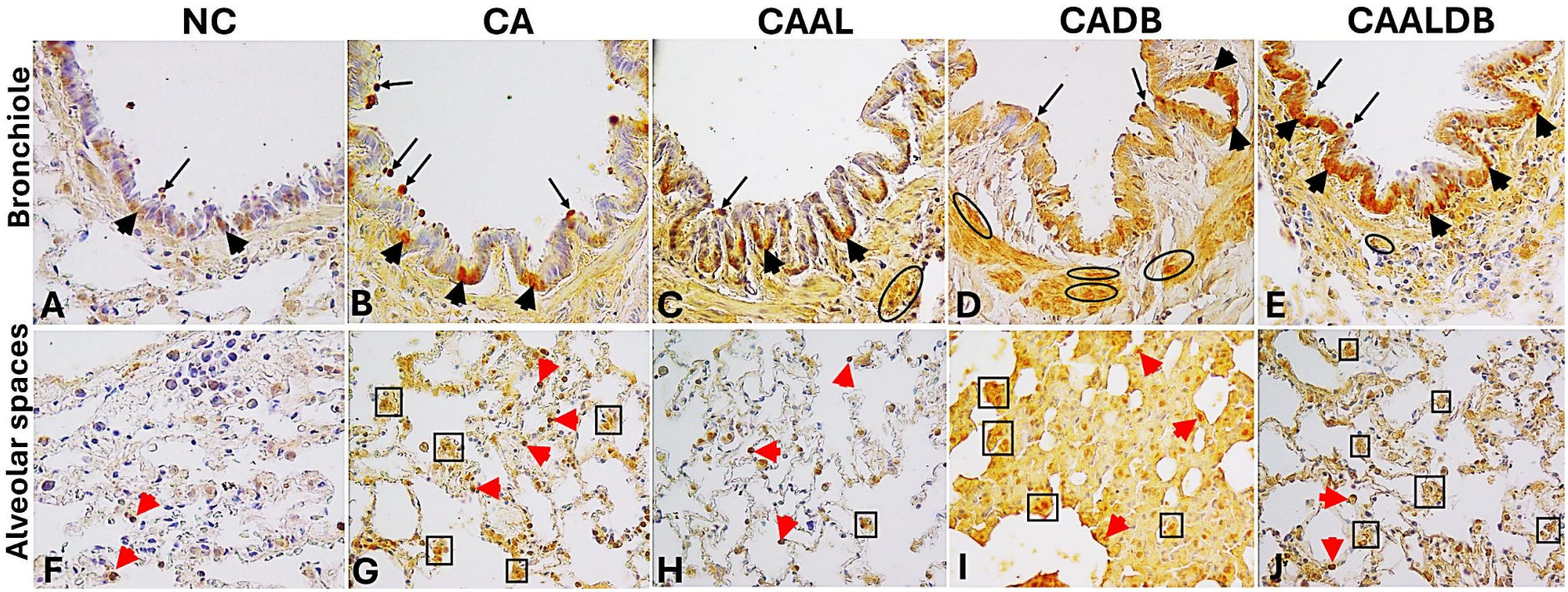

Figure 4.19: CRP Expression in The Bronchiole epithelium Alveolar Spaces.

CRP expression: Black arrowhead- bronchiole epithelium cytoplasm, black arrow- macrophage nuclei (bronchiole lumen), oval circle- smooth muscle (muscularis mucosa), red arrowhead- alveolar macrophage nuclei, and black square- pneumocyte II nuclei cluster.

Key: NC= negative control; CA= cART; CAAL= cART and alcohol; CADB= cART and diabetes; CAALDB= cART, alcohol and diabetes.

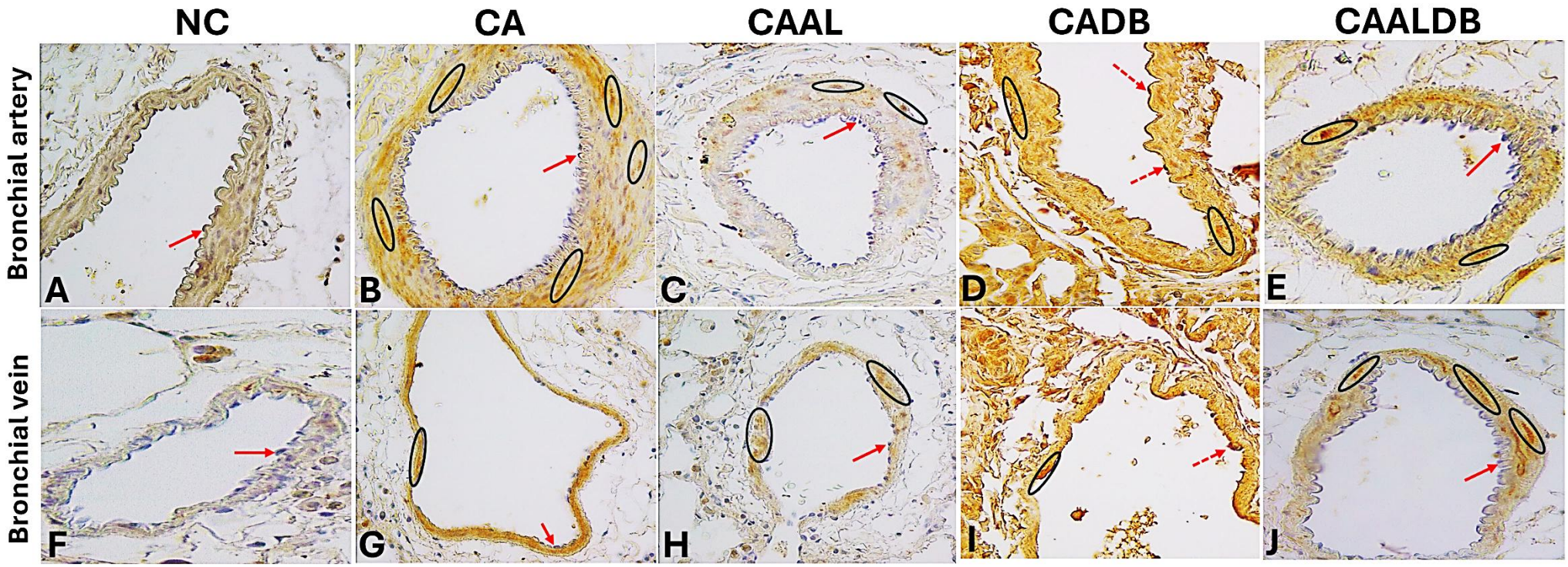

Figure 4.20: CRP Expression in The Bronchial Artery and Vein.

CRP expression: Oval circle- smooth muscle (bronchial vein, and artery), red arrow- endothelium (non-expression), broken red arrow- endothelium (expression).

Key: NC= negative control; CA= cART; CAAL= cART and alcohol; CADB= cART and diabetes; CAALDB= cART, alcohol and diabetes.

4.1.5.2. TGFβ1, MDA and Caspase 3 Trials.

The non-expression trials for TGFβ1, MDA and Caspase 3 in the parenchyma (Fig. 4.21A, C and E) and bronchial vein (Fig. 4.21B, D and F) are presented. Optimization was performed through adjusting several factors including secondary antibody, ABC kit, antigen retrieval in EDTA vs citrate buffer and primary antibody dilution (1: 100, 1: 300, 1:500 and 1:1000). However, no expression of TGFβ1 (Fig. 4.21A-B), MDA (Fig. 4.21C-D) and Caspase 3 (Fig. 4.21E-F) was observed.

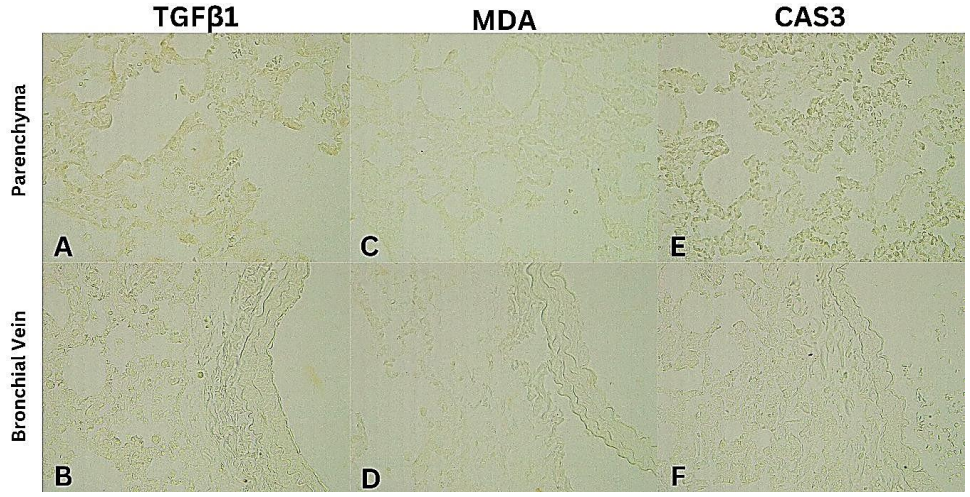

Figure 4.21: Non-Expression Trials for TGFβ1, MDA and Caspase 3.

Key; (A-B), bronchial vein, and parenchyma for TGFβ1**, (C-D),** bronchial vein, and parenchyma for MDA**; (E-F)** bronchial vein, and parenchyma observed Caspase 3.

4.2. DIABETES AND ALCOHOL INTERACTION.

The effect of alcohol-diabetes comorbidity is analyzed for interactive toxicity induced by alcohol in a diabetic condition.

4.2.1. Fasting Blood Glucose.

The overall mean FBG results of the experiment are presented in Table 4.1. There was a significant difference in FBG across groups (One-way ANOVA, p= 0.04). Both DB and DBAL showed a significant increase in FBG compared to NC (Independent-Samples T Test, p= 0.022 and 0.024 respectively, Table. 4.1), moreover, AL showed a significant decrease against DB (Independent-Samples T Test, p= 0.028, Table. 4.1) and DBAL a significant increase against AL (Independent-Samples T Test, p= 0.029, Table. 4.1).

Table 4.1: Mean Fasting Blood Glucose, Body and Lung Weights, Relative Lung Weight, Right Lung Surface Area, Serum MDA and GPX1 Concentrations and MDA To GPx1 Ratio.

Groups	FBG (mmol/L)	Body Weight (g)	Lung Weight (g)	Relative Lung Weight (%)	Right lung Surface area (cm^2)	Serum MDA (µmol/gprotein)	Serum GPx1 (µmol/ml)	MDA: GPx1 ratio (gprotein/ml)
NC	4,95± 0,13	524± 9,43	3,83± 0,31	73± 0,05	8,29± 0,29	0,014± 0,00102	58± 3,73	2,33E-04± 2,21E-05
AL	5,08± 0,20**Δ**	473± 19,56***Δ**	2,11± 0,19*	79± 0,19	6,67± 0,52*	0,035± 0,00269*	66± 1,04	5,28E-04± 3,32E-05*
DB	10,6 ± 2,40*	359± 35,09*	2,81± 0,29	45± 0,04*	7,06± 0,32*	0,033± 0,00216*	64± 5,27	5,19E-04± 5,96E-05*
DBAL	11,26± 2,72*α	323± 62,29*α	3,40± 0,27α	117± 0,16***Δ** α	7,49± 0,35	0,018± 0,00274**Δ** α	44± 3,06***Δ** α	4,04E-04± 5,34E-05

'*' indicates significant difference compared to NC, **'Δ'** against DB and 'α' against AL. The data is presented as Mean± SEM.

Key: NC= negative control; DB= diabetes; AL= alcohol; DBAL= diabetes and alcohol.

4.2.2. Body and Lung Weights and Right Lung Surface Area.

The mean body and lung weights and right lung surface area results are presented in Table 4.1. The body weight showed a significant difference across groups (One-way ANOVA, p= 0.004), groups DB and DBAL showed significantly decreased body weight compared to NC (Independent-Samples T Test, p< 0.001 and 0.007 respectively, Table. 4.1). Further, AL showed a significant decrease against NC (Independent-Samples T Test, p= 0.044, Table. 4.1) and significant increase against DB (Independent-Samples T Test, p= 0.008, Table. 4.1). Moreover, a significantly reduced body was observed in DBAL compared to AL (Independent-Samples T Test, p= 0.021, Table. 4.1).

For lung weight, comparison across the groups (One-way ANOVA, p= 0.065), AL showed a significant decrease compared to NC (Independent-Samples T Test, p< 0.001, Table. 4.1) whereas DBAL showed a significant increase against AL (Independent-Samples T Test, p= 0.003, Table. 4.1). Significant difference in relative lung weight was observed across all groups (One-way ANOVA, p= 0.01), DB showed a significantly reduced relative lung weight compared to NC (Independent- Samples T Test, p= 0001, Table. 4.1). Moreover, DBAL showed significant decrease against both NC and DB (Independent-Samples T Test, p= 0.015 and 0.001 respectively, Table. 4.1) and a significant increase against AL (Independent-Samples T Test, p= 0.001, Table. 4.1).

The representative photomicrographs and measurements for the right lung total surface area (combination of right superior, middle and inferior lobes) are presented in Figure 4.22, each lobe of the right lung is annotated with respective shape. Significant difference across groups in right lung surface area was observed (One-way ANOVA, p= 0,051). Both groups AL and DB showed a significant decrease in right lung total surface area compared to NC (Independent-Samples T Test, p= 0.003 and 0.036 respectively, Table. 4.1).

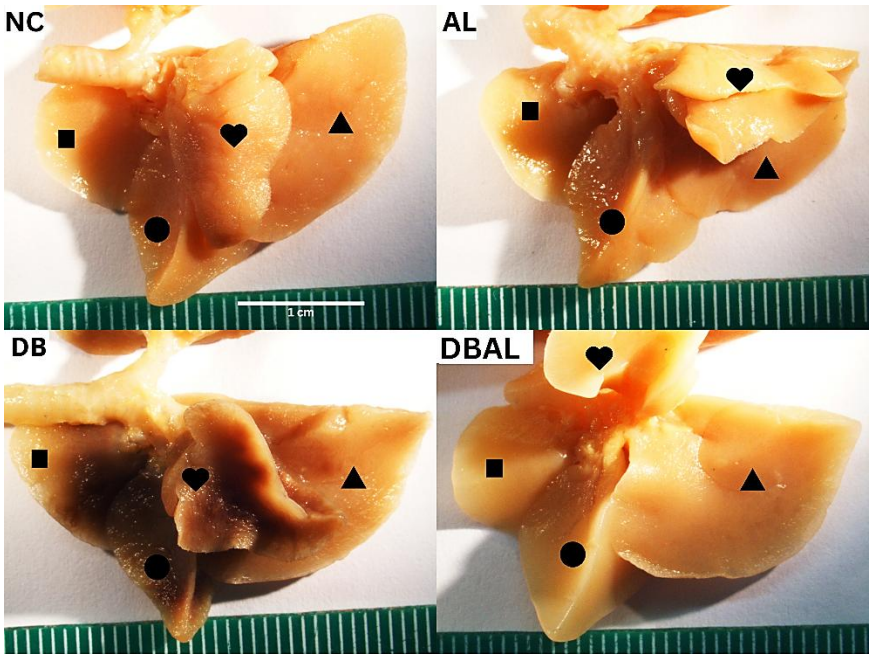

Figure 4.22: Mean Right Lung Total Surface Area.

Single arrow: Trachea, ■: Right superior lobe, ▲: Right inferior lobe, ●: Right middle lobe and ♥: Post caval lobe.

Key: NC= negative control; DB= diabetes; AL= alcohol; DBAL= diabetes and alcohol.

4.2.3. Mean Serum MDA and Gpx1 Concentrations and MDA to GPx1 Ratio.

The results for the serum MDA and GPx1 concentrations and the ratio of MDA to GPx1 are displayed in Table 4.1. The MDA concentration comparison across the different groups (One-way ANOVA, p= 0.052). Groups DB and AL showed significant increase in MDA concentration compared to NC (Independent-Samples T Test, p= 0.029 and 0.009 respectively, Table.4.1) while DBAL showed a significantly low concentration against DB (Independent- Samples T Test, p= 0.041, Table.4.1). Further, significant difference across groups in GPx1 concentration was observed (One-way ANOVA, p= 0.002.) and DBAL showed a significant decrease compared to NC and DB (Independent-Samples T Test, p= 0.010 and 0.003 respectively, Table. 4.1). Furthermore, DBAL showed significant reduction in both MDA and GPx1 compared to AL (Independent-Samples T Test, p= 0.039 and <0.001 respectively, Table. 4.1). The MDA to GPx1 ratio showed a significant difference (One-way ANOVA, p= 0.048, Table. 4.1) and DB and AL showed significant increase against NC (Independent-Samples T Test, p= 0.019 and 0.023 respectively, Table. 4.1)

4.2.4. Tracheal Epithelial Height, Cartilage Width and Lacunae Area.

The mean tracheal epithelial height, cartilage width and lacunae area are presented in Figure 4.23A-C. Significant difference across groups was observed in epithelial height, cartilage width and lacunae area (One-way ANOVA, $p< 0.001$ respectively). Groups AL and DB showed a significant decrease in tracheal epithelial height compared to NC (Independent-Samples T Test, $p= 0.018$ and < 0.001 respectively, Fig. 4.23A) while AL and DBAL showed a significant increase against DB (Independent-Samples T Test, $p= 0.002$ and < 0.001, respectively, Fig. 4.23A). Moreover, DBAL showed a significant increase in tracheal epithelial height compared to AL (Independent-Samples T Test, $p= 0.011$, Fig. 4.23A). A significant reduction in cartilage width was observed in groups AL and DBAL against NC (Independent- Samples T Test, $p= 0.009$ and 0.002 respectively, Fig. 4.23B) and a significant increase against DB (Independent-Samples T Test, $p= 0.010$ and 0.001 respectively, Fig. 4.23B). While DB showed a significant decrease against NC (Independent-Samples T Test, $p< 0.001$, Fig. 4.23B). For lacunae area, AL and DBAL showed a significant decrease compared to NC (Independent-Samples T Test, $p= 0.001$ and <0.001 respectively, Fig. 4.23C) and against DB (Independent-Samples T Test, $p< 0.001$ respectively, Fig. 4.23C) while DB showed a significant decrease against NC (Independent-Samples T Test, $p= 0.002$, Fig. 4.23C).

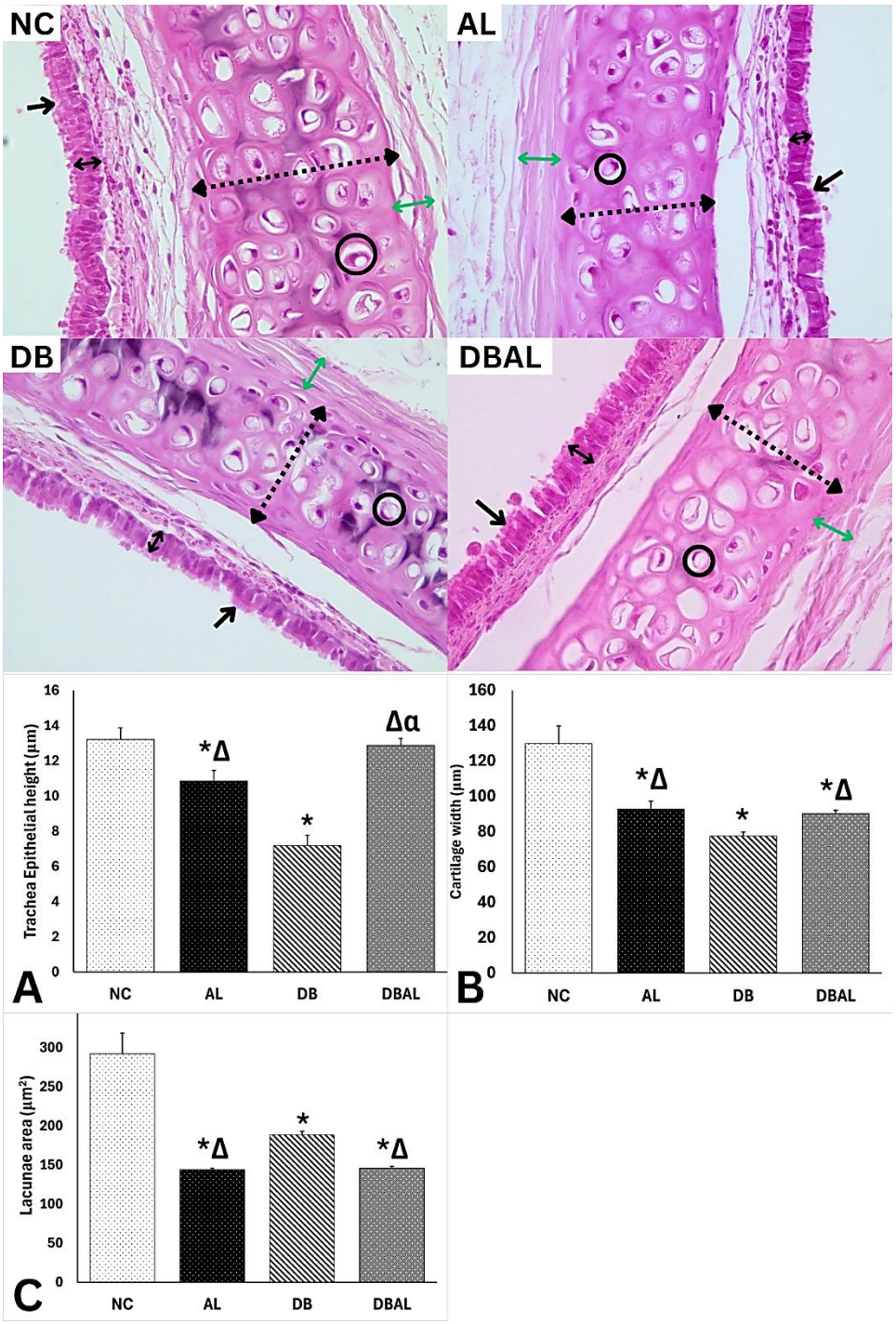

Figure 4.23: Tracheal Epithelial Height, Cartilage Width and Lacunae Area.

Double arrow: Epithelial height, Green double arrow: Perichondrium width, Broken double arrow: Cartilage width, Circle: Lacunae area and Single arrow: Cilia. **'*'** indicates significant difference compared to NC, **'Δ'** against DB and 'α' against AL.

Key: NC= negative control; DB= diabetes; AL= alcohol; DBAL= diabetes and alcohol.

4.2.5. Bronchiole Epithelial Height, Muscularis Mucosa Width and Mucosal Reticular Fibre Profile.

The mean bronchiole epithelial height, muscularis mucosa width and mucosal reticular fibre profile results are illustrated in Figure 4.24 and summarized in Table 4.2. Significant differences across groups were observed in epithelial height (Fig 4.24A-D), muscularis mucosa width (Fig 4.24E-H) and mucosal reticular fibre profile (Fig 4.24I-L) (One-way ANOVA, $p< 0.001$, 0.002 and 0.005 respectively). Groups AL, DB and DBAL showed significant decrease in epithelial height compared to NC (Independent-Samples T Test, $p< 0.001$ respectively, Table. 4.2). For muscularis mucosa width, DB and DBAL showed a significant increase against NC (Independent-Samples T Test, $p= 0.010$ and 0.009 respectively, Table. 4.2) whereas AL showed a significant decrease against DB (Independent-Samples T Test, $p < 0.001$, Table. 4.2). Moreover, DBAL showed a significant increase in muscularis mucosa width and a significant reduction in mucosal reticular fibre content against AL (Independent-Samples T Test, $p< 0.001$ and 0.011, respectively, Table. 4.2). Group AL showed a significant increase in mucosal reticular fibre profile against NC and DB (Independent-Samples T Test, $p= 0.001$ and 0.024 respectively, Table. 4.2) while DBAL showed a significant decrease against NC (Independent-Samples T Test, $p= 0.045$, Table. 4.2).

Table 4.2: Bronchiole Epithelial Height, Muscularis Mucosa Width and Mucosal Reticular Fibre Profile.

Groups	Epithelial height (µm)	Muscularis Mucosa Width (µm)	Mucosal Reticular Fibre Profile (%Area)
NC	12,08± 0,58	21,03± 1,85	13,25± 0,19
AL	8,07± 0,13*	21,79± 0,12 **Δ**	16,25± 0,63***Δ**
DB	8,27± 0,10*	26,54± 0,45*	12,57±0,80
DBAL	8,32± 0,26*	26,86± 0,67*α	12,22± 0,61*α

'*' indicates significant difference compared to NC, **'Δ'** against DB and 'α' against AL. The data is presented as Mean± SEM.

Key: NC= negative control; DB= diabetes; AL= alcohol; DBAL= diabetes and alcohol.

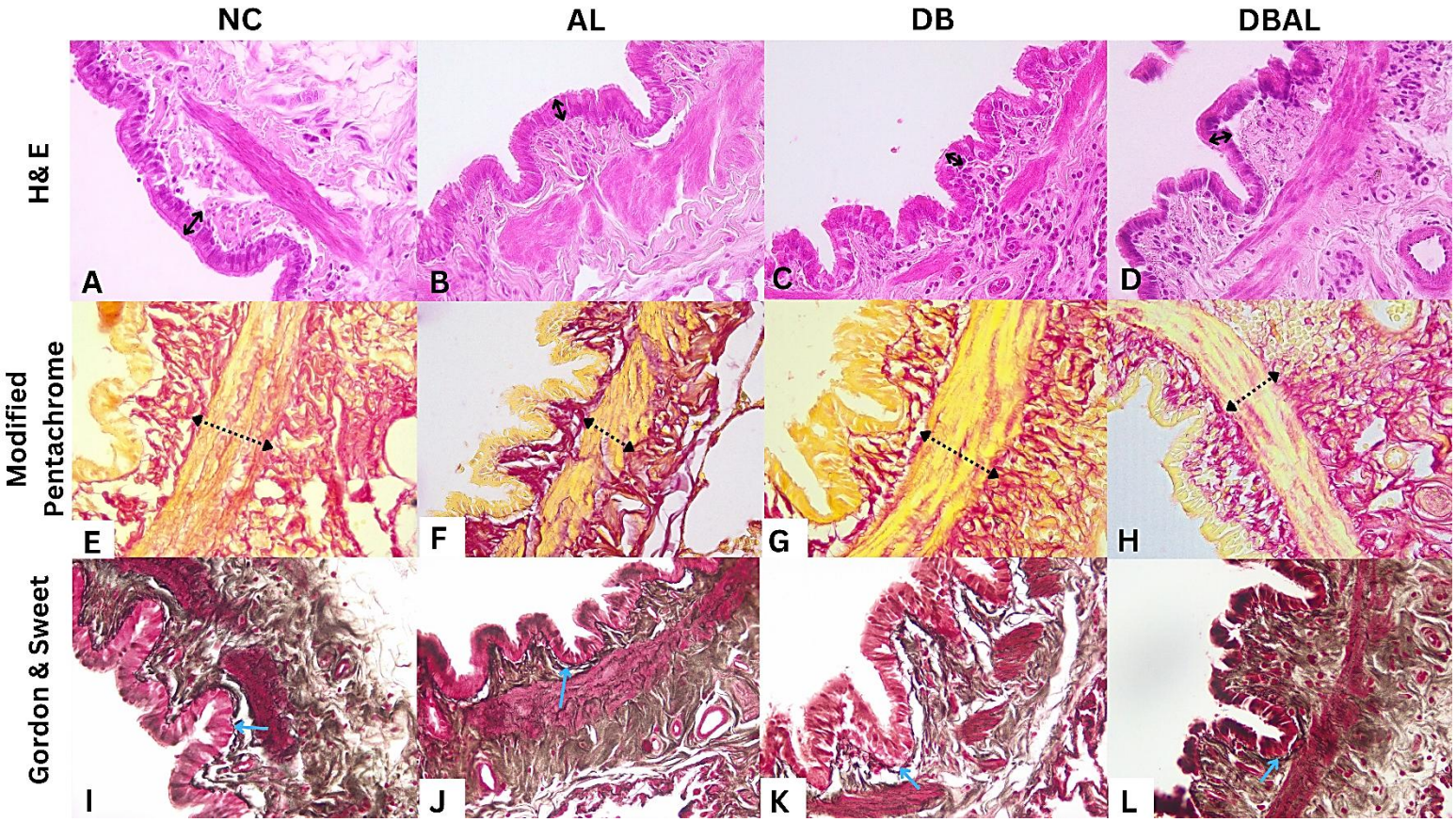

Figure 4.24: Bronchiole Epithelial Height Muscularis Mucosa Width, and Mucosal Reticular Fibre Profile.

Double arrow: Epithelial height, Broken double arrow: Muscularis mucosa width and blue arrow: Reticular fibres.

Key: NC= negative control; DB= diabetes; AL= alcohol; DBAL= diabetes and alcohol.

4.2.6. Bronchial Artery (Tunica Media and Adventitia Thickness) and Vein (Wall, Tunica Media and Adventitia Thickness, and Collagen and Elastic Fibre Profile).

The mean estimated bronchial artery wall and tunica media thickness are presented in Figure 4.25A-G, whereas the estimated bronchial vein wall, tunica media and adventitia thickness, and collagen and reticular fibre profile are presented in Figure 4.25I-U and summarized in Table 4.3. Significant difference across groups was observed in bronchial artery wall (Fig. 4.25A-D) and tunica media thickness (Fig. 4.25E-H) (One-way ANOVA, p= 0.002 and 0.013, respectively). Groups AL and DB showed a significant decrease in bronchial artery wall thickness against NC (Independent-Samples T Test, p= 0.002 and 0.018 respectively, Table. 4.3) while DBAL showed a significant increase against DB and AL (Independent-Samples T Test, p= 0.006 and 0.001 respectively, Table. 4.3). For bronchial artery tunica media thickness, AL and DBAL showed a significant decrease against NC (Independent-Samples T Test, p= 0.006 and 0.048 respectively, Tab. 4.3) and DB (Independent-Samples T Test, 0.005 and 0.044 respectively Table. 4.3), moreover, DBAL showed a significant increase in tunica media thickness against AL (Independent-Samples T Test, p< 0.001, Table. 4.3).

Bronchial vein wall (Fig. 4.25, I-L), tunica media, adventitia thickness, and collagen (Fig. 4.25M-Q) and reticular fibre profile (Fig. 4.25R-U) showed a significant difference across groups (One-way ANOVA, <0,001, respectively). Groups AL and DB showed a significant decrease in bronchial vein wall (Independent-Samples T Test, p= 0.003 and <0.001 respectively, Table. 4.3) and tunica media thickness (Independent-Samples T Test, p= 0.017 and 0.009 respectively, Table. 4.3) against NC, while DBAL showed a significant increase in bronchial vein wall and tunica media thickness against DB and AL (Independent-Samples T Test, p < 0.001 respectively, Table. 4.3). For bronchial vein tunica adventitia thickness, AL showed a significant decrease against NC and DB (Independent- Samples T Test, p< 0.001 respectively, Table. 4.3) while DB showed a significant decrease against NC (Independent-Samples T Test, p= 0.001, Table 4.3) and DBAL a significant increase against DB and AL (Independent-Samples T Test, p < 0.001, Table. 4.3). Group AL showed a significant decrease in bronchial vein collagen fibre profile against NC and DB (Independent-Samples T Test, p= 0.001 and 0.002 respectively, Table. 4.3), while DBAL showed a significant increase against AL (Independent- Samples T Test, p< 0.001, Table. 4.3). Groups AL and DB showed a significant decrease in bronchial vein elastic fibre profile against NC (Independent- Samples T Test, p< 0.001 respectively, Table. 4.3) while DBAL showed a significant increase compared to DB and AL (Independent-Samples T Test, p< 0.001, respectively, Table. 4.3).

Table 4.3: Bronchial Artery (Tunica Media and Adventitia Thickness) and Vein (Wall, Tunica Media and Adventitia Thickness, and Collagen and Elastic Fibre Profile).

	Bronchial Artery		Bronchial Vein				
Groups	**Wall Thickness (µm)**	**Tunica Media Thickness (µm)**	**Wall Thickness (µm)**	**Tunica Media Thickness (µm)**	**Tunica Adventitia Thickness (µm)**	**Collagen Fibre Profile (%Area)**	**Elastic Fibre Profile (%Area)**
NC	62,68± 3,20	30,51± 1,81*	72,62± 1,32	19,81± 1,07	50,23± 3,07	24,17± 0,63	17,17± 0,40
AL	42,58± 1,70*	22,21± 0,24 ***Δ**	48,94± 0,44*	13,52± 0,43*	29,75± 0,80* **Δ**	19,58± 0,61* **Δ**	12,50± 051*
DB	47,57± 0,97*	30,13± 1,74	50,02± 0,17*	13,58± 0,20*	34,91± 0,52*	23,00± 0,52	12,42± 0,52*
DBAL	62,00± 1,28**Δα**	24,62± 0,25***Δα**	72,18± 0,50**Δα**	16,11± 0,29**Δα**	54,07± 0,14**Δα**	23,67± 0,65α	16,88± 0,40**Δα**

'*' indicates significant difference compared to NC, **'Δ'** against DB and 'α' against AL. The data is presented as Mean± SEM.

Key: NC= negative control; DB= diabetes; AL= alcohol; DBAL= diabetes and alcohol.

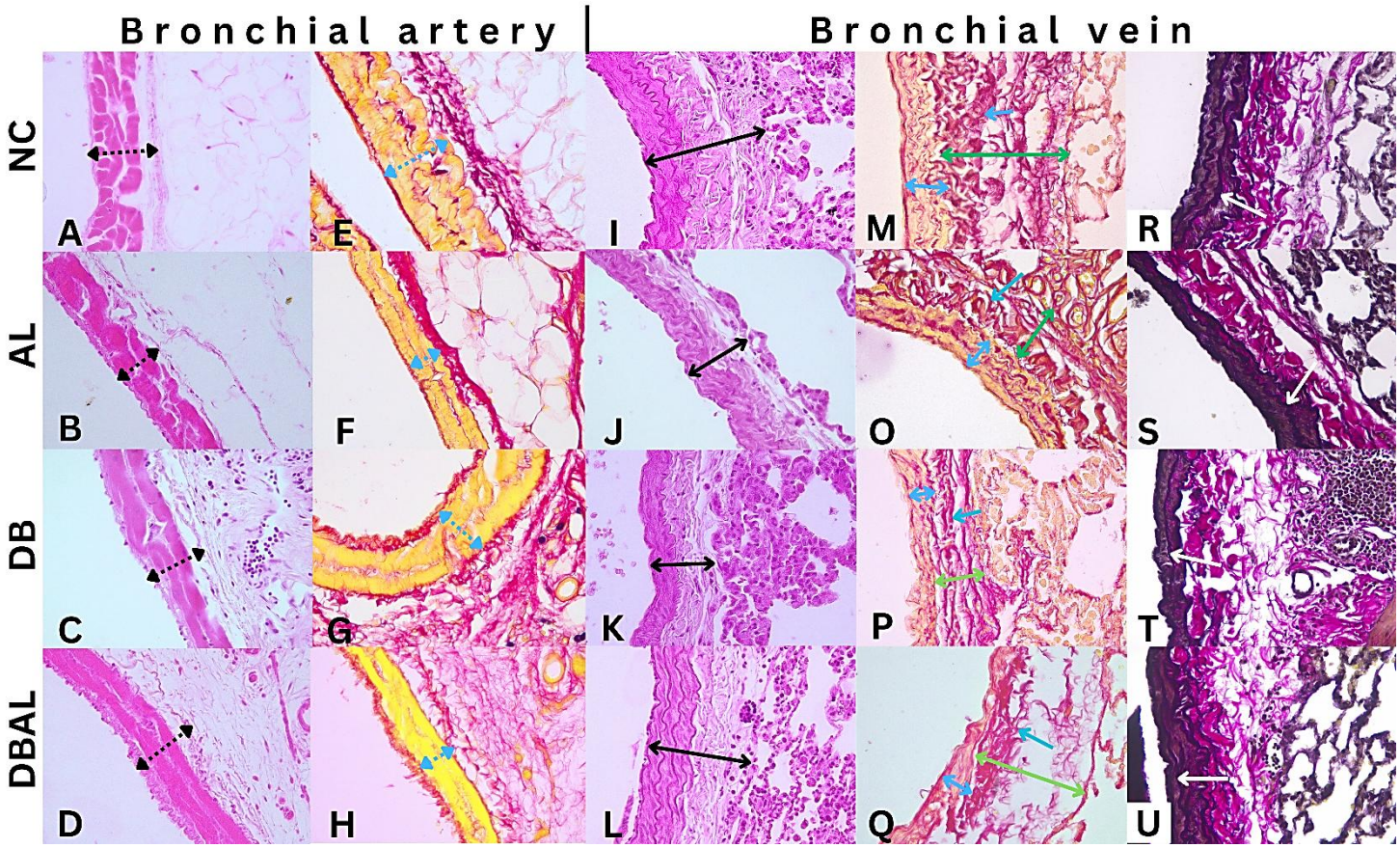

Figure 4.25: Bronchial Artery (Tunica Media and Adventitia Thickness) and Vein (Wall, Tunica Media and Adventitia Thickness, and Collagen and Elastic Fibre Profile).

Black broken double arrow: Arterial wall thickness, blue broken double arrow: Arterial tunica media thickness, black double arrow: Venal wall thickness, blue double arrow: Venal tunica media thickness, green double arrow: Venal tunica adventitia thickness, single blue arrow: Venal collagen fibres, single while arrow: Venal elastic fibres.

Key: NC= negative control; DB= diabetes; AL= alcohol; DBAL= diabetes and alcohol.

4.2.7. Parenchymal Collagen, Reticular and Elastic Fibre Profile.

The parenchymal collagen, reticular and elastic fibre profile are shown in Figure 4.26 and summarized in Table 4.4. Significant difference across groups was observed in parenchymal collagen (Fig. 26A-D), reticular (Fig. 26E-H), and elastic fibre profile (Fig. 26I-L) (One-way ANOVA, p <0,001 respectively). Groups AL and DB showed a significant increase in collagen fibre profile compared to NC (Independent-Samples T Test, p< 0.001 respectively, Table. 4.4). Moreover, AL showed a significant increase in parenchymal collagen content against DB (Independent-Samples T Test, p< 0.001, Table. 4.4) and DBAL a significant decrease against DB and AL (Independent-Samples T Test, p< 0.001 respectively, Table. 4.4). Groups AL and DB showed a significant increase in parenchymal reticular fibre content compared to NC (Independent-Samples T Test, p< 0.001 respectively, Table. 4.4) whereas DBAL showed a significant decrease compared to DB and AL (Independent-Samples T Test, p< 0.001 respectively, Table. 4.4). For elastic fibre profile, AL and DB showed a significant decrease compared to NC (Independent-Samples T Test, p< 0.001 respectively, Table. 4.4) while DBAL showed a significant increase compared to DB and AL (Independent-Samples T Test, p< 0.001 respectively, Table. 4.4).

Table 4.4: Parenchymal Collagen, Reticular and Elastic Fibre Profile.

Groups	Collagen Fibre Profile (%Area)	Reticular Fibre Profile (%Area)	Elastic Fibre Profile (%Area)
NC	14,50± 0,40	10,00± 0,56	22,13± 1,12
AL	23,19± 0,65***Δ**	16,64± 0,48*	13,31± 0,40*
DB	18,00± 0,32*	15,63± 0,33*	13,88± 0,57*
DBAL	14,25± 0,29**Δα**	9,38± 0,64**Δα**	23,06± 0,90**Δα**

'*' indicates significant difference compared to NC, **'Δ'** against DB and 'α' against AL. The data is presented as Mean± SEM.

Key: NC= negative control; DB= diabetes; AL= alcohol; DBAL= diabetes and alcohol.

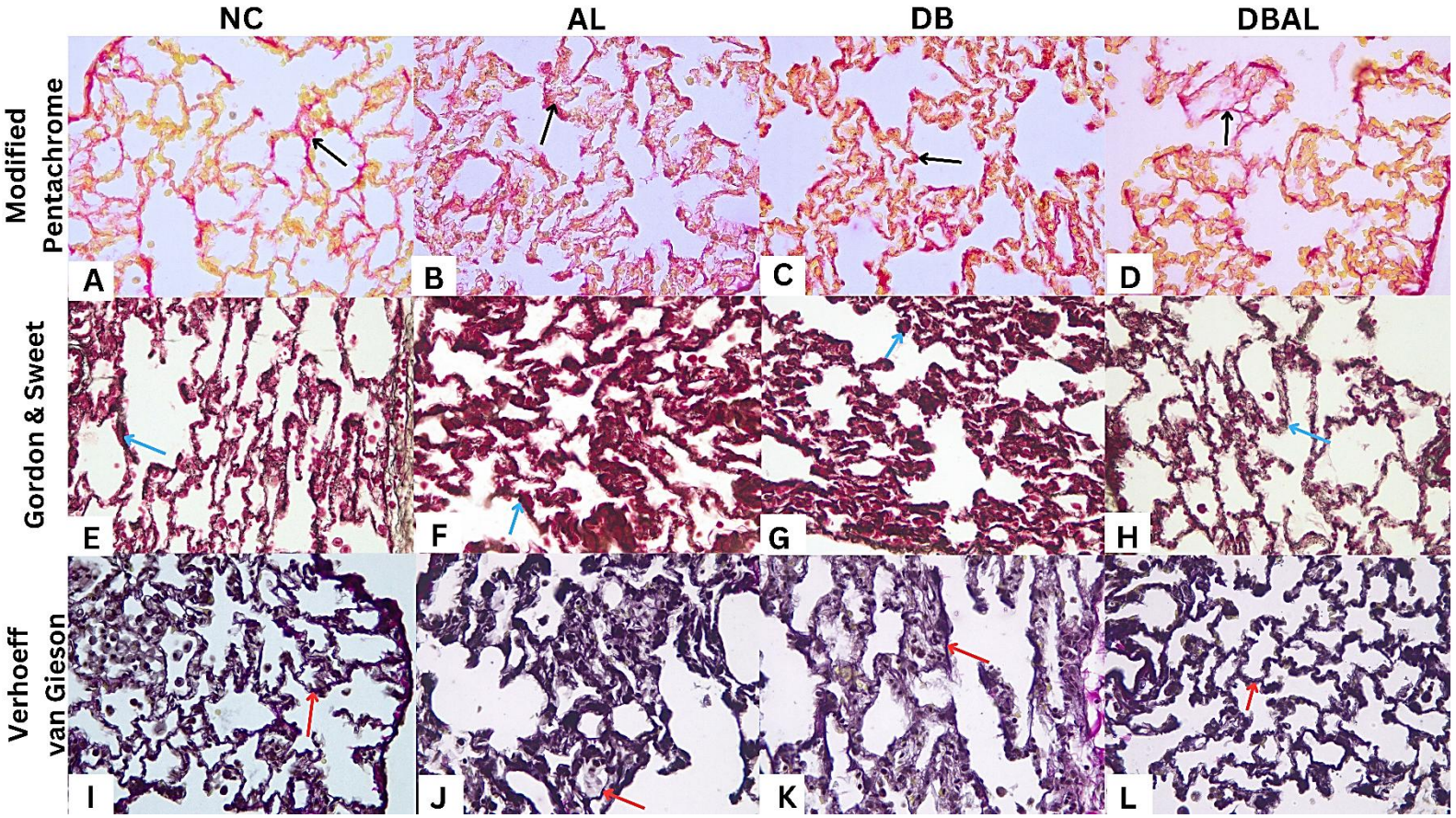

Figure 4.26: Parenchymal Collagen, Reticular and Elastic Fibre Profile.

Black single arrow: collagen fibres (stained red), blue single arrow: reticular fibres (stained black) and red single arrow: elastic fibres (stained black). **Key:** NC= negative control; DB= diabetes; AL= alcohol; DBAL= diabetes and alcohol.

4.2.8. Immunohistochemical Analysis.

4.2.8.1. C-Reactive Protein IHC Expression.

The respiratory immunohistochemistry of CRP was performed and presented in Figure 4.27 for bronchiole and alveolar spaces and Figure 4.28 for bronchial artery and vein. The expression was observed in the bronchiole, bronchial artery, vein and alveoli. In the bronchiole (Fig. 4.27A-D), all groups showed epithelial CRP expression and the presence of luminal macrophages, however, pronounced in DB and DBAL with additional expression within the muscularis mucosa. The NC group showed minimal alveolar macrophage nuclei CRP expression in contrast to the treated groups with pronounced expression, in addition to clusters of pneumocytes II (Fig. 4.27E-H). Further, all treated groups showed CRP expression in the bronchial artery (Fig. 4.28A-D) and vein (Fig. 4.28E-H) smooth muscle, additionally, DBAL also showed expression in the endothelium of the bronchial vein.

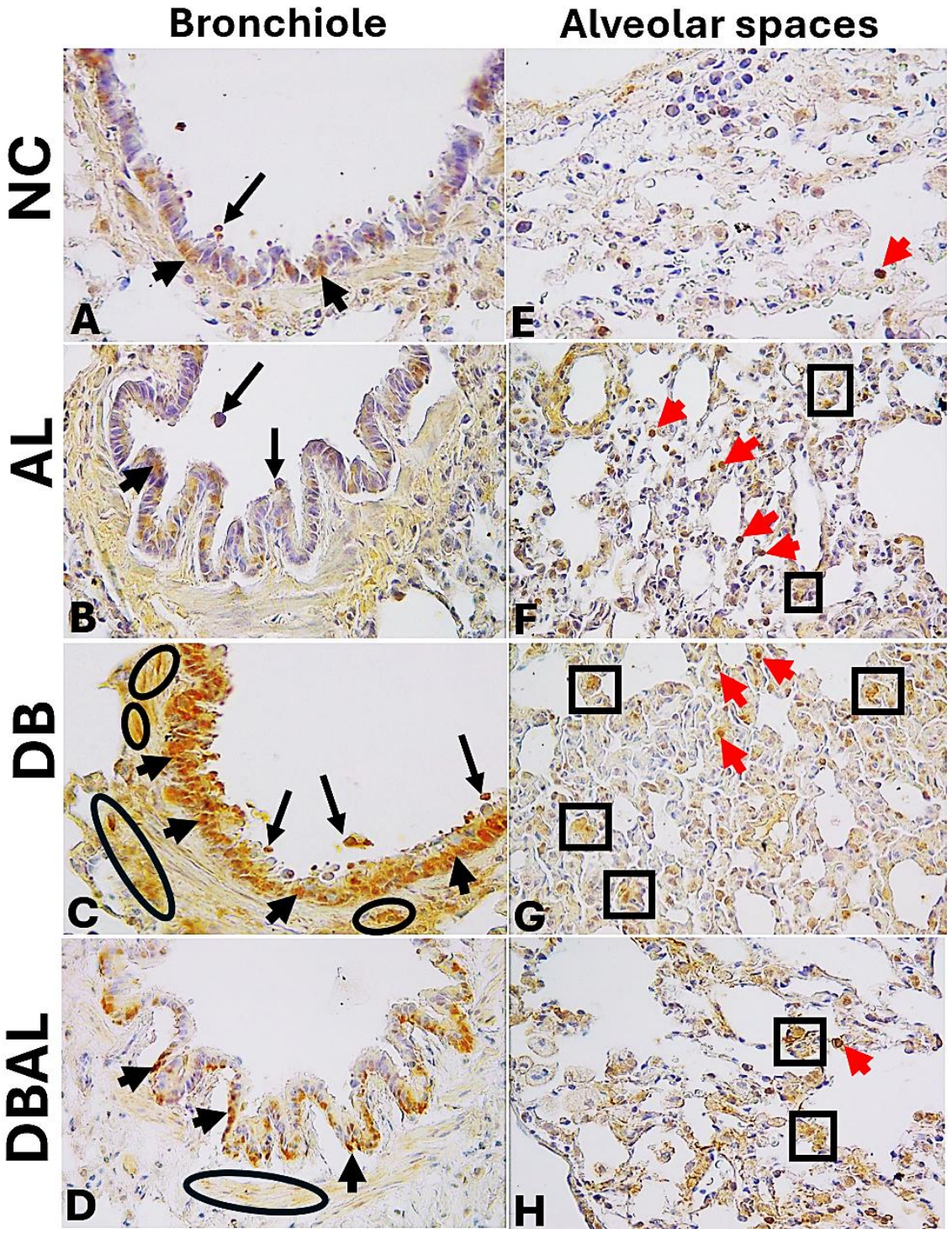

Figure 4.27: CRP Expression in The Bronchiole and Alveolar Spaces.

CRP expression: Black arrowhead- bronchiole epithelium cytoplasm, black arrow- macrophage nuclei (bronchiole lumen), oval circle- smooth muscle (muscularis mucosa) red arrowhead- alveolar macrophage nuclei, and black square- pneumocytes II nuclei cluster.

Key: NC= negative control; DB= diabetes; AL= alcohol; DBAL= diabetes and alcohol.

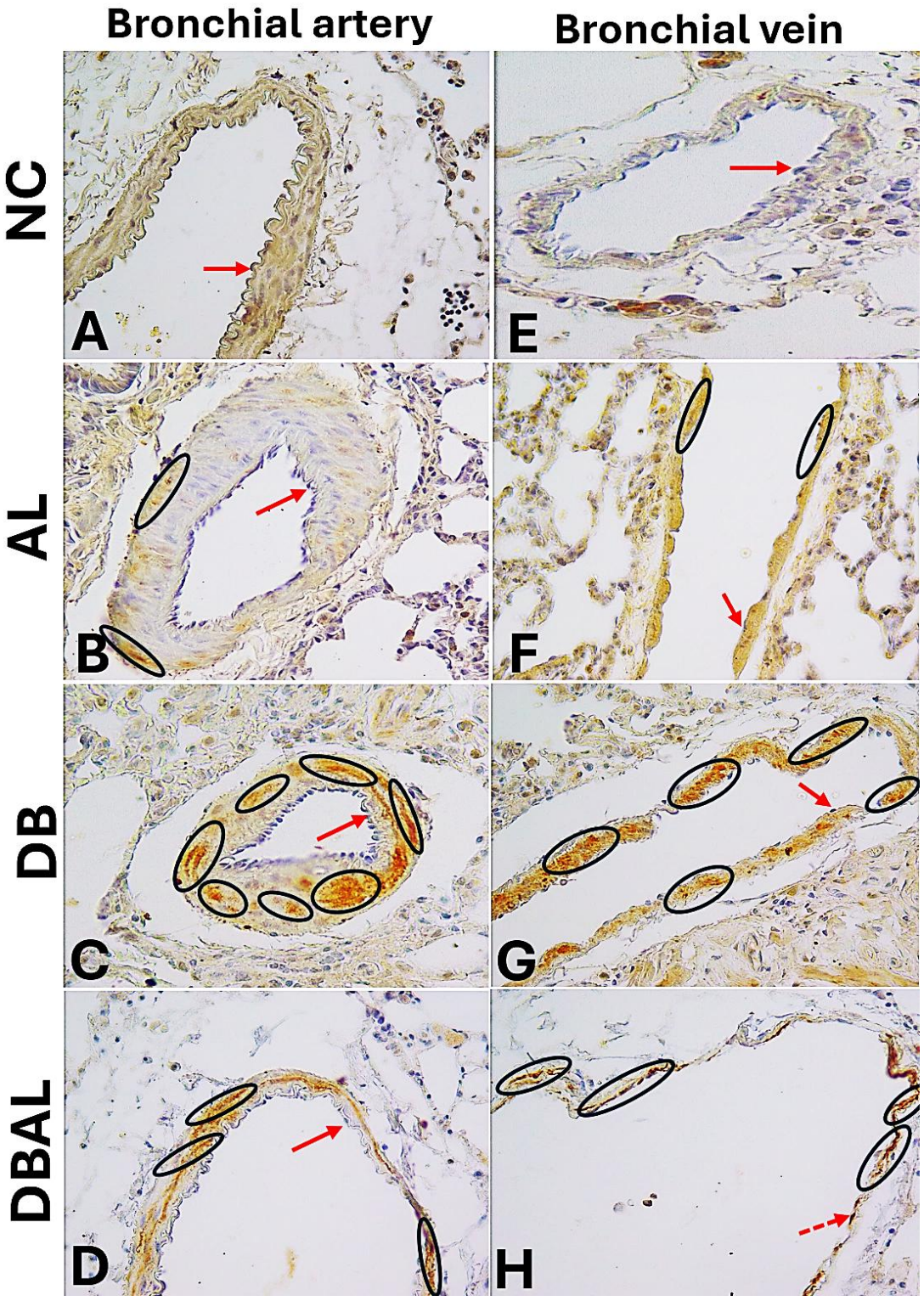

Figure 4.28: CRP Expression in The Bronchial Artery and Vein.

CRP expression: Oval circle- smooth muscle (bronchial vein, and artery), red arrow- endothelium (non-expression), broken red arrow- endothelium (expression).

Key: NC= negative control; DB= diabetes; AL= alcohol; DBAL= diabetes and alcohol.

4.2.8.2. TGFβ1, MDA and Caspase 3 Trials.

Optimization was performed for the expression of TGFβ1, MDA and Caspase 3 in the parenchyma (Fig. 4.29A, C and E) and bronchial vein (Fig. 4.29B, D and F) and the trials are presented. Several factors were calibrated including secondary antibody, primary antibody dilution (1: 100, 1: 300, 1:500 and 1:1000), ABC kit and antigen retrieval in EDTA vs citrate buffer. But no expression in positive controls within the bronchial vein and the parenchyma was observed for TGFβ1 (Fig. 4.29A-B), MDA (Fig. 4.29C-D) and Caspase 3 (Fig. 4.29E-F).

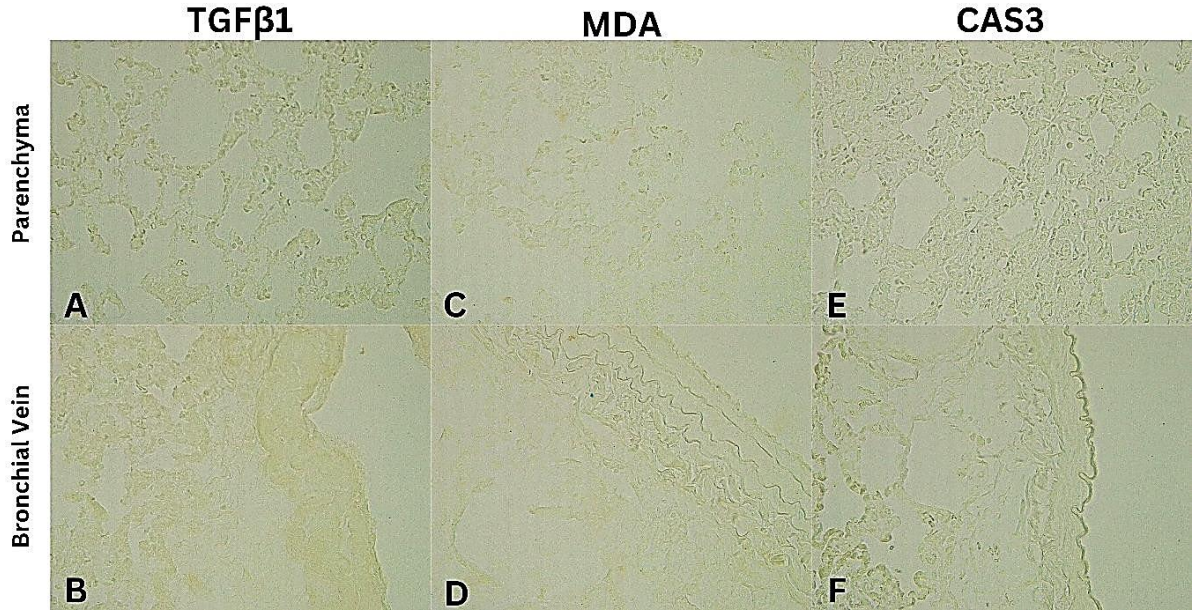

Figure 4.29: Non-expression trials for TGFβ1, MDA, and Caspase 3.

Key; (A-B), bronchial vein, and parenchyma observed for TGFβ1**, (C-D),** bronchial vein, and parenchyma observed for MDA**; (E-F)** bronchial vein, and parenchyma observed for Caspase 3.

CHAPTER FIVE: Discussion

The rollout of cART treatment to the broader population continues to rise, mainly to manage and prevent HIV transmission on the backdrop of increasing alcohol abuse and incidences of diabetes. These are lifestyle factors (alcohol abuse, sedentary life, diabetes etc) affecting the human population, especially in developing countries. While the independent effects of these factors on the respiratory system are documented (Twigg III *et al*., 2017; Knoop *et al*., 2018; Kaphalia *et al*., 2024), the possible toxicity or otherwise arising from their coexistence in HIV-negative individuals, especially on the respiratory system, is undocumented.

The results indicate successful induction of diabetes, consistent with similar studies with significantly increased biweekly blood glucose levels since week 2 of the study in diabetic groups throughout the treatment duration compared to non-diabetic groups (Ghasemi and Jeddi, 2023). Further, the results suggest that cART administration in diabetes (CADB) interactively significantly exacerbated increases in blood glucose levels (i.e. augments diabetic condition) more than cART and alcohol (AL) interaction. This supplements previous studies that reported diabetes mellitus incidences in HIV patients following cART treatment initiation (Moyo *et al*., 2014; Hailu *et al*., 2021). Additionally, alcohol and cART administration in diabetes (CAALDB) less significantly increased blood glucose levels compared to administration of only cART in diabetes.

The significantly increased mean body and lung weights observed in the cART (CA) treated group compared to the control (NC) group was contrary to decreases in mean body and lung weights observed in all the treated groups, in alcohol (AL), diabetes (DB) and diabetes+alcohol (DBAL), cART+alcohol (CAAL), cART+diabetes (CADB) and cART, alcohol and diabetes (CAALDB). The decreased mean body and lungs weights recorded in the treatment groups compared to the increases in cART (CA) treated group, suggest that cART (CA) influenced body weight increases, which is parallel with the report of other studies that highlight body weight increase in HIV-negative individuals on preexposure cART therapy (Wohl *et al*., 2024). But cART in combination with alcohol, diabetes and/or both (i.e. CAAL, CADB and/or both CAALDB) interactively led to greater mean body and lung weights losses similar to DBAL combination treatment. The highest mean body and lungs weight reductions recorded in CAALDB and CADB groups respectively, may point to differential but more adverse effects of the respective treatments on body and organ weights which corroborate with a previous report (Chao *et al*., 2019). The increases in mean relative lung weight across the treatment groups correlate with the decreases in body weight which points to proper application of the technique

and treatments effects. The mean lung surface area was significantly reduced in the treated groups except in cART-treated group compared to control (NC), suggesting that alcohol (AL) consumption in diabetes could result in organ shrinkage and consequently reduced surface area. Though cART treatment alone did not cause changes in the organ surface area, the reductions recorded in the combination treatment groups (CAAL, CADB, CAALDB) might be associated with cART since no reductions were recorded in DBAL treated group suggesting possible cART interaction with alcohol, diabetes or both.

The cART treatment (CA) showed antioxidant capacity through GPx1 increase, which is contrary to previous reports of increased oxidative stress and reduced antioxidant enzymes in HIV-infected individuals on cART (Ivanov *et al*., 2016; Yeligar *et al*., 2017; Konstantinidis *et al*., 2023). Such disparity in the results could be due to the presence and absence of HIV virus in the previous and present study respectively. Biochemical analysis signifies the presence of oxidative stress (particularly lipid peroxidation), and susceptibility to toxicity (cellular damage) with the increased MDA levels associated with alcohol (AL), diabetes (DB), cART-diabetes (CADB) and cART-alcohol-diabetes (CAALDB) combination exposures. Correspondingly, the slight increases in GPx1 levels in AL, DB and CA against the NC group, while suggesting very minimal oxidative stress, the highly significant decreases in CADB and CAALDB treated groups imply increased toxicity and cellular damage following heightened oxidative stress in the cART-diabetes (CADB) and cART-alcohol-diabetes (CAALDB) exposure combinations. The heightened oxidative stress in CADB and CAALDB treated groups is substantiated by the significantly increased MDA to GPx1 ratios.

The mean trachea and bronchiole epithelial heights were significantly reduced in all the treatment groups against the control (NC) except the tracheal epithelium in cART (CA) treated group. This may lead to reduction in the trapping of dust particles and microorganisms in the respiratory passage, implicating these treatment combinations in reducing optimal air transport function of the respiratory epithelium and probably the dysfunction of the overall respiratory system (Kiyota *et al*., 2014). Another study highlighted chronic alcohol consumption capacity to impair mucous and ciliary functioning of the respiratory lining (Sisson, 2007). Also, an analysis of respiratory functioning in HIV individuals with history of heavy alcohol consumption had reported disruption of epithelial barrier integrity (New-Aaron *et al*., 2024). Additionally, the mean tracheal cartilage width and lacuna were significantly reduced across the treatment groups against the control (NC), except in diabetes-alcohol (DBAL) treated. Such changes signify adverse effects on the cytomorphological integrity of the trachea, and consequently, may lead to structural

dysfunction (Khalid and O'Leary, 2023).

The bronchiole muscularis mucosa width significantly increased in diabetes (DB) and diabetes-alcohol treated (DBAL) groups but was significantly decreased in CAAL combination exposure compared to the control. While cART (CA) and alcohol (AL) independently did not affect the bronchiole muscularis mucosa width, they significantly increased the bronchial reticular fibre content against the control (NC), DBAL, CAAL, CADB & CAALDB treated groups. However, cART in combination with alcohol (CAAL) significantly reduced bronchial reticular fibres contrary to their independent effects, which may imply enhanced bronchial elasticity in independent CA and AL treated groups but interactively antagonize each other with resultant impairment of elasticity which corroborates with a previous report (Brusasco and Martinez, 2014).

Furthermore, the bronchial arterial wall and tunica media thicknesses were generally reduced across the treatments. However, significant reductions were recorded in both parameters in alcohol (AL), but only arterial wall thickness in diabetic group (DB) and tunica media in diabetes-alcohol combined (DBAL) treatment, indicating the differential effects of the treatments and suggests that alcohol may have a greater adverse impact on the bronchial arterial wall components than diabetes and when both are combined. Interestingly, while no significant changes were recorded in both parameters in cART (CA), CAAL and CADB treated groups, significant reduction was recorded in combination of the three factors (CAALDB), suggesting that vascular wall shrinkage defect may emanate from interactive effects of cART-alcohol therapy in diabetes.

The treatments showed slightly more severe effects with recorded significant reductions on bronchial vein morphometry (tunica media and tunica adventitia thicknesses) in alcohol and diabetes independent exposures against the effects on the arterial wall. The differential effects on the wall and media thickness of the bronchial artery and vein may be associated with the differences in structural configuration of these vessels relative to their functional requirements (Zhou *et al*., 2023). Though cART treatment recorded minimal reduction in the wall thickness of bronchial vein, significant reductions were recorded in combination with alcohol (CAAL), diabetes (CADB) and both (CAALDB) compared to control (NC) pointing to combinatorial impact of cART with alcohol, diabetes and both on the pulmonary venular system. Covid 19 reported deaths were significantly high amongst HIV/AIDS patients on cART regimen and with diabetes, high blood pressure and other related co-morbidities (Mellor et al., 2021; Ssentongo et al., 2021). Furthermore, significant reductions recorded in the thickness of adventitia in all the treatment groups with highest reduction in CA and CAALDB treatments, generally, may lead to

distorted functional efficiency of the vasculature and consequently dysfunction (Tai *et al*., 2021). Moreover, significant reductions recorded in venal fibre profiles in collagen (in AL, CADB and CAALDB) and elastic fibre (in AL, DB, CAAL) compared to NC, signifies reductions in some extra cellular matrix (ECM) structures, with consequent reductions in the rigidity and contractility property of the bronchial vein which may lead to pulmonary disorders such as pulmonary hypertension (Schermuly *et al*., 2011). Therefore, the recorded adverse effects on the vascular structural components following the treatments infer adverse structural effects and perturbations on their functional competences (Suresh and Shimoda, 2016).

Additionally, the pulmonary parenchymal collagen fibre content of bronchial arterial and vein was increased in all the treatments groups but decreased in DBAL and CAALDB groups against control (NC). While the significant increases in collagen fibre profile may lead to increased rigidity of the parenchyma, the reductions in CAALDB-treated group suggests contrary effect on the parenchyma structure. These differential effects could emanate from the interactive effects of the different combination treatments and imply slight amelioration of the effect. Similarly, the increased lung parenchyma reticular fibre profile in CAALDB and the significant reductions in cART-alcohol, and cART-diabetes combination treatments demonstrate different modulating effects of these treatment combinations, but the mechanism behind modulating effects is beyond the scope of the present study and requires further investigations. Also, the significant reductions in elastic fibre content in the AL, DB, CAAL, CADB and CAALDB groups, and lack of any change in CA treated group compared to control group mirrored the treatments effects on collagen and reticular fibres. Altogether, the results present variable adverse impact on the respiratory connective tissue fibres and function of the lungs relative to pulmonary contractility and relaxation movements (Jagadapillai *et al*., 2016; Galicia-Garcia *et al*., 2020).

Furthermore, alcohol (AL)-induced CRP expression was minimal in the bronchial epithelium and luminal macrophages, as well as in the vascular smooth muscles, but it was prominent in the parenchymal alveolar macrophages and pneumocyte II clusters. The minimal expression of CRP in alcohol-treated lung lining and vasculature is congruent with other findings that linked chronic alcohol use in middle-agers with low systemic CRP expression and consequently anti-inflammatory impact (Raum *et al*., 2007). The cART (CA) treatment increased CRP expression in bronchiole luminal macrophages, vascular smooth muscle, type II pneumocyte clusters and alveolar macrophages. This highlights the cART -associated inflammatory induction involving respiratory/the body's immune system signifying the toxicity of cART morbidities, and contrasts with a study in the United States that reported reduced inflammatory cytokines and chemokines

in HIV patients on cART (Twigg III *et al*., 2017). Such inconsistency can be implicated on the HIV-negative model of the present study compared to the reported study. The pronounced expression across the respiratory tree is a course for concern especially in cART-diabetes and cART-alcohol-diabetes treatment combinations. Correspondingly, studies have reported persistent cART-induced pulmonary CRP expression in HIV-infected individuals which later develop into chronic inflammation (Sereti *et al*., 2017; Cai and Sereti, 2021), but other studies align with pulmonary CRP upregulation observed in diabetes-treated groups (i.e. DB, CADB & CAALDB) (Stanimirovic *et al*., 2022).

CHAPTER SIX: Conclusion

The present study reports the intricate combination of cART, diabetes, and alcohol on HIV-naïve respiratory health. The interaction of these three factors intensifies hyperglycemia, oxidative stress, and pulmonary inflammation while inducing histological alterations including vascular atrophy and parenchymal fibre remodeling. These findings highlight the exacerbation of pulmonary vascular toxicity of cART and alcohol in diabetes. which potentially may lead to impaired respiratory lining epithelium. Moreover, the altered pulmonary fibre composition suggests compromised pulmonary microstructure and associated dysfunction. Mainly, the coexistence of these three factors imposes significant additive damage to the respiratory system, with diabetes acting as a multifaceted exacerbator while cART and alcohol exhibit both harmful and modulatory roles in different combinations. Indeed, alcohol demonstrates limited attenuative effects on oxidative stress and parenchymal fibrosis when combined with cART and diabetes.

The current research emphasizes the need for clinical management strategies, particularly in developing countries with high occurrence of this multiple morbidity. Further research should delve into the pathways and mechanisms that govern the interactions between these factors considering how they affect the respiratory system, and potentially other organ systems such as the cardiovascular and nervous system.

REFERENCES

1. Abu-Abeeleh, M., Bani Ismail, Z. A., Alzaben, K. R., Abu-Halaweh, S. A., Aloweidi, A. S., Al-Ammouri, I. A., Al-Essa, M. K., Jabaiti, S. K., Abu-Abeeleh, J., Alsmady, M. M., & Alshobaki, O. (2010). A preliminary study of the use of human adipose tissue-derived stem cells for the treatment of streptozotocin-induced diabetes mellitus in a rat model. *Comparative Clinical Pathology, 19(1),* 1–4. https://doi.org/10.1007/s00580-009-0912-x
2. Agarwal, V., Gupta, A., & Mehrotra, M. K. (2021). Relation of FEV1/FVC in Type 2 Diabetes Mellitus Patients. *International Journal of Science and Research*. https://doi.org/10.21275/SR211014224603
3. Agassandian, M., Shurin, G. V., Ma, Y., & Shurin, M. R. (2014). C-reactive protein and lung diseases. *The International Journal of Biochemistry & Cell Biology*, *53*, 77–88. https://doi.org/10.1016/j.biocel.2014.05.016
4. Albert, M. A., Glynn, R. J., & Ridker, P. M. (2003). Alcohol consumption and plasma concentration of C-reactive protein. *Circulation*, *107*(3), 443–447. https://doi.org/10.1161/01.CIR.0000045669.16499.EC
5. Alexandrova, Y., Costiniuk, C. T., & Jenabian, M. A. (2022). Pulmonary Immune Dysregulation and Viral Persistence During HIV Infection. *Frontiers in Immunology*, *12*, 808722. https://doi.org/10.3389/FIMMU.2021.808722/PDF
6. Alvarado, A., & Arce, I. (2016). Metabolic Functions of the Lung, Disorders and Associated Pathologies. *Journal of Clinical Medicine Research, 8(10),* 689–700. https://doi.org/10.14740/jocmr2668w
7. American Diabetes Association. (2010). Diagnosis and Classification of Diabetes Mellitus. *Diabetes Care*, *33*(1), S62–S69. https://doi.org/10.2337/dc10- S062
8. Arafath, S., Campbell, T., Yusuff, J., & Sharma, R. (2018). Prevalence of and Risk Factors for Prediabetes in Patients Infected With HIV. *Diabetes Spectrum*, *31*(2), 139–143. https://doi.org/10.2337/DS17-0009
9. Asouzu Johnson, J., Ndou, R., & Mbajiorgu, E. F. (2023). Interactions of alcohol and combination antiretroviral (cART) drug in diabetic male Sprague Dawley rats: Hippocampal perturbations and toxicosis. *Toxicology Reports*, *10*, 155–170.

https://doi.org/10.1016/J.TOXREP.2023.01.009

10. Baeten, J. M., Donnell, D., Ndase, P., Mugo, N. R., Campbell, J. D., Wangisi, J., Tappero, J. W., Bukusi, E. A., Cohen, C. R., Katabira, E., Ronald, A., Tumwesigye, E., Were, E., Fife, K. H., Kiarie, J., Farquhar, C., John-Stewart, G., Kakia, A., Odoyo, J., & Celum, C. (2012). Antiretroviral Prophylaxis for HIV Prevention in Heterosexual Men and Women. *New England Journal of Medicine*, *367*(5), 399–410. https://doi.org/10.1056/NEJMoa1108524

11. Bailin, S. S., Gabriel, C. L., Wanjalla, C. N., & Koethe, J. R. (2020). Obesity and Weight Gain in Persons with HIV. *Current HIV/AIDS Reports*, *17*(2), 138–150. https://doi.org/10.1007/S11904-020-00483-5/FIGURES/1

12. Balansky, R., Ganchev, G., Iltcheva, M., Nikolov, M., La Maestra, S., Micale, R. T., Steele, V. E., & De Flora, S. (2016). Interactions between ethanol and cigarette smoke in a mouse lung carcinogenesis model. *Toxicology*, *373*, 54–62. https://doi.org/10.1016/j.tox.2016.11.008

13. Bara, I., Ozier, A., Tunon de Lara, J.-M., Marthan, R., & Berger, P. (2010). Pathophysiology of bronchial smooth muscle remodelling in asthma. *European Respiratory Journal*, *36*(5), 1174–1184. https://doi.org/10.1183/09031936.00019810

14. Baum, M. K., Tamargo, J. A., Diaz-Martinez, J., Delgado-Enciso, I., Meade, C. S., Kirk, G. D., Mehta, S. H., Moore, R., Kipke, M. D., Shoptaw, S. J., Mustanski, B., Mandler, R. N., Khalsa, J. H., Siminski, S., Javanbakht, M., & Gorbach, P. M. (2022). HIV, psychological resilience, and substance misuse during the COVID-19 pandemic: A multi-cohort study. *Drug and Alcohol Dependence*, *231*, 109230. https://doi.org/10.1016/J.DRUGALCDEP.2021.109230

15. Be in the KNOW (2023). Origin of HIV and AIDS. Retrieved 8 March 2025, from https://www.beintheknow.org/understanding-hiv-epidemic/context/origin-hiv-and-aids

16. Bektas, A., Sen, R., & Ferrucci, L. (2016). Does a bit of alcohol turn off inflammation and improve health? *Age and Ageing*, *45*(6), 747–748. https://doi.org/10.1093/AGEING/AFW146

17. Birbrair, A., Zhang, T., & Files, D.C. (2014). Type-1 pericytes accumulate after tissue injury and produce collagen in an organ-dependent manner. *Stem Cell Res Ther, 5*, 122.

https://doi.org/10.1186/scrt512

18. Bjerk, S. M., Baker, J. V., Emery, S., Neuhaus, J., Angus, B., Gordin, F. M., Pett, S. L., Stephan, C., & Kunisaki, K. M. (2013). Biomarkers and Bacterial Pneumonia Risk in Patients with Treated HIV Infection: A Case-Control Study. *PLOS ONE*, *8*(2), e56249. https://doi.org/10.1371/JOURNAL.PONE.0056249

19. Bogers, S. J., Schim van der Loeff, M. F., Davidovich, U., Boyd, A., van der Valk, M., Brinkman, K., de Bree, G. J., Reiss, P., van Bergen, J. E. A. M., Geerlings, S. E., van Bergen, J. E. A. M., Brokx, P., Deug, F., Heidenrijk, M., Prins, M., Reiss, P., de Bree, G. J., Brokx, P., Davidovich, U., & Zimmermann, H. M. L. (2021). Promoting HIV indicator condition-guided testing in hospital settings (PROTEST 2.0): study protocol for a multicentre interventional study. *BMC Infectious Diseases*, *21*(1). https://doi.org/10.1186/S12879-021-06183-8

20. Boras, E., Slevin, M., Alexander, M. Y., Aljohi, A., Gilmore, W., Ashworth, J., Krupinski, J., Potempa, L. A., Al Abdulkareem, I., Elobeid, A., & Matou-Nasri, S. (2014). Monomeric C-reactive protein and Notch-3 co-operatively increase angiogenesis through PI3K signalling pathway. *Cytokine*, *69*(2), 165–179. https://doi.org/10.1016/J.CYTO.2014.05.027

21. Brown, L. A. S., Harris, F. L., Ping, X.-D., & Gauthier, T. W. (2004). Chronic alcohol ingestion and the risk of acute lung injury: a role for glutathione availability. *Alcohol, 33(3),* 191–197. https://doi.org/10.1016/j.alcohol.2004.08.002

22. Brusasco, V., & Martinez, F. (2014). Chronic obstructive pulmonary disease. Comprehensive Physiology, 4(1), 1–31. https://doi.org/10.1002/cphy.c110037

23. Bryda, E. (2013). The Mighty Mouse: The Impact of Rodents on Advances in Biomedical Research. Mo Med, 1103, 207–211. https://pubmed.ncbi.nlm.nih.gov/23829104/

24. Burnham, E. L., Halkar, R., Burks, M., & Moss, M. (2009). The Effects of Alcohol Abuse on Pulmonary Alveolar-Capillary Barrier Function in Humans. *Alcohol and Alcoholism*, *44*(1), 8–12. https://doi.org/10.1093/ALCALC/AGN051

25. Cai, C. W., & Sereti, I. (2021). Residual Immune Dysfunction Under Antiretroviral Therapy. *Seminars in Immunology*, *51*, 101471. https://doi.org/10.1016/J.SMIM.2021.101471

26. Canadian Foundation for AIDS Research (2017). History of HIV/AIDS. Retrieved 8 March

2025, from https://canfar.com/awareness/about-hiv-aids/history-of-hiv-aids/

27. Caterino-de-Araujo, A., Campos, K. R., Oliveira, L. M. S., & Rigato, P. O. (2022). Biomarkers in a Cohort of HIV-Infected Patients Single- or Co-Infected with HTLV-1, HTLV-2, and/or HCV: A Cross-Sectional, Observational Study. Viruses, 14(9). https://doi.org/10.3390/V14091955

28. Cerrada, A., Haller, T., Cruz, A., & Pérez-Gil, J. (2015). Pneumocytes Assemble Lung Surfactant as Highly Packed/Dehydrated States with Optimal Surface Activity. *Biophysical Journal*, *109*(11), 2295–2306. https://doi.org/10.1016/j.bpj.2015.10.022

29. Chao, A. M., Wadden, T. A., Tronieri, J. S., & Berkowitz, R. I. (2019). Alcohol Intake and Weight Loss During Intensive Lifestyle Intervention for Adults with Overweight or Obesity and Diabetes. *Obesity*, *27*(1), 30–40. https://doi.org/10.1002/oby.22316

30. Chaudhry, R., Omole, A. E., & Bordoni, B. (2024). Anatomy, Thorax, Lungs. *Treasure Island (FL): StatPearls Publishing.* https://www.ncbi.nlm.nih.gov/books/NBK470197/

31. Clumeck, N., Pozniak, A., & Raffi, F. (2008). European AIDS Clinical Society (EACS) guidelines for the clinical management and treatment of HIV-infected adults. *HIV Medicine*, *9*(2), 65–71. https://doi.org/10.1111/j.1468-1293.2007.00533.x

32. Deeks, E. D., & Perry, C. M. (2010). Efavirenz/Emtricitabine/Tenofovir Disoproxil Fumarate Single-Tablet Regimen (Atripla®). *Drugs,* 70(17). https://doi.org/10.2165/11203800-000000000-00000

33. Dungu, A. M., Ryrsø, C. K., Hegelund, M. H., Jensen, A. V., Kristensen, P. L., Krogh- Madsen, R., Ritz, C., Faurholt-Jepsen, D., & Lindegaard, B. (2023). Diabetes Status, c- Reactive Protein, and Insulin Resistance in Community-Acquired Pneumonia—A Prospective Cohort Study. Journal of Clinical Medicine 2024, Vol. 13, Page 245, 13(1), 245. https://doi.org/10.3390/JCM13010245

34. Feng, J. R., Li, X., Han, C., Chang, Y., Fu, Y., Feng, G. C., Lei, Y., Li, H. Y., Tang, P. M. K., Ji, S. R., Hou, Y., & Wu, Y. (2024). C-Reactive Protein Induces Immunosuppression by Activating FcγR2B in Pulmonary Macrophages to Promote Lung Metastasis. *Cancer Research*, *84*(24), 4184–4198. https://doi.org/10.1158/0008-5472.can-24-0253/749005/am/c-reactive-protein-induces- immunosuppression-by

35. Fernandez-Bargiela, N., Rotea-Salvo, S., Margusino-Framiñán, L., Balboa-Barreiro,

V., Martín-Herranz, I., Castro-Iglesias, Á., Mena-De-Cea, Á., López-Calvo, S., Vázquez-Rodríguez, P., Míguez-Rey, E., & Cid-Silva, P. (2022). Discontinuation due to neuropsychiatric adverse events with efavirenz- and dolutegravir-based antiretroviral therapy: a comparative real-life study. Eur J Hosp Pharm, 29(4): 207- 211. https://doi.org/10.1136/ejhpharm-2020-002374

36. Ferreiro, J. L., & Angiolillo, D. J. (2011). Diabetes and antiplatelet therapy in acute coronary syndrome. Circulation, 123 (7), 798- 813. https://doi.org/10.1161/CIRCULATIONAHA.109.913376

37. Festa, A., D'Agostino, R., Tracy, R. P., & Haffner, S. M. (2002). Elevated Levels of Acute-Phase Proteins and Plasminogen Activator Inhibitor-1 Predict the Development of Type 2 Diabetes: The Insulin Resistance Atherosclerosis Study. *Diabetes*, *51*(4), 1131–1137. https://doi.org/10.2337/DIABETES.51.4.1131Fitzpatrick, M. E., Kunisaki, K. M., & Morris, A. (2018). Pulmonary Disease in HIV- Infected Adults in the Era of Antiretroviral Therapy. *AIDS (London, England)*, *32*(3), 277. https://doi.org/10.1097/QAD.0000000000001712

38. Forgiarini, L. A., Jr, Kretzmann, N. A., Porawski, M., Dias, A. S., & Marroni, N. A. (2009). Experimental diabetes mellitus: oxidative stress and changes in lung structure. *Jornal brasileiro de pneumologia: publicacao oficial da Sociedade Brasileira de Pneumologia e Tisilogia, 35(8),* 788–791. https://doi.org/10.1590/s1806-37132009000800011

39. Foster, D. J., Ravikumar, P., Bellotto, D. J., Unger, R. H., & Hsia, C. C. W. (2010). Fatty diabetic lung: altered alveolar structure and surfactant protein expression. *American Journal of Physiology-Lung Cellular and Molecular Physiology*, *298*(3), L392–L403. https://doi.org/10.1152/ajplung.00041.2009

40. Furman, B. L. (2021). Streptozotocin-Induced Diabetic Models in Mice and Rats. *Current Protocols*, *1*(4). https://doi.org/10.1002/CPZ1.78

41. Galicia-Garcia, U., Benito-Vicente, A., Jebari, S., Larrea-Sebal, A., Siddiqi, H., Uribe, K. B., Ostolaza, H., & Martín, C. (2020). Pathophysiology of Type 2 Diabetes Mellitus. *International Journal of Molecular Sciences*, *21*(17), 6275. https://doi.org/10.3390/IJMS21176275

42. Gambineri A., & Pelusi, C. (2019). Sex hormones, obesity and type 2 diabetes: is there a link. *Endocr Connect, 1; 8(1):* R1-R9. https://doi.org/10.1530/EC-18-0450.

43. García-Benayas, T., Rendón, A. L., Rodríguez-Novóa, S., Barrios, A., Maida, I., Blanco, F., Barreiro, P., Rivas, P., González-Lahoz, J., & Soriano, V. (2006). Higher risk of hyperglycemia in HIV-infected patients treated with didanosine plus tenofovir. *AIDS research and human retroviruses, 22(4),* 333–337. https://doi.org/10.1089/aid.2006.22.333

44. Gebrie, A., Tesfaye, B., Gebru, T., Adane, F., Abie, W., & Sisay, M. (2020). Diabetes mellitus and its associated risk factors in patients with human immunodeficiency virus on anti-retroviral therapy at referral hospitals of Northwest Ethiopia. *Diabetology & Metabolic Syndrome*, *12*(1), 20. https://doi.org/10.1186/s13098-020-00527-1

45. Ghasemi, A., & Jeddi, S. (2023). Streptozotocin as a tool for induction of rat models of diabetes: a practical guide. *EXCLI Journal, 22,* 274. https://doi.org/10.17179/EXCLI2022-5720

46. Gould, J. M., & Weiser, J. N. (2001). Expression of C-Reactive Protein in the Human Respiratory Tract. *Infection and Immunity*, *69*(3), 1747–1754. https://doi.org/10.1128/IAI.69.3.1747-1754.2001

47. Greene, W. C. (2007). A history of AIDS: looking back to see ahead. *European Journal of Immunology*, *37 Suppl 1*(SUPPL. 1). https://doi.org/10.1002/EJI.200737441

48. Green, A. S., & Grahame, N. J. (2008). Ethanol drinking in rodents: is free choice drinking related to the reinforcing effects of ethanol. *Alcohol (Fayetteville, N.Y.), 42(1),* 1–11. https://doi.org/10.1016/j.alcohol.2007.10.005

49. Guidot, D. M., & Hart, C. M. (2005). Alcohol abuse and acute lung injury: epidemiology and pathophysiology of a recently recognized association. *Journal of investigative medicine: the official publication of the American Federation for Clinical Research, 53(5),* 235–245. https://doi.org/10.2310/6650.2005.53506

50. Hailu, W., Tesfaye, T., & Tadesse, A. (2021). Hyperglycemia After Dolutegravir-Based Antiretroviral Therapy. *International Medical Case Reports Journal, 14,* 503. https://doi.org/10.2147/IMCRJ.S323233

51. Hale, Z. E., Singhal, A., & Hsia, R. Y. (2018). Causes of Shortness of Breath in the Acute Patient: A National Study. *Academic Emergency Medicine, 25(11),* 1227–1234.

https://doi.org/10.1111/ACEM.13448/FULL

52. Hamden, K., Carreau, S., Jamoussi, K., Miladi, S., Lajmi, S., Aloulou, D., Ayadi, F., & Elfeki, A. (2009). 1Alpha,25 dihydroxyvitamin D3: therapeutic and preventive effects against oxidative stress, hepatic, pancreatic and renal injury in alloxan-induced diabetes in rats. *Journal of nutritional science and vitaminology*, *55(3),* 215–222. https://doi.org/10.3177/jnsv.55.215

53. Harkema, J. R., Nikula, K. J., & Haschek, W. M. (2013). Respiratory System. In *Haschek and Rousseaux's Handbook of Toxicologic Pathology* (pp. 1935–2003). Elsevier. https://doi.org/10.1016/B978-0-12-415759-0.00051-0

54. Honnapurmath, V., & Patil, V. (2017). Antiretroviral therapy-induced insulin resistance and oxidative deoxy nucleic acid damage in human immunodeficiency virus-1 patients. *Indian Journal of Endocrinology and Metabolism*, *21*(2), 316. https://doi.org/10.4103/2230-8210.202029

55. Horberg, M., & Klein, D. B. (2010). An update on the use of Atripla® in the treatment of HIV in the United States. *HIV/AIDS - Research and Palliative Care*, 2, 135–140. https://doi.org/10.2147/HIV.S6366

56. Hukkanen, J., Pelkonen, O., Hakkola, J., & Raunio, H. (2002). Expression and Regulation of Xenobiotic-Metabolizing Cytochrome P450 (CYP) Enzymes in Human Lung. *Critical Reviews in Toxicology*, *32*(5), 391–411. https://doi.org/10.1080/20024091064273

57. Hurwitz, B. E., Klimas, N. G., & Llabre, M. M. (2004). Metabolic syndrome x, inflammation, oxidative stress and coronary heart disease risk. *Cardiovascular Toxicology, 4(3),* 303-315. https://doi.org/10.1385/ct:4:3:303

58. Ivanov, A. V., Valuev-Elliston, V. T., Ivanova, O. N., Kochetkov, S. N., Starodubova, E. S., Bartosch, B., & Isaguliants, M. G. (2016). Oxidative Stress during HIV Infection: Mechanisms and Consequences. *Oxidative Medicine and Cellular Longevity*, *2016*, 8910396. https://doi.org/10.1155/2016/8910396

59. Jagadapillai, R., Rane, M. J., Lin, X., Roberts, A. M., Hoyle, G. W., Cai, L., & Gozal, E. (2016). Diabetic Microvascular Disease and Pulmonary Fibrosis: The Contribution of Platelets and Systemic Inflammation. *International Journal of Molecular Sciences 2016, Vol. 17, Page 1853*, *17*(11), 1853. https://doi.org/10.3390/IJMS17111853

60. Jantarapakde, J., Phanuphak, N., Chaturawit, C., Pengnonyang, S., Mathajittiphan, P., Takamtha, P., Dungjun, N., Pinyakorn, S., Pima, W., Prasithsirikul, W., & Phanuphak, P. (2014). Prevalence of Metabolic Syndrome Among Antiretroviral-Naive and Antiretroviral-Experienced HIV-1 Infected Thai Adults. *AIDS Patient Care and STDs*, *28*(7), 331–340. https://doi.org/10.1089/apc.2013.0294

61. Jerrells, T. R., Pavlik, J. A., DeVasure, J., Vidlak, D., Costello, A., Strachota, J. M., & Wyatt, T. A. (2007). Association of chronic alcohol consumption and increased susceptibility to and pathogenic effects of pulmonary infection with respiratory syncytial virus in mice. *Alcohol*, *41*(5), 357–369. https://doi.org/10.1016/j.alcohol.2007.07.001

62. Jin, L., Wang, Z., & Qi, X. (2018). Diffuse idiopathic pulmonary neuroendocrine cell hyperplasia. *Medicine*, *97*(52), e13806. https://doi.org/10.1097/MD.0000000000013806

63. Joshi, P. C., Applewhite, L., Ritzenthaler, J. D., Roman, J., Fernandez, A. L., Eaton, D. C., Brown, L. A. S., & Guidot, D. M. (2005). Chronic Ethanol Ingestion in Rats Decreases Granulocyte-Macrophage Colony-Stimulating Factor Receptor Expression and Downstream Signaling in the Alveolar Macrophage. *The Journal of Immunology*, *175*(10), 6837–6845. https://doi.org/10.4049/jimmunol.175.10.6837

64. Joshi, P. C., & Guidot, D. M. (2007). The alcoholic lung: epidemiology, pathophysiology, and potential therapies. *American Journal of Physiology-Lung Cellular and Molecular Physiology, 292(4)*, L813–L823. https://doi.org/10.1152/ajplung.00348.2006

65. Jung, K.-I., Ju, A., Lee, H.-M., Lee, S.-S., Song, C.-H., Won, W.-Y., Jeong, J.-S., Hong, O.-K., Kim, J.-H., & Kim, D.-J. (2011). Chronic ethanol ingestion, type 2 diabetes mellitus, and brain-derived neurotrophic factor (BDNF) in rats. *Neuroscience Letters*, *487*(2), 149–152. https://doi.org/10.1016/j.neulet.2010.10.011

66. Juta, P. M., Jansen van Vuuren, J. M., & Mbaya, K. J. (2024). A multidisciplinary approach for people with HIV failing antiretroviral therapy in South Africa. *Southern African Journal of HIV Medicine*, *25*(1), 1–11. https://doi.org/10.4102/SAJHIVMED.V25I1.1579

67. Kanmani, S., Kwon, M., Shin, M. K., & Kim, M. K. (2019). Association of C-Reactive Protein with Risk of Developing Type 2 Diabetes Mellitus, and Role of Obesity and

Hypertension: A Large Population-Based Korean Cohort Study. *Scientific Reports 2019 9:1*, *9*(1), 1–8. https://doi.org/10.1038/s41598-019-40987-8

68. Kanters, S., Vitoria, M., Zoratti, M., Doherty, M., Penazzato, M., Rangaraj, A., Ford, N., Thorlund, K., Anis, P. A. H., Karim, M. E., Mofenson, L., Zash, R., Calmy, A., Kredo, T., & Bansback, N. (2020). Comparative efficacy, tolerability and safety of dolutegravir and efavirenz 400mg among antiretroviral therapies for first-line HIV treatment: A systematic literature review and network meta-analysis. *EClinicalMedicine*, *28*, 100573. https://doi.org/10.1016/J.ECLINM.2020.100573

69. Kaphalia, L., & Calhoun, W. J. (2013). Alcoholic lung injury: Metabolic, biochemical and immunological aspects. *Toxicology Letters*, *222*(2), 171–179. https://doi.org/10.1016/j.toxlet.2013.07.016

70. Kaphalia, L., Srinivasan, M. P., Kakumanu, R. D., Kaphalia, B. S., & Calhoun, W. J. (2019). Ethanol Exposure Impairs AMPK Signaling and Phagocytosis in Human Alveolar Macrophages: Role of Ethanol Metabolism. *Alcoholism, Clinical and Experimental Research*, *43*(8), 1682–1694. https://doi.org/10.1111/ACER.14131

71. Kaphalia, L., Srinivasan, M. P., Kaphalia, B. S., & Calhoun, W. J. (2024). Alcohol and its metabolites dysregulate cellular bioenergetics and induce oxidative and endoplasmic reticulum stress in primary human bronchial epithelial cells. *Alcohol, Clinical & Experimental Research*, *48*(4), 596–611. https://doi.org/10.1111/ACER.15278

72. Khalid, T., & O'Leary, C. (2023). Engineering Large Airways. *Advances in Experimental Medicine and Biology*, *1413*, 121–135. https://doi.org/10.1007/978-3-031-26625-6_7

73. Khateeb, J., Fuchs, E., & Khamaisi, M. (2019). Diabetes and Lung Disease: An Underestimated Relationship. *The Review of Diabetic Studies : RDS*, *15*(1), 1. https://doi.org/10.1900/RDS.2019.15.1

74. Kim, S.-J., & Kim, D.-J. (2012). Alcoholism and Diabetes Mellitus. *Diabetes & Metabolism Journal*, *36*(2), 108. https://doi.org/10.4093/dmj.2012.36.2.108

75. Kiyota, K., Ueno, H., Numayama-Tsuruta, K., Haga, T., Imai, Y., Yamaguchi, T., & Ishikawa, T. (2014). Fluctuation of cilia-generated flow on the surface of the tracheal lumen. *American Journal of Physiology. Lung Cellular and Molecular Physiology*, 306(2). https://doi.org/10.1152/AJPLUNG.00117.2013

76. Knoop, J., Gavrisan, A., Kuehn, D., Reinhardt, J., Heinrich, M., Hippich, M., Eugster, A., Ockert, C., Ziegler, A. G., & Bonifacio, E. (2018). GM-CSF-producing autoreactive CD4 T cells in type 1 diabetes. Clinical Immunology (Orlando, Fla.), 188, 23–30. https://doi.org/10.1016/J.CLIM.2017.12.002

77. Konstantinidis, I., Crothers, K., Kunisaki, K. M., Drummond, M. B., Benfield, T., Zar, H. J., Huang, L., & Morris, A. (2023). HIV-associated lung disease. *Nature Reviews. Disease Primers*, *9*(1), 39. https://doi.org/10.1038/S41572-023-00450-5

78. Kuhlmann, C. R. W., Li, F., Lüdders, D. W., Schaefer, C. A., Most, A. K., Backenköhler, U., Neumann, T., Tillmanns, H., Waldecker, B., Erdogan, A., & Wiecha, J. (2004). Dose-dependent activation of Ca2-activated K channels by ethanol contributes to improved endothelial cell functions. *Alcoholism, Clinical and Experimental Research*, *28*(7), 1005–1011. https://doi.org/10.1097/01.ALC.0000130811.92457.0D

79. Kumar, S., Jin, M., Ande, A., Sinha, N., Silverstein, P. S., & Kumar, A. (2012). Alcohol consumption effect on antiretroviral therapy and HIV-1 pathogenesis: role of cytochrome P450 isozymes. *Expert Opinion on Drug Metabolism & Toxicology*, *8*(11), 1363–1375. https://doi.org/10.1517/17425255.2012.714366

80. Lam, B. Q., Srivastava, R., Morvant, J., Shankar, S., & Srivastava, R. K. (2021). Association of Diabetes Mellitus and Alcohol Abuse with Cancer: Molecular Mechanisms and Clinical Significance. *Cells, 10(11)*, 3077. https://doi.org/10.3390/CELLS10113077

81. Lau, K. A., & Wong, J. J. L. (2013). Current trends of HIV recombination worldwide. *Infectious Disease Reports, 5(1),* 4. https://doi.org/10.4081/idr.2013.s1.e4

82. Lazić, A., Danković, G., Korobeinikov, G., Cadenas-Sanchez, C., & Trajković, N. (2025). Acute effects of different "exercise snacking'' modalities on glycemic control in patients with type 2 diabetes mellitus (T2DM): study protocol for a randomized controlled trial. *BMC Public Health, 25(1)*, 1–9. https://doi.org/10.1186/S12889-025-21669-9/FIGURES/B

83. Liang, Y., Yeligar, S. M., & Brown, L. A. S. (2012). Chronic-Alcohol-Abuse-Induced Oxidative Stress in the Development of Acute Respiratory Distress Syndrome. *The Scientific World Journal*, *2012*(1), 740308. https://doi.org/10.1100/2012/740308

84. Lieber, C. S. (2004). Alcoholic fatty liver: its pathogenesis and mechanism of

progression to inflammation and fibrosis. *Alcohol*, *34*(1), 9–19. https://doi.org/10.1016/j.alcohol.2004.07.008

85. Liu, J., Tian, Z., Gao, B., & Kunos, G. (2002). Dose-dependent activation of antiapoptotic and proapoptotic pathways by ethanol treatment in human vascular endothelial cells: differential involvement of adenosine. *The Journal of Biological Chemistry*, *277*(23), 20927–20933. https://doi.org/10.1074/JBC.M110712200

86. López-Campos, J. L., Calero, C., Rojano, B., López-Porras, M., Sáenz-Coronilla, J., Blanco, A. I., Sánchez-López, V., Tobar, D., Montes-Worboys, A., & Arellano, E. (2013). C-Reactive Protein and Serum Amyloid A Overexpression in Lung Tissues of Chronic Obstructive Pulmonary Disease Patients: A Case-Control Study. *International Journal of Medical Sciences*, *10*(8), 938–947. https://doi.org/10.7150/IJMS.6152

87. Lopez-Lopez, J. G., Moral-Sanz, J., Frazziano, G., Gomez-Villalobos, M. J., Flores-Hernandez, J., Monjaraz, E., Cogolludo, A., & Perez-Vizcaino, F. (2008). Diabetes induces pulmonary artery endothelial dysfunction by NADPH oxidase induction. *American Journal of Physiology-Lung Cellular and Molecular Physiology*, *295*(5), L727–L732. https://doi.org/10.1152/ajplung.90354.2008

88. Malecki, M. T. (2005). Genetics of type 2 diabetes mellitus. *Diabetes Research and Clinical Practice*, *68*, S10–S21. https://doi.org/10.1016/j.diabres.2005.03.003

89. Maraldi, C., Volpato, S., Kritchevsky, S. B., Cesari, M., Andresen, E., Leeuwenburgh, C., Harris, T. B., Newman, A. B., Kanaya, A., Johnson, K. C., Rodondi, N., & Pahor, M. (2006). Impact of inflammation on the relationship among alcohol consumption, mortality, and cardiac events: The health, aging, and body composition study. *Archives of Internal Medicine*, *166*(14), 1490–1497. https://doi.org/10.1001/archinte.166.14.1490

90. Marsh Sung, J., & M. Margolis, D. (2018). HIV persistence on antiretroviral therapy and barriers to a cure. *Advances in Experimental Medicine and Biology*, *1075*, 165–185. https://doi.org/10.1007/978-981-13-0484-2_7

91. Martinez-Picado, J., & Deeks, S. (2016). Persistent HIV-1 replication during antiretroviral therapy. *Journals.Lww.ComJ*. https://journals.lww.com/co-hivandaids/fulltext/2016/07000/Persistent_HIV_1_replication_during_antiretroviral.11.aspx

92. Mellor, M. M., Bast, A. C., Jones, N. R., Roberts, N. W., Ordonez-Mena, J. M., Reith,

A. J. M., Butler, C. C., Matthews, P. C., & Dorward, J. (2021). Risk of adverse coronavirus disease 2019 outcomes for people living with HIV. AIDS, 35(4), F1–F10. https://doi.org/10.1097/QAD.0000000000002836

93. McCance-Katz, E. F., Lum, P. J., Beatty, G., Gruber, V. A., Peters, M., & Rainey, P. M. (2012). Untreated HIV infection is associated with higher blood alcohol levels. *Journal of acquired immune deficiency syndromes (1999), 60(3),* 282–288. https://doi.org/10.1097/QAI.0b013e318256625f

94. McCormick, T. S., Hejal, R. B., Leal, L. O., & Ghannoum, M. A. (2022). GM-CSF: Orchestrating the Pulmonary Response to Infection. *Front Pharmacol, 12:* 735443. https://doi.org/10.3389/fphar.2021.735443

95. Meintjes, G., Moorhouse, M. A., Carmona, S., Davies, N., Dlamini, S., Van Vuuren, C., Manzini, T., Mathe, M., Moosa, Y., Nash, J., Nel, J., Pakade, Y., Woods, J., Van Zyl, G., Conradie, F., & Venter, F. (2017). Adult antiretroviral therapy guidelines 2017. *Southern African Journal of HIV Medicine, 18(1)*. https://doi.org/10.4102/SAJHIVMED.V18I1.776

96. Melhuish, A., & Lewthwaite, P. (2022). Natural history of HIV and AIDS. *Medicine (United Kingdom), 50(5),* 298–303. https://doi.org/10.1016/j.mpmed.2022.02.011

97. Moyo, D., Tanthuma, G., Mushisha, O., Kwadiba, G., Chikuse, F., Cary, M. S., Steenhoff, A. P., BCh, M., & A Reid, M. J. (2014). Diabetes mellitus in HIV-infected patients receiving antiretroviral therapy. *South African Medical Journal (SAMJ), 104(1)*. https://doi.org/10.7196/SAMJ.6792

98. Mpinganjira, M. G., Chirwa, T., Kabudula, C. W., Gómez-Olivé, F. X., Tollman, S., & Francis, J. M. (2023). Association of alcohol use and multimorbidity among adults aged 40 years and above in rural South Africa. *Scientific Reports 2023 13:1*, *13*(1), 1–11. https://doi.org/10.1038/s41598-023-35018-6

99. Mzimela, N., Dimba, N., Sosibo, A., & Khathi, A. (2024). Evaluating the impact of type 2 diabetes mellitus on pulmonary vascular function and the development of pulmonary fibrosis. *Frontiers in Endocrinology*, *15*, 1431405. https://doi.org/10.3389/FENDO.2024.1431405

100. New-Aaron, M., Kang, M., & Yeligar, S. M. (2024). Pulmonary symptoms associated with heavy alcohol consumption among people living with HIV: an analysis

of the NHANES 1999-2010. *Alcohol and alcoholism (Oxford, Oxfordshire), 59(3)*, 21. https://doi.org/10.1093/alcalc/agae021

101. Newling, M., Sritharan, L., van der Ham, A. J., Hoepel, W., Fiechter, R. H., de Boer, L., Zaat, S. A. J., Bisoendial, R. J., Baeten, D. L. P., Everts, B., & den Dunnen, J. (2019). C-Reactive Protein Promotes Inflammation through FcγR-Induced Glycolytic Reprogramming of Human Macrophages. *The Journal of Immunology, 203(1)*, 225–235. https://doi.org/10.4049/JIMMUNOL.1900172

102. Obradovic, M., Sudar, E., Zafirovic, S., Stanimirovic, J., Labudovic-Borovic, M., & Isenovic, E. R. (2015). Estradiol in vivo induces changes in cardiomyocytes size in obese rats. *Angiology*, *66*(1), 25–35. https://pubmed.ncbi.nlm.nih.gov/24327768/

103. Oguntibeju O. O. (2019). Type 2 diabetes mellitus, oxidative stress and inflammation: examining the links. *International journal of physiology, pathophysiology and pharmacology, 11(3),* 45–63. https://pubmed.ncbi.nlm.nih.gov/31333808/

104. Otieno, G., Whiteside, Y. O., Achia, T., Kwaro, D., Zielinski-Gutierrez, E., Ojoo, S., Sewe, M., Musingila, P., Akelo, V., Obor, D., Nyaguara, A., De Cock, K. M., & Borgdorff, M. W. (2019). Decreased HIV-associated mortality rates during scale-up of antiretroviral therapy, 2011–2016. *AIDS*, *33*(15). https://doi.org/10.1097/QAD.0000000000002374

105. Patwa, A., & Shah, A. (2015). Anatomy and physiology of respiratory system relevant to anaesthesia. *Indian Journal of Anaesthesia*, *59*(9), 533. https://doi.org/10.4103/0019-5049.165849

106. Pechlivani, N., & Ajjan, R. A. (2018). Thrombosis and Vascular Inflammation in Diabetes: Mechanisms and Potential Therapeutic Targets. *Frontiers in Cardiovascular Medicine*, *5*. https://doi.org/10.3389/fcvm.2018.00001

107. Pignone, M., Alberts, M. J., Colwell, J. A., Cushman, M., Inzucchi, S. E., Mukherjee, D., Rosenson, R. S., Williams, C. D., Wilson, P. W., Kirkman, M. S., American Diabetes Association, American Heart Association, & American College of Cardiology Foundation. (2010). Aspirin for primary prevention of cardiovascular events in people with diabetes. *Journal of the American College of Cardiology, 55(25),*

2878- 2886. https://doi.org/10.1016/j.jacc.2010.04.003

108. Pitocco, D., Fuso, L., Conte, E. G., Zaccardi, F., Condoluci, C., Scavone, G., Incalzi, R. A., & Ghirlanda, G. (2012). The Diabetic Lung - A New Target Organ? *The Review of Diabetic Studies*, *9*(1), 23–35. https://doi.org/10.1900/RDS.2012.9.23

109. Pohlers, D., Brenmoehl, J., Löffler, I., Müller, C. K., Leipner, C., Schultze-Mosgau, S., Stallmach, A., Kinne, R. W., & Wolf, G. (2009). TGF-β and fibrosis in different organs — molecular pathway imprints. *Biochimica et Biophysica Acta (BBA)-Molecular Basis of Disease*, *1792*(8), 746–756. https://doi.org/10.1016/j.bbadis.2009.06.004

110. Probst, C., Parry, C. D. H., Wittchen, H.-U., & Rehm, J. (2018). The socioeconomic profile of alcohol-attributable mortality in South Africa: a modelling study. *BMC Medicine*, *16*(1), 97. https://doi.org/10.1186/s12916-018-1080-0

111. Qin, G., & Meng, Z. (2006). The expressions of protooncogenes and CYP1A in lungs of rats exposed to sulfur dioxide and benzo(a)pyrene. *Regulatory Toxicology and Pharmacology*, *45*(1), 36–43. https://doi.org/10.1016/j.yrtph.2006.02.006

112. Rahman, M. S., Hossain, K. S., Das, S., Kundu, S., Adegoke, E. O., Rahman, Md. A., Hannan, Md. A., Uddin, M. J., & Pang, M.-G. (2021). Role of Insulin in Health and Disease: An Update. *International Journal of Molecular Sciences*, *22*(12), 6403. https://doi.org/10.3390/ijms22126403

113. Raum, E., Gebhardt, K., Buchner, M., Schiltenwolf, M., & Brenner, H. (2007). Long-term and short-term alcohol consumption and levels of C-reactive protein. *International Journal of Cardiology*, *121*(2), 224–226. https://doi.org/10.1016/J.IJCARD.2006.08.104

114. Sapra, A., & Bhandari, P. (2023). Diabetes. *StatPearls*. https://www.ncbi.nlm.nih.gov/books/NBK551501/

115. Sato, S., Bartol, Ã., Suki, E., Parameswaran, H., Hamakawa, H., & Suki, B. (2015). Scale dependence of structure-function relationships in the emphysematous mouse lung. *Frontiers in Physiology*, *6*. https://doi.org/10.3389/fphys.2015.00146

116. Schamberger, A. C., Schiller, H. B., Fernandez, I. E., Sterclova, M., Heinzelmann, K., Hennen, E., Hatz, R., Behr, J., Vašáková, M., Mann, M., Eickelberg, O., & Staab-Weijnitz, C. A. (2016). Glutathione peroxidase 3 localizes to the epithelial

lining fluid and the extracellular matrix in interstitial lung disease. *Scientific reports, 6,* 29952. https://doi.org/10.1038/srep29952

117. Savin, I. A., Zenkova, M. A., & Sen'kova, A. V. (2022). Pulmonary Fibrosis as a Result of Acute Lung Inflammation: Molecular Mechanisms, Relevant In Vivo Models, Prognostic and Therapeutic Approaches. *International Journal of Molecular Sciences, 23(23),* 14959. https://doi.org/10.3390/IJMS232314959

118. Schermuly, R. T., Ghofrani, H. A., Wilkins, M. R., & Grimminger, F. (2011). Mechanisms of disease: pulmonary arterial hypertension. *Nature Reviews. Cardiology, 8(8)*, 443. https://doi.org/10.1038/NRCARDIO.2011.87

119. Schneider, M., Norman, R., Parry, C., Bradshaw, D., Plüddemann, A., & South African Comparative Risk Assessment Collaborating Group (2007). Estimating the burden of disease attributable to alcohol use in South Africa in 2000. *South African medical journal = Suid-Afrikaanse tydskrif vir geneeskunde, 97(8 Pt 2), 664–672.* https://pubmed.ncbi.nlm.nih.gov/17952223/

120. Sereti, I., Krebs, S. J., Phanuphak, N., Fletcher, J. L., Slike, B., Pinyakorn, S., O'Connell, R. J., Rupert, A., Chomont, N., Valcour, V., Kim, J. H., Robb, M. L., Michael, N. L., Douek, D. C., Ananworanich, J., & Utay, N. S. (2017). Persistent, Albeit Reduced, Chronic Inflammation in Persons Starting Antiretroviral Therapy in Acute HIV Infection. *Clinical Infectious Diseases*, *64*(2), 124–131. https://doi.org/10.1093/CID/CIW683

121. Sexton, S. M. (2003). Alcohol Consumption and C-Reactive Protein. *American Family Physician*, *68*(5), 959–960. https://www.aafp.org/pubs/afp/issues/2003/0901/p959.html

122. Sharma, B. (2014). Oxidative stress in HIV patients receiving antiretroviral therapy. *Current HIV Research, 12(1),* 13–21. https://doi.org/10.2174/1570162X12666140402100959

123. Shelburne, S. A., Hamill, R. J., Rodriguez-Barradas, M. C., Greenberg, S. B., Atmar, R. L., Musher, D. M., Gathe, J. C., Visnegarwala, F., & Trautner, B. W. (2002). Immune Reconstitution Inflammatory Syndrome. *Medicine*, *81*(3), 213–227. https://doi.org/10.1097/00005792-200205000-00005

124. Shen, C. J., Kao, C. H., Hsu, T. Y., Chen, C. Y., Lin, C. L., & Shih, H. M.

(2017). Effect of alcohol intoxication on the risk of venous thromboembolism: A nationwide retrospective cohort study. *Medicine*, *96*(42), e8041. https://doi.org/10.1097/MD.0000000000008041

125. Silva, A. F., Sousa-Nunes, F., Faria-Costa, G., Rodrigues, I., Guimarães, J. T., Leite-Moreira, A., Henriques-Coelho, T., Negrão, R., & Moreira-Gonçalves, D. (2021). Effects of chronic moderate alcohol consumption on right ventricle and pulmonary remodelling. *Experimental Physiology*, *106*(6), 1359–1372. https://doi.org/10.1113/EP088788

126. Simet, S. M., & Sisson, J. H. (2015). Alcohol's Effects on Lung Health and Immunity. *Alcohol Research: Current Reviews*, *37*(2), 199–208. https://pmc.ncbi.nlm.nih.gov/articles/PMC4590617/

127. Sisson, J. H. (2007). Alcohol and Airways Function in Health and Disease. *Alcohol (Fayetteville, N.Y.), 41(5)*, 293. https://doi.org/10.1016/J.ALCOHOL.2007.06.003

128. Slovinsky, W. S., Romero, F., Sales, D., Shaghaghi, H., & Summer, R. (2019). The involvement of GM-CSF deficiencies in parallel pathways of pulmonary alveolar proteinosis and the alcoholic lung. *Alcohol, 80,* 73–79. https://doi.org/10.1016/j.alcohol.2018.07.006

129. Ssentongo, P., Heilbrunn, E. S., Ssentongo, A. E., Advani, S., Chinchilli, V. M., Nunez, J. J., & Du, P. (2021). Epidemiology and outcomes of COVID-19 in HIV-infected individuals: a systematic review and meta-analysis. Scientific Reports, 11(1), 1–12. https://doi.org/10.1038/S41598-021-85359-3;SUBJMETA

130. Stanimirovic, J., Radovanovic, J., Banjac, K., Obradovic, M., Essack, M., Zafirovic, S., Gluvic, Z., Gojobori, T., & Isenovic, E. R. (2022). Role of C-Reactive Protein in Diabetic Inflammation. *Mediators of Inflammation*, *2022*, 3706508. https://doi.org/10.1155/2022/3706508

131. Steiner, J. L., Crowell, K. T., & Lang, C. H. (2015). Impact of Alcohol on Glycemic Control and Insulin Action. *Biomolecules*, *5*(4), 2223–2246. https://doi.org/10.3390/BIOM5042223

132. Stewart, S. H., Mainous, A. G., & Gilbert, G. (2002). Relation between alcohol consumption and C-reactive protein levels in the adult US population. *The Journal of*

the American Board of Family Practice, *15*(6), 437–442. https://www.jabfm.org/content/15/6/437.long.

133. Stewart, J. (2021). Trivicay FDA approval history. *Drugs.com*. https://www.drugs.com/history/tivicay.html

134. Suresh, K., & Shimoda, L. A. (2016). Lung Circulation. *Comprehensive Physiology, 6(2)*, 897. https://doi.org/10.1002/CPHY.C140049

135. Sueblinvong, V., Kerchberger, V. E., Saghafi, R., Mills, S. T., Fan, X., & Guidot, D. M. (2014). Chronic Alcohol Ingestion Primes the Lung for Bleomycin-Induced Fibrosis in Mice. *Alcoholism: Clinical and Experimental Research*, *38*(2), 336–343. https://doi.org/10.1111/acer.12232

136. Suki, B., & Bates, J. H. T. (2008). Extracellular matrix mechanics in lung parenchymal diseases. *Respiratory Physiology & Neurobiology*, *163*(1–3), 33–43. https://doi.org/10.1016/j.resp.2008.03.015

137. Tai, H., Jiang, X., Yao, S., Liu, Y., Wei, H., Li, L., Jiao, Z., Wang, T., Kuang, J., Jia, L. (2021). Vascular Endothelial Function as a Valid Predictor of Variations in Pulmonary Function in T2DM Patients Without Related Complications. *Frontiers in Endocrinology*, *12*, 622768. https://doi.org/10.3389/FENDO.2021.622768

138. Takahashi, T., Yoshihisa, A., Sugimoto, K., Yokokawa, T., Misaka, T., Kaneshiro, T., Oikawa, M., Kobayashi, A., Nakazato, K., Ishida, T., & Takeishi, Y. (2018). Associations between diabetes mellitus and pulmonary hypertension in chronic respiratory disease patients. *PloS one, 13(10),* e0205008. https://doi.org/10.1371/journal.pone.0205008

139. Talakatta, G., Sarikhani, M., Muhamed, J., Dhanya, K., Somashekar, B. S., Mahesh, P. A., Sundaresan, N., & Ravindra, P. V. (2018). Diabetes induces fibrotic changes in the lung through the activation of TGF-β signaling pathways. *Scientific Reports*, *8*(1), 11920. https://doi.org/10.1038/s41598-018-30449-y

140. Tangvarasittichai, S. (2015). Oxidative stress, insulin resistance, dyslipidemia and type 2 diabetes mellitus. *World Journal of Diabetes*, *6*(3), 456. https://doi.org/10.4239/wjd.v6.i3.456

141. Taylor, B., Irving, H. M., Kanteres, F., Room, R., Borges, G., Cherpitel, C.,

Greenfield, T., & Rehm, J. (2010). The more you drink, the harder you fall: A systematic review and meta-analysis of how acute alcohol consumption and injury or collision risk increase together. *Drug and Alcohol Dependence*, *110*(1–2), 108–116. https://doi.org/10.1016/j.drugalcdep.2010.02.011

142. Thapa, S., & Shrestha, U. (2022). *Immune Reconstitution Inflammatory Syndrome*. Treasure Island (FL): StatPearls Publishing. https://www.ncbi.nlm.nih.gov/books/NBK567803/

143. Triplette, M., Justice, A., Attia, E. F., Tate, J., Brown, S. T., Goetz, M. B., Kim, J. W., Rodriguez-Barradas, M. C., Hoo, G. W. S., Wongtrakool, C., Akgün, K., & Crothers, K. (2018). Markers of chronic obstructive pulmonary disease are associated with mortality in people living with HIV. *AIDS*, *32*(4), 487–493. https://doi.org/10.1097/QAD.0000000000001701

144. Twigg III, H. L., & Knox, K. S. (2013). Impact of Antiretroviral Therapy on Lung Immunology and Inflammation. *Clinics in Chest Medicine*, *34*(2), 155–164. https://doi.org/10.1016/j.ccm.2013.01.004

145. Twigg III, H. L., Weinstock, G. M., & Knox, K. S. (2017). Lung microbiome in human immunodeficiency virus infection. *Translational Research, 179,* 97–107. https://doi.org/10.1016/J.TRSL.2016.07.008

146. UNAIDS. (2024.) The path that ends AIDS. *UNAIDS Global AIDS* |. Retrieved 8 March 2025, from https://www.unaids.org/en/resources/documents/2023/global-aids-update-2023

147. Vaillant, A. A. J., & Naik, R. (2023). HIV-1–Associated Opportunistic Infections. *StatPearls*. https://www.ncbi.nlm.nih.gov/books/NBK539787/

148. Wagner, P. D. (2015). The physiological basis of pulmonary gas exchange: implications for clinical interpretation of arterial blood gases. *European Respiratory Journal*, *45*(1), 227–243. https://doi.org/10.1183/09031936.00039214

149. Wang, X., Chai, H., Lin, P. H., Yao, Q., & Chen, C. (2009). Roles and Mechanisms of Human Immunodeficiency Virus Protease Inhibitor Ritonavir and Other Anti-Human Immunodeficiency Virus Drugs in Endothelial Dysfunction of Porcine Pulmonary Arteries and Human Pulmonary Artery Endothelial Cells. *The American Journal of Pathology*, *174*(3), 771.

https://doi.org/10.2353/AJPATH.2009.080157

150. Wheatley, C. M., Baldi, J. C., Cassuto, N. A., Foxx-Lupo, W. T., & Snyder, E. M. (2011). Glycemic control influences lung membrane diffusion and oxygen saturation in exercise-trained subjects with type 1 diabetes. *European Journal of Applied Physiology*, *111*(3), 567–578. https://doi.org/10.1007/s00421-010-1663-8

151. Witkiewitz, K., Litten, R. Z., & Leggio, L. (2019). Advances in the science and treatment of alcohol use disorder. *Science Advances*, *5*(9). https://doi.org/10.1126/sciadv.aax4043

152. Wohl, D. A., Koethe, J. R., Sax, P. E., Mccomsey, G. A., Kuritzkes, D. R., Moyle, G., Kaplan, L., Van Wyk, J., Campo, R. E., & Cohen, C. (2024). Antiretrovirals and Weight Change: Weighing the Evidence. *Clinical Infectious Diseases, 79(4),* 999–1005. https://doi.org/10.1093/CID/CIAE191

153. Wu, Y., Ding, Y., Tanaka, Y., & Zhang, W. (2014). Risk factors contributing to Type 2 Diabetes and recent advances in treatment and prevention. *Int J Med Sci*, *11*, 1185–1200. https://doi.org/10.7150/ijms.10001

154. Wyatt, T. A., Kharbanda, K. K., McCaskill, M. L., Tuma, D. J., Yanov, D., DeVasure, J., & Sisson, J. H. (2012). Malondialdehyde–acetaldehyde-adducted protein inhalation causes lung injury. *Alcohol*, *46*(1), 51–59. https://doi.org/10.1016/J.ALCOHOL.2011.09.001

155. Xiang, Y., Cheng, J., Wang, D., Hu, X., Xie, Y., Stitham, J., Atteya, G., Du, J., Tang, W. H., Lee, S. H., Leslie, K., Spollett, G., Liu, Z., Herzog, E., Herzog, R. I., Lu, J., Martin, K. A., & Hwa, J. (2015). Hyperglycemia repression of miR-24 coordinately upregulates endothelial cell expression and secretion of von Willebrand factor. *Blood, 125(22),* 3377–3387. https://doi.org/10.1182/blood-2015-01-620278

156. Wynn, T. A & Ramalingam, T. R. (2012). Mechanisms of fibrosis: therapeutic translation for fibrotic disease. *Nat Med, 18(7):* 1028–1040. https://doi.org/10.1038/nm.2807

157. Yeligar, S. M., Ward, J. M., Harris, F. L., Brown, L. A. S., Guidot, D. M., & Cribbs, S. K. (2017). Dysregulation of Alveolar Macrophage PPARγ, NADPH Oxidases, and TGFβ1 in Otherwise Healthy HIV-Infected Individuals. *AIDS Research and Human Retroviruses*, *33*(10), 1018. https://doi.org/10.1089/AID.2016.0030

158. Zhang, J., Guo, Y., Mak, M., & Tao, Z. (2024a). Translational medicine for acute lung injury. *Journal of Translational Medicine*, *22*(1). https://doi.org/10.1186/S12967-023-04828-7

159. Zhang, J., Gong, S., Li, Q., Zhang, S., & Feng, G. (2024b). Lysosome-Targeted Polarity-Sensitive NIR Fluorescence Probe for Imaging Injured Lung and Liver in Diabetes. *Analytical Chemistry*. https://doi.org/10.1021/ACS.ANALCHEM.4C03214

160. Zhang, R. H., Zhou, J. B., Cai, Y. H., Shu, L. P., Simó, R., & Lecube, A. (2020). Non-linear association between diabetes mellitus and pulmonary function: a population-based study. *Respiratory Research*, *21*(1). https://doi.org/10.1186/S12931-020-01538-2

161. Zheng, Y., Ley, S. H., & Hu, F. B. (2018). Global aetiology and epidemiology of type 2 diabetes mellitus and its complications. *Nature Reviews. Endocrinology*, *14*(2), 88–98. https://doi.org/10.1038/NRENDO.2017.151

162. Zhou, Q., Tan, W., Li, Q., Li, B., Zhou, L., Liu, X., Yang, J., & Zhao, D. (2023). A new segment method for pulmonary artery and vein. *Health Information Science and Systems*, *11*(1), 1–17. https://doi.org/10.1007/S13755-023-00245-8/TABLES/3

163. Zimmet, P. Z. (2017). Diabetes and its drivers: the largest epidemic in human history. *Clinical Diabetes and Endocrinology*, *3*(1), 1. https://doi.org/10.1186/s40842-016-0039-3

APPENDICES

7.1. Microscope slide-coating.

7.1.1. Saline.

The slides were treated with 3% aminopropyltriethoxysilane (APES) in acetone for 30 minutes, then rinsed in two changes of acetone. The slides were then allowed to air dry for a minimum of an hour, then left to dry overnight at 37 ℃. These slides were used for immunohistochemistry.

7.1.2. Gelatine.

Chrome Alum Gelatine solution was made using Gelatine type A, Chromium potassium sulfate and distilled water in this proportion 2.5 g: 0.415 g: 250 ml. The gelatin was completely dissolved in heated distilled water at 60 ℃ and the chromium potassium sulfate was added and stirred till the solution turned pale blue. Then 1 g of thymol was added to preserve the solution. Microscope slides were treated with gelatine solution maintained at 40 to 50 ℃ and the slides were covered with foil to protect from dust and left to dry overnight at 37 ℃. These slides were used for routine staining.

7.2. Serum biochemical analysis.

7.2.1. TBA test for MDA.

I) Reagents preparation.

Reagent 1: The reagent was warmed from 2 ℃ storage in water bath at 37 ℃ until clear.

Reagent 2: The reagent was diluted with double distilled water and fully mixed at 1.2:34 ratio.

Reagent 3: The reagent was dissolved fully in 14 ml double distilled water at approximately 95 ℃ and added 14 ml glacial acetic acid to the solution, then cooled to room temperature.

50% acetic acid: 8 ml of acetic acid was added to 8 ml of double distilled water gradually and thoroughly mixed.

Table 7.1: The preparation of the TBA assay.

Measurements of the samples and reagents into respective tubes.

	Standard tube	Sample tube	Control tube
Standard solution with different concentrations (mL)	0.02		
Sample (mL)		0.02	0.02
Reagent 1 (mL)	0.02	0.02	0.02
Reagent 2 application solution (mL)	0.6	0.6	0.6
Reagent 3 application solution (mL)	0.02	0.02	
50% acetic acid (mL)			0.02

II) Preparation of standard curve.

Table 7.2: Preparation of standard curve.

The recommended dilution gradient comprised of the standard solution and absolute ethyl alcohol for the preparation of the standard curve.

Number	Standard concentrations (µmol/L)	50 µmol/L Standard (µL)	Absolute ethyl alcohol (µL)
A	0	0	100
B	5	10	90
C	10	20	80
D	15	30	70
E	20	40	60
F	25	50	50
G	30	60	40
H	40	80	20

7.2.2. ELISA for GPx1.

I) Reagent preparation.

All reagents were brought to ambient temperature ~ 18- 25 ℃ before starting the experiment.

- **Wash buffer:** 30 ml of the concentrated wash buffer was diluted with 720 ml of distilled water to make up to 750 ml of wash buffer.
- **Standard working solution:** The standard solution was centrifuged at 10 000g for a minute, then added 1 ml of reference standard and sample diluent. The solution was then allowed to mix for 10 minutes by gentle inversion several times and further mixed thoroughly with a pipette, producing a working solution of 2000 pg/ml. Serial dilutions for the dilution gradient were made as follow: 2000, 1000, 500, 250, 125, 62.5, 31.25 and 0 pg/ml, dilution method is illustrated in Figure 7.1.
- **Biotinylated detection Ab working solution:** The solution was prepared at 100 µl/well. The concentrated biotinylated detection Ab was centrifuged at 800g for a minute, then diluted the 100x concentrated HRP conjugate to 1x working solution with HRP conjugate diluent at 1:99 ratio (Concentrated HRP conjugate: HRP conjugate diluent).

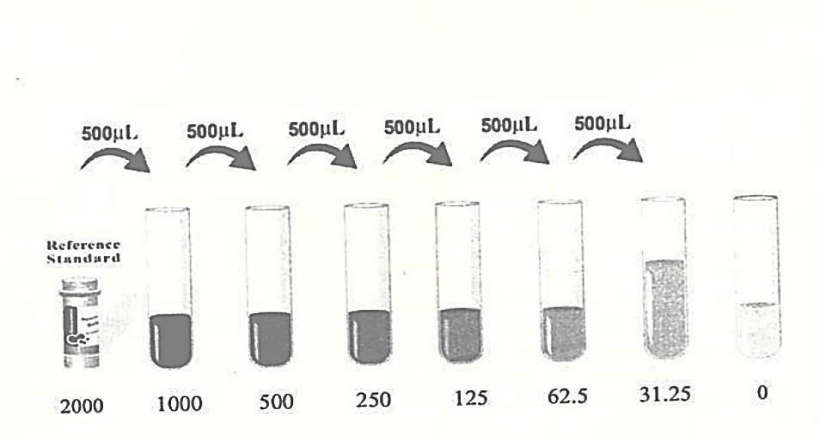

Figure 7.1: Preparation of the standard working solution.

Dilution method for the recommended dilution gradient for GPx ELIZA.

7.2.3. Optical density for concentration calculation.

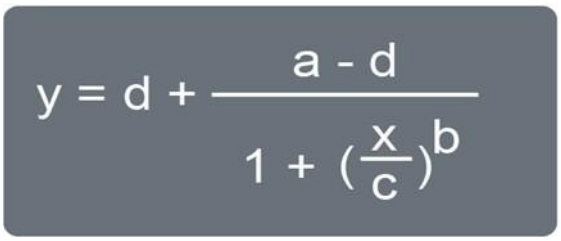

Figure 7.2: Equation to convert optical density to concentration.

Formula used to calculate concentrations for plasma protein, serum MDA and GPx1 concentrations from optical density values for plasma protein, MDA and GPx1.

Table 7.3: Optical density for concentration formular values.

Descriptions and values of symbols of the equation used to calculate actual concentrations from optical density values.

Symbol	Description	Value
a	Theoretical response at [o]	0.009191
b	Slope factor	1.162363
c	Inflection point (EC50/IC50)	951.3686
d	Theoretical response at [infinite]	4.094045
x	Optical density	
y	Concentration	

7.3. Routine stains.

7.3.1. H&E stain.

The hematoxylin solution was made by dissolving 100g of potash alum in 800 ml boiling distilled water. Separately, 4g hematoxylin powder was dissolved in 60 ml ethanol. The hematoxylin solution was then added to the potash alum solution followed by gradual addition of 2g mercury at low heat until the mercury is dissolved, and the solution adopts a pink hue. After the solution has cooled it was filtered for impurities.

7.3.2. Modified Verhoeff's van Gieson stain.

The modified Verhoeff working elastic solution was made by 3 parts of 3% Alcoholic Hematoxylin, 2 parts of aqueous Ferric chloride and 1 part of Lugol's iodine. To make Lugol's

iodine, 1g of Lugol's iodine and 2g of potassium iodide were dissolved in 100 ml of distilled water. To Van Gieson solution, 100 ml of saturated aqueous Picric acid, 18 ml of 1% aqueous Acid Fuchsin were mixed with 100 ml of distilled water.

7.3.3. Modified pentachrome stain.

Toluidine blue was made by dissolving 0.5g of toluidine blue in 100 ml of distilled water, adjusted pH to 1.5 with 0.5% HCL. To make picrosirius solution, 0.5g of Sirius red was dissolved in 500 m of distilled water saturated with picric acid.

7.3.4. Gordon and sweets stain.

The working silver solution was prepared by adding concentrated ammonia drop by drop to 5 ml of aqueous silver nitrate solution until precipitates form and dissolve. Then 5 ml of 3% sodium hydroxide was added, dissolving forming precipitates with drops of concentrated ammonia till the solution acquires opalescence. The solution was then made up to 50 ml with distilled water and stored in a dark bottle.

AREC 2017 MCE

Please note that only typewritten applications will be accepted.

UNIVERSITY OF THE WITWATERSRAND

ANIMAL RESEARCH ETHICS COMMITTEE
MODIFICATIONS AND EXTENSIONS TO EXPERIMENTS

a. Name: Prof Ejikeme Mbajiorgu Staff number: A

b. School and email address: Anatomical Sciences, Ejikeme.mbajiorgu@wits.ac.za

c. Experiment to be modified / extended

Original AESC number	**2018**	**011**	**58C**
Other MCEs :			04

d. Project Title: CHARACTERIZATION OF STREPTOZOTOCIN INDUCED DIABETIC MALE SPRAGUEDAWLEY RATS WITH CHRONIC ALCOHOL INTAKE AND ANTIRETROVIRAL THERAPY.

		No.	**Species**
e.	Number and species of animals originally approved:	120	*Sprague- Dawley rats*
f.	Number of additional animals previously allocated on MCEs:	N/A	
g.	Total number of animals allocated to the experiment to date:	107	
h.	Number of animals used to date:	107	

i. Specific modification ~~/ extension requested~~:

Change of Permit or PI:

a. 1.This was a group research project which I initiated and accepted three of my students who enrolled (Dr I Eguvoen, Ms Jaclyn Johnson and Mr Vaughan) in the project. Jaclyn has completed her PhD, Dr Eguvoen and Mr Vaughan (SMU staff) has moved to SMU.

b. 2. However, the ethics permit was issued on the name of DR. I Eguvoen, Student ID 0616737M, who is finalizing his thesis analysis at SMU.

c. 3. But, I have admitted two new master's students to continue the work on other tissues that I collected during the experiment.
d. In other to facilitate their studies, I am therefore requesting for the ethics permit to be transferred to my name as the original PI to enable the use of the tissues collected for further studies without hindrance.

Inclusion of MSc students

a. Inclusion of **Mcebo Zwane** (student number; 1473425) and **Mmotong Mahloko** (student number; 1863024) as co-workers for their M.Sc. degree projects in the School Anatomical Sciences.
b. The students will use the heart, lungs, vascular tissue, and blood samples already harvested from the study for the purpose of a M.Sc. degree with Prof Ejikeme Mbajiorgu and Dr Jaclyn Asouzu Johnson as supervisors.
c. The student will use already harvested tissue for the study of treatment effects on organs, which does not involve any new animal, treatment or extra use of the WRAF facility.

AREC 2017 MCE

---

j. Motivation for modification / extension:

This will enable this student, **Mcebo Zwane** (student number; 1473425) and **Mmotong Mahloko** (student number; 1863024) to use the tissue and avoid wasting this tissue, extra-funding and thereby maximising the use of the animals in the study as approved.

Date: 30/11/2022 Signature:

RECOMMENDATIONS

Extension of the study until the 31 December 2023.
Approval for the transfer of the study to Prof. Mbajiorgu as the PI.
Approval for the inclusion of MSc students; M. Zwane and M. Mahloko as co-workers on the protocol, and to access the described, stored tissue samples for in vitro analysis.

Date: 18 December 2022 Signature:

Deputy Chair, AREC